We thank Lev and another anonymous reviewer for their constructive comments, which have helped improve the quality of the manuscript. To address their concerns, we have made substantial revisions. Specifically, we have expanded and clarified the description of the coupling mechanism between the climate and ice sheet model. We have expanded discussions about parameter uncertainty and included a table and figure of the entire ensemble of experiments performed. We have also added more discussions of our results in the context of previous studies of reconstructions. Detailed responses to the issues raised by them can be found below along with excerpts from the revised manuscript in boxes. A bibliography of the references cited here is present at the end of the document. We would like to emphasize that excerpts presented here are only a handful of the changes made to the manuscript, which are relevant to the reviewer's distinct comments. Besides these, there are many other changes designed to improve the overall appeal of the study.

Reviewer 1:
Specific comments:

1- Methods:
I found the coupling strategy not very clear. If I understand correctly, the surface mass balance model is a submodel of PSUISM. From Fig. 2 it seems that PSUISM only takes SAT, solar radiation, precipitation and Tocean. How these fields are downscaled onto the higher resolution ice sheet model grid? Then, what is the "solar radiation" (not explained in Sec. 2.3)? I find it a bit strange that surface albedo is not part of the fields that are given to PSUISM. Eq.1 and Eq.2 suggest that PSUISM compute its own albedo from rs and rl. Where do these rs and rl come from? Also, you do not explain how you compute the sub-shelf melt from Tocean. Is this a simple scaling after a bilinear spatial interpolation? What about ice shelves developing where there is no oceanic grid points (e.g. Kara and Barents seas)? I am sure that we can find all this information in the different papers that use a similar LOVECLIP framework but it would facilitate the reading to have a synthetic and integrated view in this paper as well.

A. We have now expanded the section on the climate-ice sheet coupling to be more complete and easier to read. First, we present answers to each specific question below:
   - LOVECLIM outputs of temperature, radiation and precipitation are downscaled using bilinear remapping and ocean temperature is downscaled using a conservative remapping approach.
   - Solar radiation refers to the incoming solar radiation at the surface (used in Eq. 3 for calculating the surface mass balance).
   - PSUIM calculates albedo based on the fraction of area that is covered by snow (r_s) and that without ($1 - r_s$) \. For the snow-covered areas, the fraction of area corresponding to wet and dry snow is also explicitly considered using the ratio between liquid water contained in the snow mass and the maximum embedded liquid capacity (r_l). All of this information is obtained from the last year of its previous chunk of PSUIM run. This provides a more realistic estimate of the albedo than downscaling from LOVECLIM.
   - The sub-ice-shelf ocean melting is calculated as per Pollard et al. (2015) using ocean temperature at 400m depth (T_o) from LOVECLIM as follows:
     $$OM = \frac{KK_T\rho_w c_w}{\rho_i L_f}\left|T_{oc} - T_f\right|\left(T_{oc} - T_f\right) \quad (5)$$
     where OM is the subshelf ocean melting rate (myr^{-1}), T_{oc} is the LOVECLIM ocean temperature at 400m depth (℃), T_f is the ocean freezing temperature at depth z (m) calculated as $T_f = 0.0939 - 0.057 \times 34.5 - 0.000764 \times z$, $K_T = 15.77myr^{-1}K^{-1}$ is a coefficient; K is a non-dimensional factor of order 1, $K = 3$; $\rho_w = 1028kgm^{-3}$ is the density of ocean water; $\rho_i = 910kgm^{-3}$ is the ice density; $c_w = 4218Jkg^{-1}K^{-1}$ is the specific heat of ocean water; and $L_f = 0.335 \times 10^6 Jkg^{-1}$ is the latent heat of fusion .
   - T_{oc}, used in calculating the ocean sub-ice-shelf melting (Eq. 5) is interpolated to PSUIM grid using conservative remapping. For some of the floating ice (shelves) in PSUIM (Eq. 2), the ocean points underneath may not get an ocean temperature assigned on interpolation from LOVECLIM, since the land-sea mask in LOVECLIM is kept constant. For each of such grid points, the algorithm averages over the neighboring eight PSUIM grid points and this process is repeated until all PSUIM ocean points get ocean temperatures.
     Eq. 2 referred here is:
     $$\left.\begin{array}{l} \rho_w(S - h_b) < \rho_i h;\ \text{and}\ h_s = h + h_b;\ \text{for grounded ice (ice sheet)} \\ \rho_w(S - h_b) > \rho_i h;\ \text{and}\ h_s = S + h\left(1 - \frac{\rho_i}{\rho_w}\right);\ \text{for floating ice (ice shelves)} \end{array}\right\} \quad (2)$$
     where $\rho_w = 1028kgm^{-3}$ is the density of ocean water; $\rho_i = 910kgm^{-3}$ is the ice density; S is the sea level (m); h_b is the bedrock elevation (m); h is the ice thickness (m); and h_s is the ice surface elevation (m).

We have now addressed all of these issues in the model description sections of PSUIM (Sect. 2.2) and LOVECLIP (Sect. 2.3). Some relevant sections from the revised manuscript are attached below.
The criterion for grounding and floating ice is defined in *Lines 151-154* in *Section 2.2*:

> The ice is determined to be grounded or floating based on buoyancy, as per:
>
> $$\left.\begin{array}{l} \rho_w(S-h_b) < \rho_i h;\ \text{and}\ h_s = h + h_b;\ \text{for grounded ice (ice sheet)} \\ \rho_w(S-h_b) > \rho_i h;\ \text{and}\ h_s = S + h\left(1-\frac{\rho_i}{\rho_w}\right);\ \text{for floating ice (ice shelves)} \end{array}\right\} \quad (1)$$
>
> where $\rho_w = 1028 kgm^{-3}$ is the density of ocean water; $\rho_i = 910 kgm^{-3}$ is the ice density; S is the sea level (m); h_b is the bedrock elevation (m); h is the ice thickness (m); and h_s is the ice surface elevation (m).

Calculation of the ocean sub-ice-shelf melting is defined in *Lines 175-181* in *Section 2.2*:

> The sub-ice-shelf ocean melting is calculated as per Pollard et al. (2015) using ocean temperature at 400m depth (T_o) from LOVECLIM as follows:
>
> $$OM = \frac{KK_T\rho_w c_w}{\rho_i L_f}\left|T_{oc} - T_f\right|\left(T_{oc} - T_f\right) \quad (5)$$
>
> where OM is the subshelf ocean melting rate (myr^{-1}), T_{oc} is the LOVECLIM ocean temperature at 400m depth (°C), T_f is the ocean freezing temperature at depth z (m) calculated as $T_f = 0.0939 - 0.057 \times 34.5 - 0.000764 \times z$, $K_T = 15.77 myr^{-1}K^{-1}$ is a coefficient; K is a non-dimensional factor of order 1, $K = 3$; $c_w = 4218 Jkg^{-1}K^{-1}$ is the specific heat of ocean water; and $L_f = 0.335 \times 10^6 Jkg^{-1}$ is the latent heat of fusion.

Downscaling of solar radiation, albedo and subshelf melting over locations without oceanic grid points in LOVECLIM are explained further in *Lines 250-257* in *Section 2.3*:

> Surface incoming shortwave radiation from LOVECLIM (Q, Eq. (3)) is bilinearly interpolated to PSUIM grid and then used to calculate the surface mass balance. PSUIM calculates albedo using snow covered fraction (r_s) and the ratio between liquid water contained in the snow mass and the maximum embedded liquid capacity (r_l) from the last year of its previous chunk. This provides a more realistic estimate of the albedo than downscaling from LOVECLIM. T_{oc}, used in calculating the ocean sub-ice-shelf melting (Eq. 5) is interpolated to PSUIM grid using conservative remapping. For some of the floating ice (shelves) in PSUIM (Eq. 2), the ocean points underneath may not get an ocean temperature assigned on interpolation from LOVECLIM, since the land-sea mask in LOVECLIM is kept constant. For each of such grid points, the algorithm averages over the neighboring eight PSUIM grid points and this process is repeated until all PSUIM ocean points get ocean temperatures.

On the coupling strategy again, but from the ice sheet to the climate model this time. I understand the use of the acceleration factor. However, I do not understand how you can ensure water conservation between the ice sheet and the rest of the climate system with this acceleration factor. It seems to me that when we use an acceleration factor we can only conserve the volume or the flux, but not the two quantities at the same time (already reported by Heinemann et al., 2014). For example, let's assume that the ice sheet model runs 10 years for each year computed by the rest of the climate model. Let's say that the ice sheet model produces 10 km3 of volume loss integrated over the 10 years (1km3/yr). What do you give to the ocean model? 1 km3 or 10 km3 ? The second option conserves the volume but the fluxes that arrive to the ocean are overestimated which can ultimately result in unrealistic oceanic evolution. In any case, I think it needs a bit more of description in the paper. Also, what is the routing strategy to transfer the ice loss to the ocean? Do you use the atmospheric model runoff model? In case of an ice sheet inception, do you have a negative flux at the surface of the ocean that increases the salinity? Is this spatially resolved?

A. In the current setup, we are conserving freshwater flux and not the freshwater volume. As the reviewer rightly points out, conserving the net volume instead would lead to huge fluxes into the ocean. However, as we are conserving flux, there is an underestimation of the net freshwater volume and thus could lead to unrealistic circulation changes. This meltwater flux from the ice model is dynamically routed based on PSUIM topography till it reaches the ocean or the domain edge, and then is routed to the nearest ocean grid point in LOVECLIM. During an inception, since the precipitation is used for building ice, the runoff from PSUIM into LOVECLIM is reduced, which in turn increases the salinity in the ocean. This salinity change is spatially resolved.

We have now added discussions regarding this in *Lines 263-273* in *Section 2.3*:

> The total meltwater from basal melting and liquid runoff in PSUIM is dynamically routed based on PSUIM topography till it reaches the ocean or the domain edge, and then is routed to the nearest ocean grid point in LOVECLIM. The calving flux is channeled into CLIO's iceberg model (Schloesser et al., 2019;Jongma et al., 2009) in the Southern Hemisphere (SH) and as an iceberg melt flux (freshwater flux and heat flux) in the NH (Schloesser et al., 2019). While both freshwater flux and freshwater volume cannot be simultaneously conserved in an accelerated run (Heinemann et al., 2014), we conserve freshwater flux in the current setup. The primary rational for this being that surface freshwater and meltwater fluxes are balanced by the convergence of ocean salt fluxes in equilibrium states, and adjustments of the ocean circulation are thought to occur rapidly compared to those of ice sheets. PSUIM is forced by LOVECLIM precipitation and LOVECLIM by PSUIM runoff. During a glacial inception (termination), the runoff from PSUIM into LOVECLIM reduces (increases) as ice sheets grow. This reduction (increase) in runoff into the ocean, relative to the evaporation, increases (decreases) the salinity of the ocean. This salinity change is spatially resolved.

Have you run a pre-industrial control run (for example a 10-kyr long simulation with the LGM bathymetry under pre-industrial orbital and GHG forcing)? Such simulation could be nice to validate your model setup, or at least to quantify the bias in the coupled model trajectory.

A. We ran a pre-industrial control run with constant forcings set at 1850 with LGM bathymetry. The figure is attached below for reference.

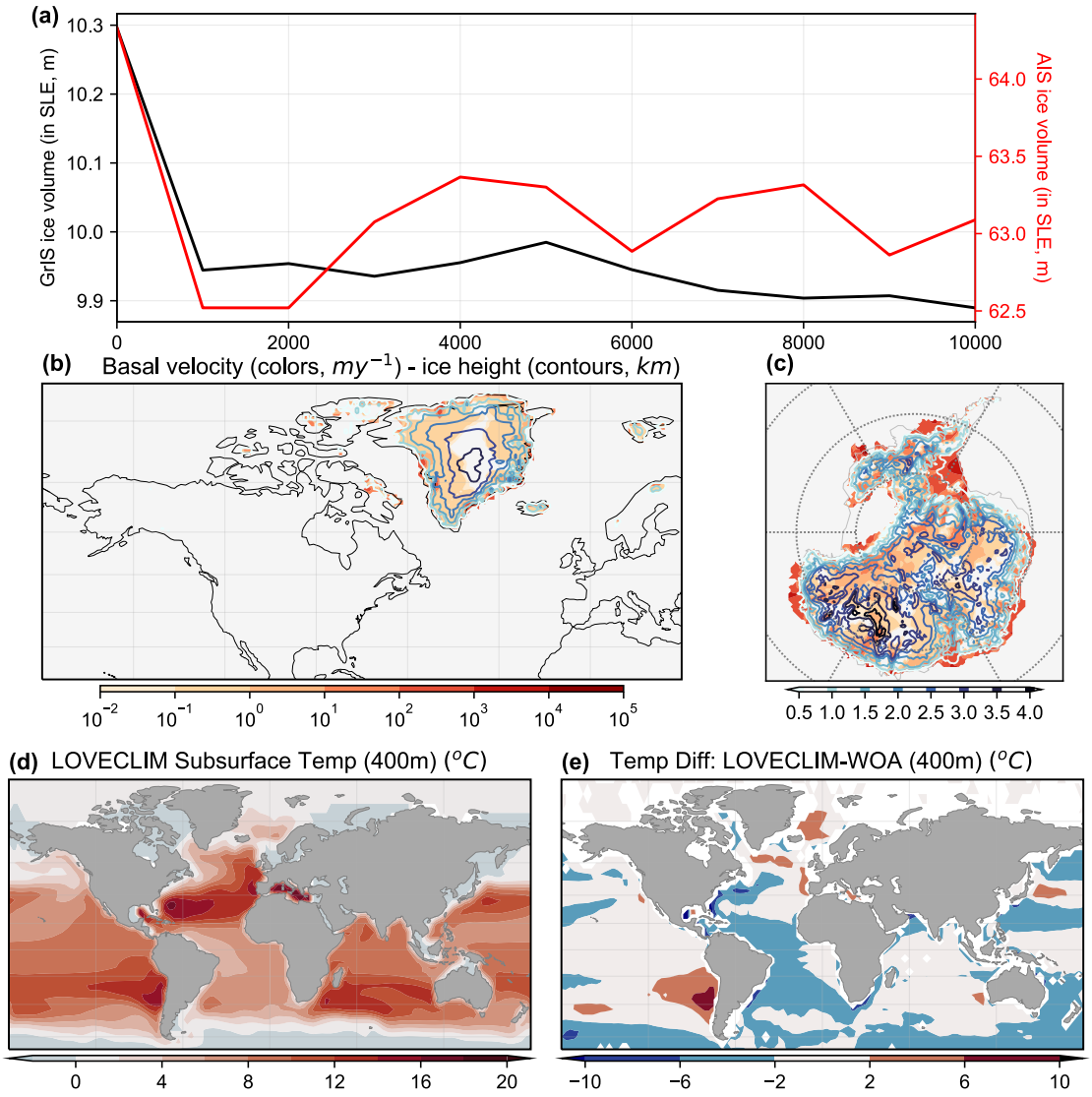

Figure R1: LOVECLIP simulation forced with constant 1850 forcing and LGM bathymetry. (a) Simulated ice volumes over Greenland (black) and Antarctica (red) in sea level equivalents (m). (b) Equilibrium basal ice velocity (solid colors, my^{-1}) and ice thickness (colored contours, km) for NH. (c) Same as (b) but for SH. (d) Equilibrium subsurface ocean temperature at 400m depth

simulated by LOVECLIM. (e) Subsurface ocean temperature difference between LOVECLIM and WOA (Locarnini et al., 2013) dataset.

We have clarified in the text now that the biases are based on present day simulations using an LGM bathymetry and that we do not find large-scale differences in the biases when running with present day bathymetry. This is addressed in *Lines 228-230* in *Section 2.3*:

> These LOVECLIM biases are calculated for PD simulations using an LGM bathymetry. We did compare the biases between using a PD or LGM bathymetry, and while there were regional differences, the large-scale structure was found to be similar (not shown).

By starting at 240 ka, you start towards the end of a deglaciation. Do you think that the long-term climate trajectory has an impact on your results? For example do you think that a restart from a full glacial state at 250 ka would result in a similar global ice volume evolution across MIS7?

A. We agree with the reviewer's comment that our simulated evolution could depend on the initial condition. To restart the model from 250ka with realistic ice volumes, we would need initial conditions at that time that comes from re-running the whole setup from the previous interglacial, MIS 9 (~320ka). If we get a realistic inception and the re-adjusted parameter set can simulate a termination into MIS 7e, then we expect to get a similar ice volume evolution across MIS 7. We fully acknowledge that our results are dependent on the parameter choices and are sensitive to the initial conditions. We have now addressed this in *Lines 543-545* in *Section 4*:

> The simulated ice sheet volume is well within the range of reconstructions for a rather narrow range of parameters. Small changes in parameter values can produce strongly diverging trajectories, and the emergence of multiple equilibrium states may also suggest the model's dependence on initial conditions.

You use a simple bias correction for surface temperature and precipitation. Why not use a similar technique for the radiative inputs of the ice sheet model and for the oceanic temperature as well?

A. Thank you for this suggestion. We agree that including additional bias corrections as suggested above might further improve the representation of ice sheets in our model, however, neither radiation nor ocean temperature bias correction is implemented in the model version used for this study. We have recently started experimenting with implementing ocean temperature bias correction, and found that this helps simulating a somewhat more realistic, present-day Antarctic ice sheet. The effects on Northern Hemisphere ice sheets appear to be relatively smaller, presumably because of smaller coastal ocean temperature biases (e.g., Fig. R1). We have included this in the discussion for future improvements in *Lines 561-569* in *Section 4*:

> Nevertheless, there is scope of further improving the current setup. For instance, we only implement temperature and precipitation bias corrections in the current setup, and including bias corrections for radiation and ocean temperature might improve our representation of ice sheets. Future research might further improve the current setup by including the advective precipitation downscaling scheme (Bahadory and Tarasov, 2018) to account for orographic forcing, which is not captured in LOVECLIM. We are also investigating the possibilities of using a dynamical, an altitude-dependent and a CO_2-dependent lapse rate corrections while downscaling temperature from LOVECLIM to PSUIM. This is because the atmospheric lapse rate depends on the atmospheric CO_2 concentration – an effect that has not been considered so far in glacial dynamics. Furthermore, improving our basal sliding coefficient map for the NH using information of sediment sizes, instead of simply using a binary coefficient map, has the potential of further improving the simulations.

The hydrofracturing and cliff collapse parametrisation embedded in PSUISM is controversial (e.g. Edwards et al., 2019). Do you think that you would end up with different ice volume trajectories using a model that does not account for the MICI?

A. The contributions from hydrofracturing and cliff instabilities were negligible in our simulations and hence were not presented in the mass balance figure. Just to be sure, we repeated our analysis with hydrofracturing and cliff melt inactive in PSUIM and found no change in our ice evolutions. This is mentioned in *Lines 320-322* in *Section 3.1*:

Following the concerns raised in Edwards et al. (2019), we ran a BLS simulation with hydrofracturing and cliff instability inactive and found no differences in the ice evolutions. This finding illustrates the complexity of the task to better constrain associated parameters in comparison of paleo climate simulations and data.

We also added discussions on the implication of these parameterizations for future studies in *Lines 546-551* in *Section 4*:

In this context, we note that parameterizations associated with hydrofracturing and cliff instability did not impact our ice sheet trajectories. These processes have provided substantial contributions to the rapid Antarctic ice sheet retreat simulated in response to future climate projections (DeConto and Pollard, 2016), and better constraining these parameterizations is important to reduce uncertainties related to future sea level trajectories (e.g., Edwards et al., 2019). Presumably, these processes did not play an important role in our present simulations, because the climate is generally too cold, suggesting that opportunities for constraining these parameters in glacial simulations may be limited.

2- Results:

From my understanding of your model results, the respective role of orbital configuration with respect to CO2 is pretty much linked to the choice of the alpha / m combination. From Fig. 3 it seems that you cannot guarantee the uniqueness of your calibrated alpha / m (higher m but lower alpha might works equally well than lower m and higher alpha). As a result how robust is your conclusion on the respective role of orbital versus CO2?

A. Although we agree that results presented here could be influenced by parameter values, we believe our results to be robust over this time period. While Figure 3 showed only a handful of ensembles that best explain the effects of the *'α'* and *'m'* parameters, the Fig. S3 (underneath) shows the whole ensemble of simulations considered in the study. These ensembles correspond to different values of *'α'*, *'m'*, acceleration factor, $N_A = T_P/T_L$ (PSUIM chunk length corresponding to LOVECLIM chunk length), and the maps of sliding coefficient *'C'*, in Eq. (6) and Eq. (7):

$$\widetilde{u_b} = C'|\tau_b|^{\mu-1}\widetilde{\tau_b}\ , \qquad (6)$$

where $\widetilde{u_b}$ is the basal sliding velocity, $\widetilde{\tau_b}$ is the basal stress; μ is the basal sliding exponent (=2); C' is the basal sliding coefficient which is a function of the basal homologous temperature:

$$C' = (1-r)C_{froz} + rC(x,y)\ , \qquad (7)$$

with $r = max\left[0, min[1, (T_b+3)/3]\right]$; where T_b(°C) is the basal homologous temperature relative to the pressure melting point ($T_m = -0.000866h$, h being the ice thickness in m); and $C_{froz} = 10^{-20}$m yr^{-1}Pa^{-2} (which cannot be zero to avoid numerical inconsistencies but is small enough to allow essentially no sliding).

We tried different combinations of all the parameter sets and have updated Table 1 to show all the ensemble runs performed in this study. While we performed a total of 50 separate experiments, we reported only 15 of them in Figure 3 that best describe the parameter sensitivities. We have now clarified this in in *Lines 293-300* in *Section 2.4:*

Furthermore, sensitivity experiments with different GHG sensitivities (α, Sect. 2.1) and melt parameterizations (m, Sect. 2.2) are run with full forcing. Generally, higher α leads to a stronger sensitivity to CO_2 concentrations, and higher values of m strengthen buildup and weaken melting of ice during interglacial climates. These experiments are presented in the first row of Table 1 (1-15) and Fig. 3. Additional simulations with different combinations of acceleration (N_A), GHG sensitivity (α), melt parameter (m), basal sliding coefficient maps over the NH ($C(x,y)$) and higher ice model resolution ($0.5 \times 0.25°$ for NH, 20×20 km polar stereographic for Antarctica) have been performed (experiments 16-50 in Table 1). The whole ensemble of simulations is presented in Fig. S3. Although we note that these experiments do not present a systematic evaluation of the full parameter space, ice sheet trajectories are consistent with and thereby support the conclusions presented in this paper.

The updated *Table 1* is as below:

Expt Number	Orb Forced	GHG Forced	N_A	α	m (Wm^{-2})	C (myr^{-1}Pa^{-2})-NH
1 **(BLS)**	**Y**	**Y**	**5**	**2**	**125**	Binary distribution
2	**N**	**N**	5	2	125	
3	Y	**N**	5	2	125	**1.**Ocean:

4	**N**	Y	5	2	125	$C(x,y)$=10^{-6}; representing deformable sediments **2.**Land: $C(x,y)$=10^{-10}; representing non-deformable rock.
5	Y	Y	5	2	125	
6	Y	Y	5	**1.8**	125	
7	Y	Y	5	**2.2**	125	
8	Y	Y	5	**2.5**	125	
9	Y	Y	5	**3**	125	
10	Y	Y	5	2	**80**	
11	Y	Y	5	2	**100**	
12	Y	Y	5	2	**120**	
13	Y	Y	5	2	**130**	
14	Y	Y	5	2	**140**	
15	Y	Y	5	2	**150**	
16-20	*Y*	*Y*	*5*	***1.5***	***120,125,130,140,150***	*Binary*
21-24	*Y*	*Y*	*5*	***3.5***	***80,100,120,125***	
25-27	*Y*	*Y*	***1 (30ky run)***	*2*	***110,120,130***	
28-30	*Y*	*Y*	***2 (30ky run)***	*2*	***110,120,130***	
31-33	*Y*	*Y*	***10***	*2*	***110,130,150***	
34-36	*Y*	*Y*	***10***	***2.5***	***110,120,130***	
37-38	*Y*	*Y*	***20***	***2.5, 3***	*125*	
39-41	*Y*	*Y*	*5*	*2*	*125*	*Tertiary* ***1.***Ocean: $C(x,y)$=10^{-6}; ***2.1*** Land (soft tills): $C(x,y)$=$\mathbf{10^{-7},10^{-8},10^{-9}}$ *over northeastern North America* ***2.2*** Land (hard bed): $C(x,y)$=10^{-10}
42-44	*Y*	*Y*	*5*	*2*	***150***	
45-47	*Y*	*Y*	*5*	***2.5***	*125*	
High Resolution Runs: 0.5 × 0.25° *for NH*, 20 × 20 km *polar stereographic for Antarctica*						
48-50	*Y*	*Y*	*5*	*2*	***110,130,150***	*Binary*

Table 1: List of all ensemble runs performed for the study study (shown in Fig. S3). The first 15 experiments are discussed in Sect. 3.1 and shown in Fig. 3. Values in bold represent the difference from the baseline simulation (BLS, experiment number 1). N_A represents the PSUIM vs LOVECLIM acceleration factor (Sect 2.3). α represents the GHG sensitivity scaling factor (Eq. 1, Sect. 2.1) and m represents the constant parameter in the surface energy balance equation (Eq. 3, Sect. 2.2). C represents the basal sliding coefficient map used for the NH (Eq. 7, Sect. 2.2).

The whole ensemble of experiments is shown under in Fig. S3 (in supplementary):

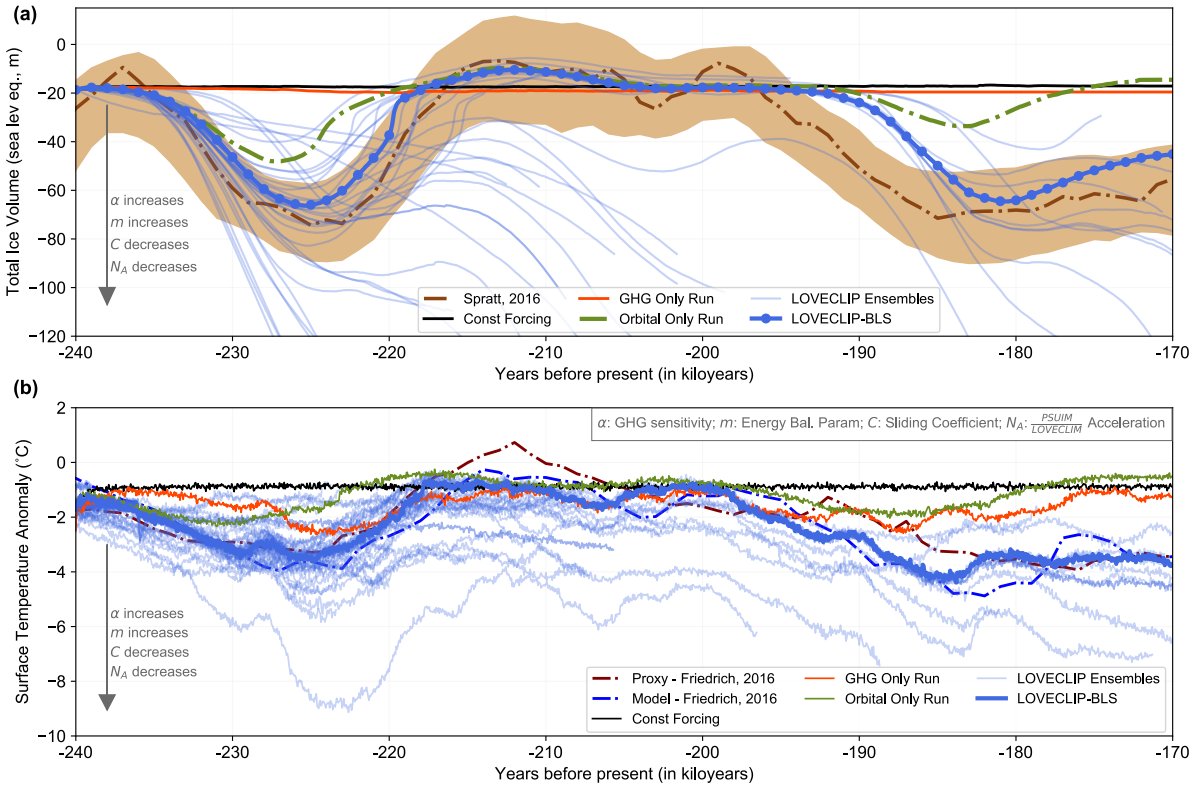

Figure S3: Transient LOVECLIP ensemble simulations over MIS7 with varying GHG sensitivities (α = 1.5-3.5), energy balance parameter (m = 80-150Wm^{-2}), basal sliding coefficient (C = 10^{-6}-10^{-8} myr^{-1}Pa^{-2}) and PSUIM-vs-LOVECLIM acceleration factor (N_A = 1,2,5,10,20). The best results are obtained for α=2, m=125 Wm^{-2}, binary sliding map (ocean: C=10^{-6} myr^{-1}Pa^{-2} and land: C=10^{-8} myr^{-1}Pa^{-2}) and N_A=5 (experiment 1 in Table 1, BLS).

Although we could get the model to glaciate from MIS 7e to MIS 7d for a low *'α'* and high 'm', the model does not terminate from the glaciation of MIS 7d.

Further, to verify our result that glacial inceptions are driven primarily by orbital forcings, we performed orbital-only simulations with CO_2 values of 180,200,220,240,260 and 280 ppmv in Fig. R2. These runs are similar to the blue line in Figure 5 (and the green line in Fig. S3 above), but with different background CO_2 values instead of keeping CO_2 constant at 240ka values (~245 ppmv). The results suggest that we can get a glacial inception over MIS 7e-7d, even for a high CO_2 value of 280 ppmv. Thus, we think our conclusion of glacial inceptions being primarily driven by orbital forcings is robust over this period.

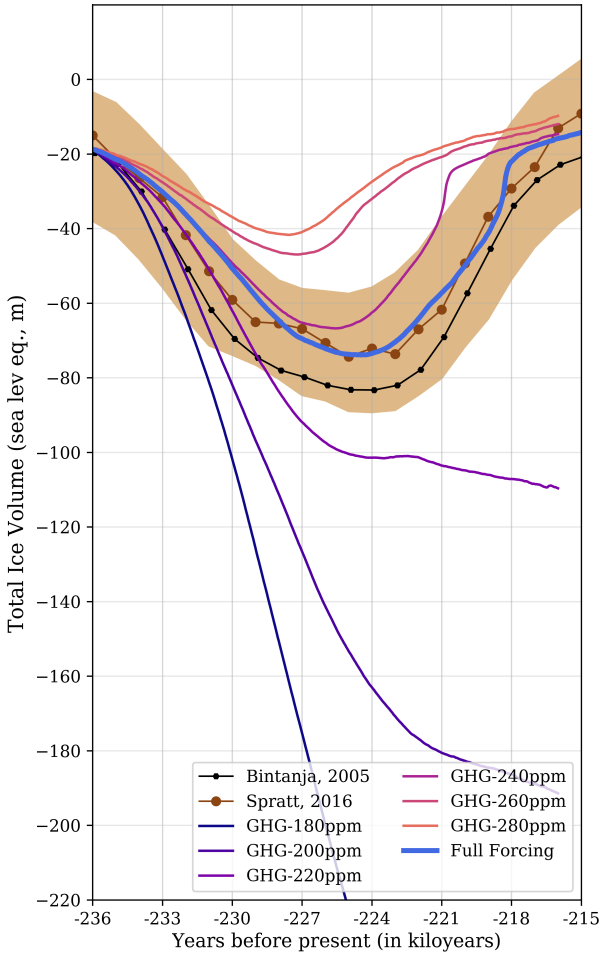

Figure R2: LOVECLIP simulations forced with transient orbital forcings, but constant background CO_2 values. All experiments are conducted with an α value of 2 and *m* of 125 Wm^{-2}.

You justify the use of the alpha parameter to correct for the lack of sensitivity of the climate model. There are alternative way to modify the climate sensitivity in the model. For example Loutre et al. (2011) modify a set of model parameters in order to have a similar pre-industrial climate but different sensitivity to the change in CO2. With your approach you might give too much importance to the radiative effect of CO2.

A. We agree that climate sensitivity could depend on responses to many different forcings. Here, we use a simple alpha parameter to change only the longwave sensitivity to CO_2, and not to other greenhouse gases. We have acknowledged this in *Lines 122-134* in *Section 2.1*:

> The effect of CO_2 variations with respect to the reference CO_2 concentration (356 ppm) on the longwave radiation flux is scaled up by a factor α (Eq. 1), to account for the low default sensitivity of ECBilt to changes in CO_2 concentrations (Friedrich and Timmermann, 2020;Timmermann and Friedrich, 2016;Timm et al., 2010). The effect of CO_2 on the longwave radiation is given as:
>
> $$LWR = \alpha . a(\lambda, \phi, p, t_{season}) . \log\left[\frac{CO_2(t)}{CO_2^{ref}}\right] \quad (1)$$
>
> where LWR is the longwave radiation flux from CO_2; α is our scaling factor for the transfer coefficient, a, which is a function of longitude, latitude, height and season; CO_2^{ref} is the reference CO_2 value set at 356 ppm. α changes the sensitivity of our model. For reference, the equilibrium climate sensitivity for CO_2 doubling is 3.69K for α of 2. Climate sensitivity is a non-trivial measure that can be changed in many different ways. For instance, changing the cloud parameterization or surface parameters would change both the longwave and shortwave forcings. Adjusting multiple parameters may not necessarily lead to more realistic simulations. While it is possible that the climate sensitivity to some of the other forcings are also weak (Timm and Timmermann, 2007), we use a simple alpha (α) parameter to change only

the longwave sensitivity to CO_2, and not to other greenhouse gases. α is determined based on transient past and future simulations.

The Eurasian ice sheet in your simulation does not grow at all which seems in contra- diction with palaeo data (e.g. Batchelor et al., 2019). Even in the run-away glaciation presented in Fig. S6, it seems that there is only very little ice developing in Eurasia. I know that it is not trivial to simulate satisfactorily the Eurasian ice sheet inception, particularly the Kara-Barents sector. Do you have any idea on how to improve on this? Do you think that it is an oceanic problem, e.g. too warm waters in the Kara and Barents seas? Or an atmospheric problem, e.g. shift in storm tracks?

A. We think this to be primarily an atmospheric problem because of the coarse T21 resolution and 3-layered atmosphere of LOVECLIM; and the best way to improve on this would be to use a model with more realistic atmosphere. We have now added more discussions on our ice sheet distribution in *Lines 344-376* in *Section 3.2*:

In the context of previous modelling studies and geological records over this MIS 7-6 period, our ice sheet distribution at MIS 7c (212ka, Fig. 4g and 219.5ka, Fig. S7) is very similar to that reported in Colleoni and Liakka (2020). However, we simulate a stronger inception compared to that of Colleoni et al. (2014) over the corresponding 236-230ka period. They also reported a bifurcated but connected North American ice sheet at MIS 6 (157ka) from both their control (100km) and high resolution (40km) experiments. Our simulation results in separate Laurentide and Cordilleran ice sheets but generates neither a Eurasian nor a Siberian ice sheet, albeit at 170ka. On a side note, our North American ice sheet distribution at 180ka (Fig. 7) is closer to that of Colleoni and Liakka (2020) at 157ka. Studies of NH reconstructions during MIS 6 such as Svendsen et al. (2004), over 160-140ka, Rohling et al. (2017), around 140ka, and Batchelor et al. (2019), over 190-132ka, have all reported glacial geological records to indicate a larger extent of the Eurasian ice sheet at MIS 6 glacial maximum compared to the LGM, while our simulations only show a persistent Fenno-Scandian ice sheet and a relatively small Eurasian ice sheet at 170ka. More recently, Zhang et al. (2020) reported the existence of a Northeast Siberia-Beringian ice sheet at MIS 6e (190-180ka) using NorESM-PISM simulations validated by North Pacific geological records. However, our model does not simulate any ice over Alaska, Beringia and northeast Siberia over MIS 7-6.

Our model's difficulty in simulating the Eurasian ice sheet can be attributed to the competition between Laurentide and Eurasian ice sheet growth, which makes it arduous to realistically simulate them simultaneously alongside generating the right atmospheric patterns. Some previous studies have suggested that teleconnections from stationary wave patterns induced by a large Laurentide ice sheet could lead to warming over Europe and influence Eurasian ice sheet evolution (Roe and Lindzen, 2001;Ullman et al., 2014). The Laurentide building up first in our simulations could have changed the storm tracks and dried out Eurasia. It is also worth reiterating that LOVECLIM has a coarse T21 grid with a simple 3-layered atmosphere. While the circulation changes reported here maybe model dependent, Lofverstrom and Liakka (2018) reported that at least a T42 grid was needed in their atmospheric model (CAM3) to generate a Eurasian ice sheet using SICOPOLIS, albeit for the LGM. They attribute this discrepancy to lapse rate induced warming due to reduced and smoother topography and higher cloudiness leading to increased re-emitted longwave radiation towards the surface. These teleconnection patterns are further discussed in Sect. 3.6. Our LOVECLIM setup also uses a fixed lapse rate for downscaling LOVECLIM surface temperatures (Eq. 10 and 11), while both Roche et al. (2014) and Bahadory and Tarasov (2018) used a dynamic lapse rate, which is estimated locally for the ice model grids in each LOVECLIM grid. Bahadory and Tarasov (2018) reported ice thickness differences up to 1km on using the dynamic lapse rate scheme compared to a fixed 6.5˚Ckm^{-1}. Nevertheless, for runaway trajectories, our model can build up a Eurasian ice sheet for ice volumes greater than -200m SLE once the Laurentide growth slows down (not shown). Our modelling setup also does not account for sub-grid mass balances, which can be especially relevant over mountainous regions with large sub-grid relief such as Alaska (Le Morzadec et al., 2015). Coarse grids tend to average out tall peaks and low valleys and thus don't capture the non-linear combination of accumulation zones on the high peaks and ablation zones in the valleys. These shortcomings could explain the lack of Eurasian, Siberian and Beringian ice sheets in our simulations.

And acknowledged this in the discussion in *Lines 556-558* in *Section 4*:

Our present setup has difficulties in realistically simulating both Laurentide and Eurasian ice sheets simultaneously and generates a smaller Eurasian ice sheet compared to reconstructions, which could be a model dependent feature of

LOVECLIM, given it is a T21 grid with only three levels in the atmosphere, and so could vary with the choice of the climate model used.

While the runaway simulation in Fig. S6 (Fig. S9 in the revised version) shows a very small Eurasian ice sheet, our Eurasian ice sheet grows once Laurentide growth slows down for ice volumes > 200m SLE (Fig. R3). This suggests that the relatively small Eurasian may not result from large biases in the Barents-Kara sector (also see subsurface temperature biases in Fig. R1 above), but from the timing of Laurentide and Eurasian growth alongside changes in atmospheric patterns.

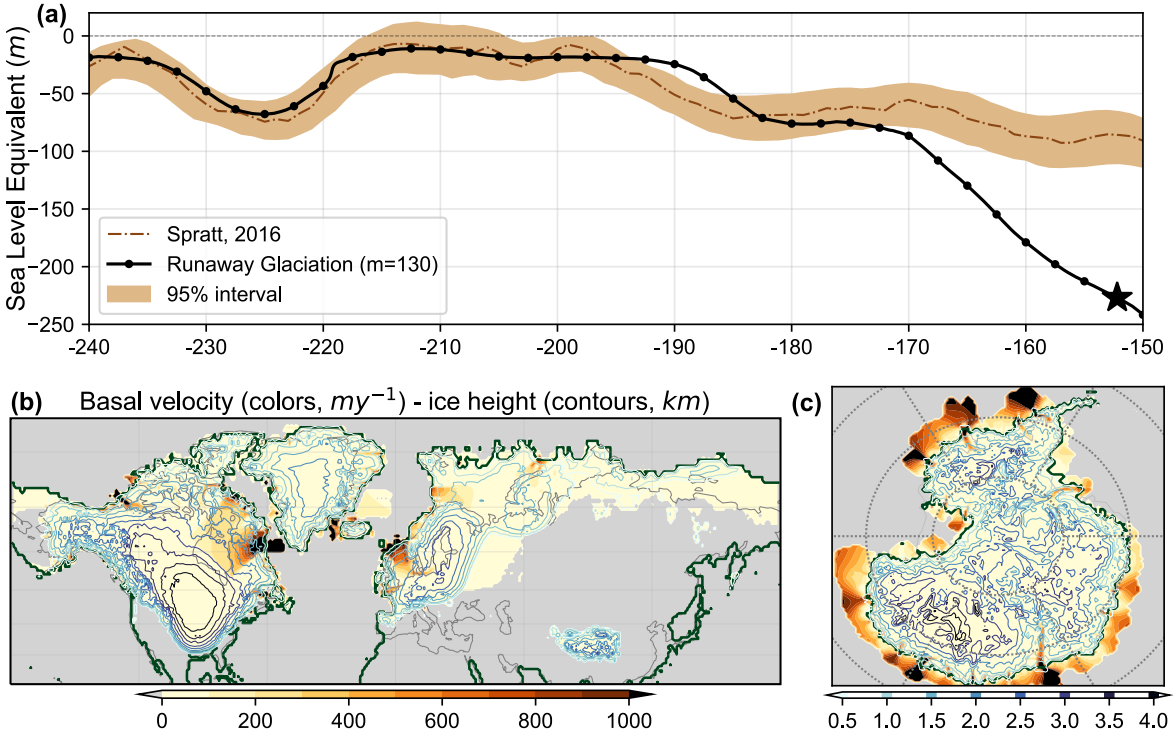

Figure R3: Transient LOVECLIP simulation with α=2 and m=130 Wm^{-2} (runaway simulation). (a) Sea level reconstruction (m) and 95% confidence interval of Spratt and Lisiecki (2016) (brown). Total ice volume from LOVECLIP run in black (SLE, m). The star shows ice volume at 152ka corresponding to 225m. (b) Basal ice velocity (solid colors, my^{-1}); ice thickness (colored contours, km) and the grounding line (solid green lines) for the Northern Hemisphere at 152ka. (c) Same as (b) but for Southern Hemisphere.

For the two step inception (Sec. 3.4), you claim that CO2 explains the later full inception. If the insolation signal is indeed similar for both periods, it shows nonetheless a greater amplitude in MIS 7e-7d-7c with respect to MIS 7a-6e-6d. The insolation maxima is thus slightly smaller for the later period. This slight difference in the insolation maxima could explain the ice retreat in the older inception, with the full glaciation being the result of an insolation threshold? Of course CO2 should help but it is hard to distinguish the role of the two forcings (especially also because the results depend on the value of the chosen alpha parameter).

A. We agree with the reviewer that the insolation maximum is indeed smaller for the later period (Figure 6a). But we believe CO_2 to drive the later inception because our orbital only run shows a much weaker inception and subsequent termination over MIS 7a-6e-6d compared to MIS 7e-7d-7c in Figure 5. We have now clarified this in *Lines 408-415* in *Section 3.4*:

In spite of orbital forcing being similar over the second half of the composite figure, model trajectories diverge markedly. The successful glacial termination coincides with increasing CO_2 concentrations (dashed line), whereas the aborted termination during MIS 6e-6d (180-170ka, solid line) is associated with flat-lined glacial CO_2 values (Fig. 6a-6c). Although the insolation maximum is weaker for the later period (MIS 7a-6e-6d) compared to the earlier period (MIS 7e-7d-7c), we argue the full inception of the later period to be primarily driven by changes in CO_2. This is further supported by the orbital-only run showing a substantially weaker inception and subsequent termination over MIS 7a-6e-6d compared to MIS 7e-7d-7c (Figure 5), suggesting that the latter full inception could not be attributed only to an insolation threshold.

I wonder how robust are the atmospheric circulation changes discussed in Sec. 3.6. For example, don't you think that the atmospheric circulation might be potentially largely affected by the presence of an ice sheet in Eurasia?

A. A high pressure cold anticyclonic pattern over ice sheets such as the Laurentide has previously been reported and was shown to be robust by Roe and Lindzen (2001). They suggest a balance between precipitation maxima alongside increased melting over the south western edges from warmer winds upslope and reduced precipitation over the rest of the ice sheet due to cold northerly winds can lead to either an equilibrium ice sheet configuration or runaways in either directions. However, it goes without saying that such patterns and runaways could change when using more realistic atmospheric models. While the presence of a Eurasian ice sheet would definitely affect the atmospheric circulation, we believe the Laurentide developing rapidly in our simulation changes the atmospheric circulation causing some warming over Europe and changed storm tracks that prevent the growth of a Eurasian ice sheet. As mentioned in the response to a previous question, our model simulates a Eurasian ice sheet only when the Laurentide growth slows down. While the circulation changes reported here maybe model dependent, Lofverstrom and Liakka (2018) reported that at least a T42 grid was needed in their atmospheric model (CAM3) to generate a Eurasian ice sheet using SICOPOLIS, albeit for the LGM. We have now mentioned this in *Lines 488-493* in *Section 3.6*:

> Roe and Lindzen (2001) suggested that the topography of an ice sheet such as the Laurentide induces a high-pressure anticyclonic circulation over the western end of the ice sheet. The associated cooling and upslope flow lead to enhanced rainfall over the western and southwestern ends of Laurentide. However, the prevailing cold northerlies downslope cause a reduction in rainfall over the ice sheet. This interplay between cooling associated with anticyclonic circulations alongside enhanced rainfall over western Laurentide and the reduction in rainfall over most of the ice sheet due to cold northerlies, can lead to an equilibrium ice sheet configuration or ice sheet growth/decay.

and in *Lines 516-522* in *Section 3.6*:

> While these stationary wave feedbacks are similar to the ones described by Roe and Lindzen (2001) and they suggested these patterns to be robust for a range of parameters, it is possible that such circulation patterns could change when using a more realistic atmospheric model or by the presence of a Eurasian ice sheet. The atmospheric patterns strengthen over the next 10ky and the runaway run simulates ~30m SLE greater ice volume than the stable run (Fig. S9). The difference between the two runs at 180ka and 170ka are presented in Fig. S10. As mentioned earlier in Sect. 3.2, it is important to acknowledge the low horizontal and vertical resolutions of LOVECLIM's atmosphere, which could mean the circulation changes reported here to be model dependent.

3- Miscellaneous:
l64-78 You could refer to your figure 1 somewhere around here to facilitate the reading.

A. Done.

towards l194 and Fig. S1 From my understanding of your methods your reference climate model uses a last glacial maximum bathymetry (since bathymetry is fixed to a LGM value). Would it have been appropriate to compute the bias for the modern climate using a LGM bathymetry? More generally it would be very interesting to see the effect of the sole bathymetry on the simulated climate (under PI forcing for example).

A. Yes, LOVECLIM biases are calculated for LGM bathymetry. We agree that the impact of bathymetry on climate is interesting and important. With regard to the bias correction, we did assess the impact of using bias corrections calculated for LGM vs PI bathymetry (though not for the simulations presented in this manuscript). The figure below shows temperature and precipitation bias corrections calculated for the different bathymetries, and while there are regional differences, the large-scale structure is (surprisingly) similar. While there are other issues related to the bias correction (for example, it is not obvious that the bias should be the same under LGM and PI boundary conditions), we believe that choosing LGM vs PI bathymetry does not substantially alter the results.

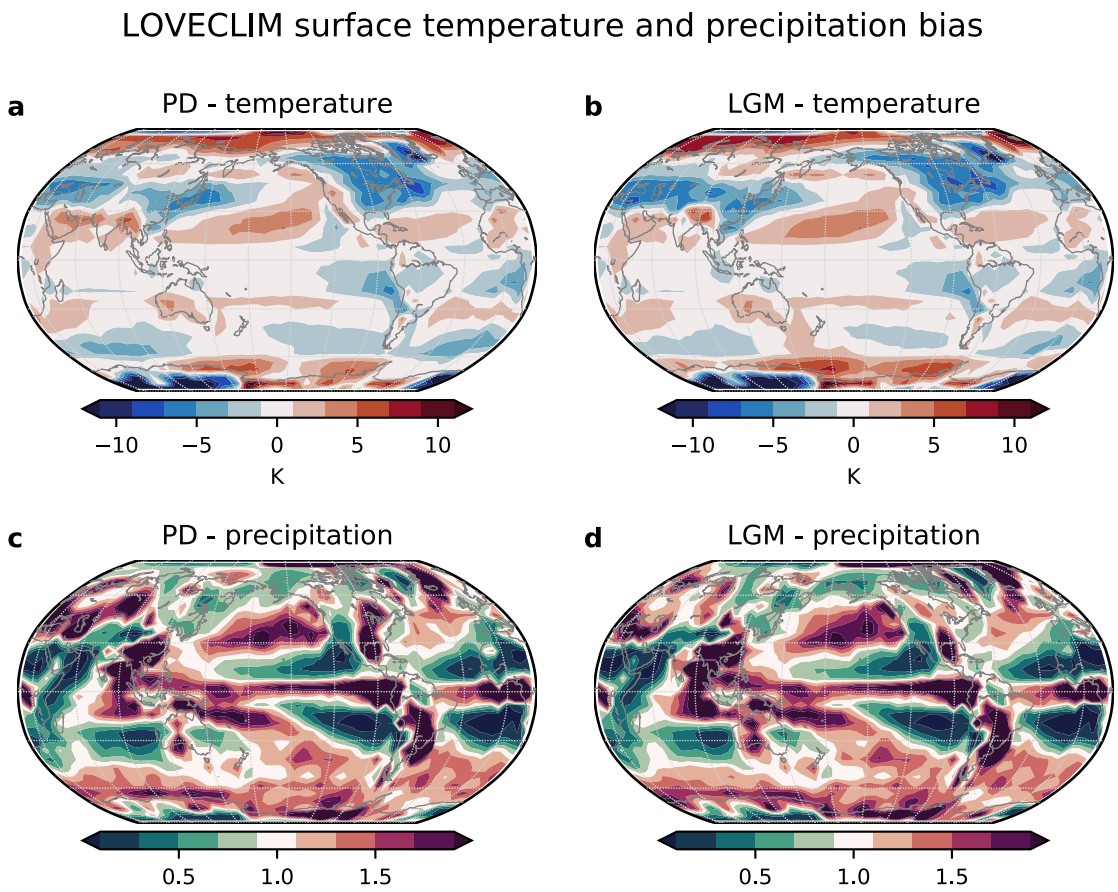

Figure R4: LOVECLIM biases for present-day simulations for temperature (a) and (b); and precipitation (c) and (d). (a) and (c) use PD bathymetry, while (b) and (d) use LGM bathymetry.

We have now clarified this in *Lines 219-233* in *Section 2.3*:

PSUIM uses surface air temperature (T), precipitation (P), solar radiation (Q), and ocean temperature at 400m depth (T_o) as inputs from LOVECLIM. These are downscaled using a bilinear interpolation approach. The surface temperature and precipitation outputs from LOVECLIM which are used for the PSUIM surface mass balance are bias-corrected in the coupler, following Pollard and DeConto (2012), Heinemann et al. (2014) and Tigchelaar et al. (2018).

$$T(t) = T_{LC}(t) + T_{obs} - T_{LC,PD} \quad (8)$$

$$P(t) = P_{LC}(t) \times P_{obs}/P_{LC,PD} \quad (9)$$

where T is monthly surface air temperature and P is monthly precipitation forcing from LOVECLIM at timestep t. Subscripts 'LC', 'obs' and 'LC,PD' refer to LOVECLIM chunk output, observed present day climatology, and LOVECLIM present day control run, respectively. The observed present day climatology is obtained from the European Centre for Medium-Range Weather Forecasts reanalysis dataset, ERA-40 (Uppala et al., 2005). These LOVECLIM biases are calculated for PD simulations using an LGM bathymetry. We did compare the biases between using a PD or LGM bathymetry, and while there were regional differences, the large-scale structure was found to be similar (not shown). The annual mean of the monthly mean bias correction terms $T_{obs} - T_{LC,PD}$ and $P_{obs}/P_{LC,PD}$ are presented in Fig. S1. Temperature biases in LOVECLIM for boreal summer (JJA) and austral summer (DJF) are shown in Fig. S2 for reference, since summer temperatures are more crucial for ice sheet growth and decay.

l252 The Filchner-Ronne ice shelf is advancing but there is almost no change for the Ross ice shelf. Any idea why?

A. While our simulation does not show much variations in Antarctica, the small changes over the Filchner-Ronne shelf unlike the Ross ice shelf might be because of small differences in subsurface ocean temperature. The present study focusses more on the mechanisms underlying the response of the Northern Hemisphere ice sheets, and hence we have not performed a

detailed analysis of the processes underlying the regional response of the Antarctic ice sheets and shelves. We do agree, however, that this is an interesting and important issue, that will be further explored in future studies.

l306-312 You show in the figure the mean SMB/ablation/accumulation over the ice sheet. In doing the spatial average, we can end up with very similar values for very different ice sheet extent. In addition, we cannot quantify the importance of the different processes to explain the total mass change (for example the sub-shelf melt is much more negative than SMB but it may concern only a very small fraction of the ice sheet). Instead, it could be interesting to have the integrated value over the ice sheet but not divided by the extent (Gt or km3 per year), to have a better idea of the respective role of SMB and sub-shelf melting to explain the total ice volume change.

A. We have now updated Figure 6 to show integrated values of the mass balance terms:

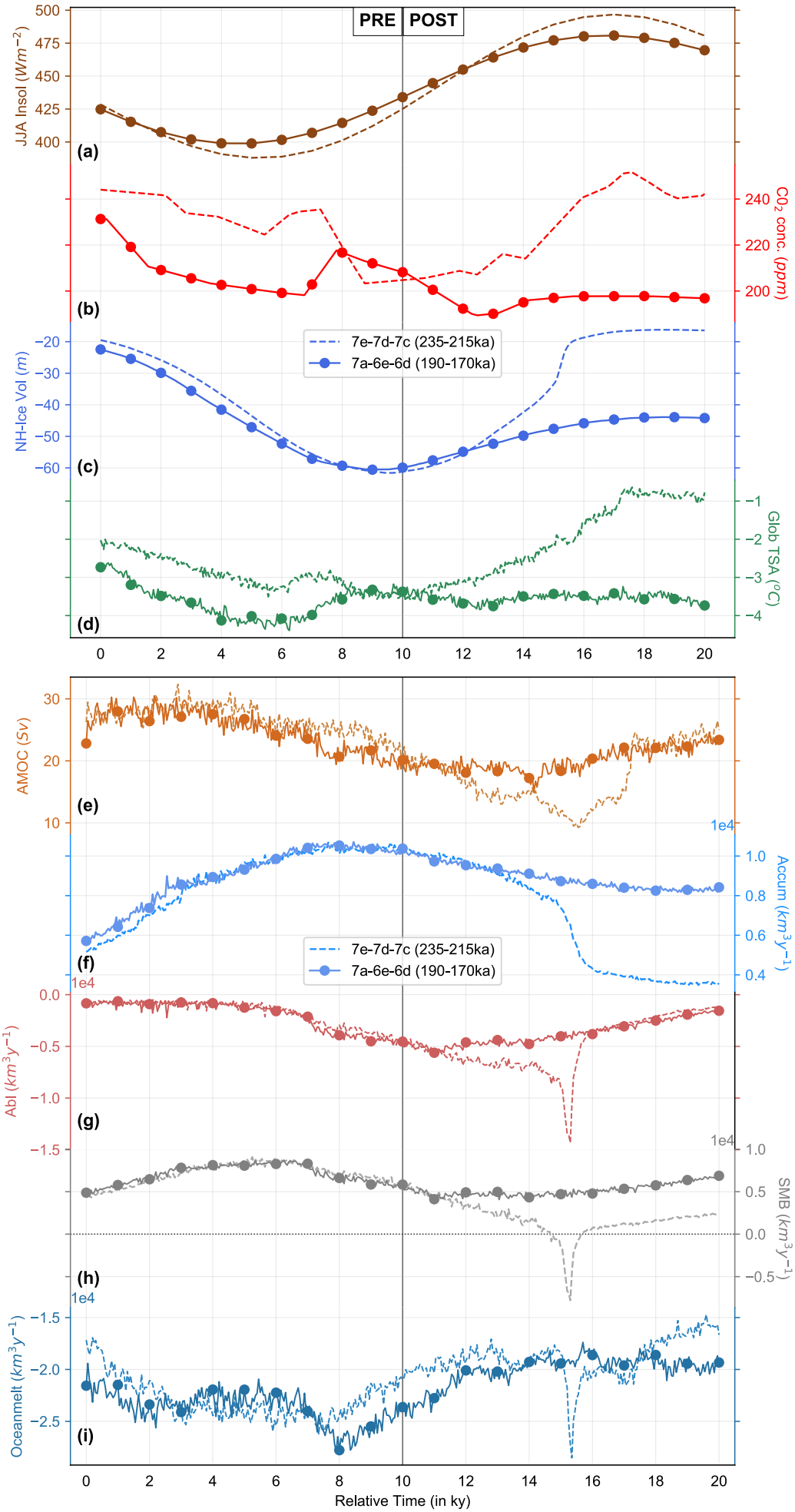
PRE
POST
JJA Insol (Wm^{-2})
(a)
CO_2 conc. (ppm)
(b)
7e-7d-7c (235-215ka)
7a-6e-6d (190-170ka)
NH-Ice Vol (m)
(c)
Glob TSA (^oC)
(d)
AMOC (Sv)
(e)
Accum (km^3y^{-1})
(f)
Abl (km^3y^{-1})
(g)
SMB (km^3y^{-1})
(h)
Oceanmelt (km^3y^{-1})
(i)
1e4
Relative Time (in ky)

Figure 6: Comparison between two glacial inception scenarios. Different variables over two 20k year periods (relative time) during pre-inception (left half) and post inception (right half) over the Northern Hemisphere are plotted. Variables from the earlier period (235-215ka) are plotted in dashed lines while that of the later period (190-170ka) are plotted in circled solid lines. (a) JJA mean insolation at 65°N (Wm^{-2}, *(Laskar et al., 2004)*). (b) CO_2 concentration (ppm, *(Lüthi et al., 2008)*). (c) Simulated Northern Hemisphere ice volume, in sea level equivalents (m). (d) Global average surface temperature anomaly (°C). (e) Temporal evolution of AMOC (Sv). (f) Net integrated accumulation rate over Northern Hemisphere ice (km^3y^{-1}). (g) Net integrated surface melt rate over Northern Hemisphere ice (km^3y^{-1}). (h) Net integrated surface mass balance over the Northern Hemisphere ice (km^3y^{-1}). (i) Net integrated subshelf melt rate over Northern Hemisphere (km^3y^{-1}).

l319-322 The spike in SMB is very impressive but I am even more surprised by the spike in shelf melting. I think it could be useful to show maps of surface mass balance and sub-shelf melting for temporal snapshots in the vicinity of this event (circa 210 ka?). In doing so, it will illustrate the saddle-collapse as well as the spike in sub- shelf melt. Again, maybe the spike in sub-shelf melt is affecting a tiny area and is not representative of the total mass loss (previous comment)?

A. The spike in subshelf melting could result from higher subsurface warming following a weakening of AMOC as reported in Liu et al. (2009) and Clark et al. (2020). We have also included a new supplementary figure, Fig. S6, showing maps of SMB and sub-shelf melting around the spikes shown in Figure 6h and 6i.

We have added the AMOC effect on subshelf melting in *Lines 418-422* in *Section 3.4*:

> For both periods the Atlantic Meridional Overturning Circulation (AMOC) is strongest during the inception phase, and weaker during termination (Fig. 6e). The AMOC weakening is substantially more pronounced in the earlier period, following the successful termination. In both periods, the AMOC recovers almost to its full interglacial state. The reduced AMOC (Fig. 6e) could lead to increased subsurface warming (Liu et al., 2009;Clark et al., 2020) causing the higher subsurface melting in Fig. 6i.

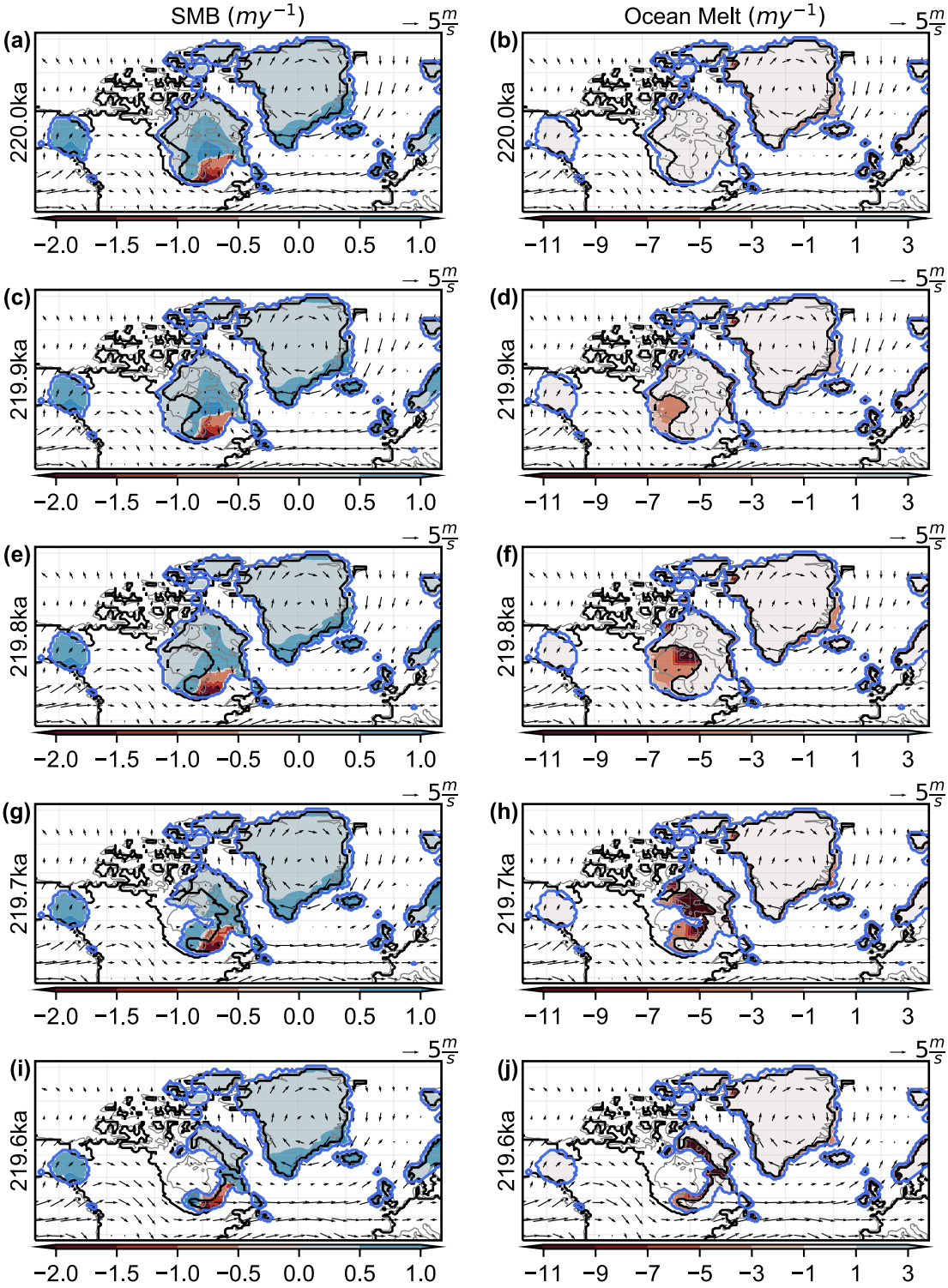

Figure S6: Temporal snapshots around the spikes in SMB and Ocean melt of Figure 6h and 6i (~15ky relative time of the dashed lines, corresponds to ~ 220ka in real time). Simulated surface mass balance (left column) and subshelf melt (right column) values at (a,b) 220ka, (c,d) 219.9ka, (e,f) 219.8ka, (g,h) 219.7ka and (I,j) 219.6ka. The blue lines mark the boundaries of the ice sheets and the black lines show the grounding line.

We have added discussions on the figure in the text in *Lines 462-469* in *Section 3.5*:

> Temporal snapshots every 0.1ky in the vicinity of the spikes in ablation (Fig. 6g), SMB (Fig. 6h) and ocean melting (Fig. 6i) are shown in Figure S6. It shows that the spikes in ablation and SMB predominantly come from a small area in the southern end of the Laurentide, while the spike in subshelf melting results only from the western part of the Laurentide with a receding grounding line. Although our model simulates sub shelf melting along the western Hudson Bay, we did not find any geologic evidence of such subsurface melting around 219.5ka. It is also worth mentioning that our setup does not simulate forebulges or other specific mechanisms modelled by more comprehensive full-Earth models. But Tigchelaar et

al. (2018) have reported such changes in mass balance arising due to changing of ice sheets to ice shelves near the grounding line.

l345-346 Do you know the reason for this? It would be nice to understand this circulation change (which produce the spike in sub-shelf melt?). It happens during the deglaciation and thus, in the meantime, you probably have a lot of freshwater flux that is discharged to the ocean. Does the two processes (increase in sub-shelf melt and freshwater flux) are related in some way? If yes, how realistic are your freshwater fluxes (see previous comment on the acceleration factor).

A. We think the spike in subsurface melt to result from relatively warm ocean waters seeping in through the gap in the grounding line on the western end of Laurentide. Following the reviewer's suggestion, Fig. S6 shows the temporal snapshots of ocean melting during the spike seen in Figure 6i. The spike in subshelf melting (Fig. 6i) as well as surface ablation (Fig. 6g) during this period would definitely lead to an increase of the freshwater flux into the ocean. This would also explain the synchronization with the AMOC slowdown seen during this period in Fig. 6e. However, since the model is run at an acceleration and we are conserving the freshwater flux, the net freshwater volume dumped into the ocean would be underestimated and thus freshwater flux changes from PSUIM into LOVECLIM may not be very realistic.

We have now discussed this in *Lines 461-473* in *Section 3.5*:

Further, relatively warm subsurface ocean water (>-1˚C) seeps along the west bank of Hudson Bay leading to a more pronounced negative mass balance (Fig. S5d). This shows up as a spike in the subsurface ocean melt values in Fig. 6i. Temporal snapshots every 0.1ky in the vicinity of the spikes in ablation (Fig. 6g), SMB (Fig. 6h) and ocean melting (Fig. 6i) are shown in Figure S6. It shows that the spikes in ablation and SMB predominantly come from a small area in the southern end of the Laurentide, while the spike in subshelf melting results only from the western part of the Laurentide with a receding grounding line. Although our model simulates sub shelf melting along the western Hudson Bay, we did not find any geologic evidence of such subsurface melting around 219.5ka. It is also worth mentioning that our setup does not simulate forebulges or other specific mechanisms modelled by more comprehensive full-Earth models. But Tigchelaar et al. (2018) have reported such changes in mass balance arising due to changing of ice sheets to ice shelves near the grounding line. The spike in subshelf melting (Fig. 6i) as well as surface ablation (Fig. 6g) during this period lead to an increase of the freshwater flux into the ocean. This could explain the synchronization with the AMOC slowdown seen during this period in Fig. 6e. However, since our model is run at an acceleration ($N_A = 5$) and we conserve the freshwater flux (Sec. 2.3), the total freshwater volume dumped into the ocean is being underestimated, which may distort the LOVECLIM response.

Fig. 2 You could also mention on the figure how the interpolation / downscaling to the different grids is done. Also, by "landmask" you mean "ice mask" (albedo)?

A. We have clarified that we use first order conservative remapping to interpolate the data across the different grids. These are mentioned in *Line 219-220* in *Section 2.3*:

PSUIM uses surface air temperature (T), precipitation (P), solar radiation (Q), and ocean temperature at 400m depth (T_o) as inputs from LOVECLIM. These are downscaled using a bilinear interpolation approach.

"Land mask" means "ice mask" in Figure 2. We have now changed this.

Technical comments:

Fig. 4 The grounding line is hardly distinguishable.

A. We have now changed it to solid green lines for all the figures.

Fig. 4 (and Fig. S2, S3, S4 and S5) I find the maps of mixed information thickness / ice velocity hard to read. Maybe using the contours for thickness and the solid colours for velocity would look nicer?

A. Done. We have also applied the same to Figure 7, S3, S6, S6 and S8. The updated Fig. 7 is attached here as an example.

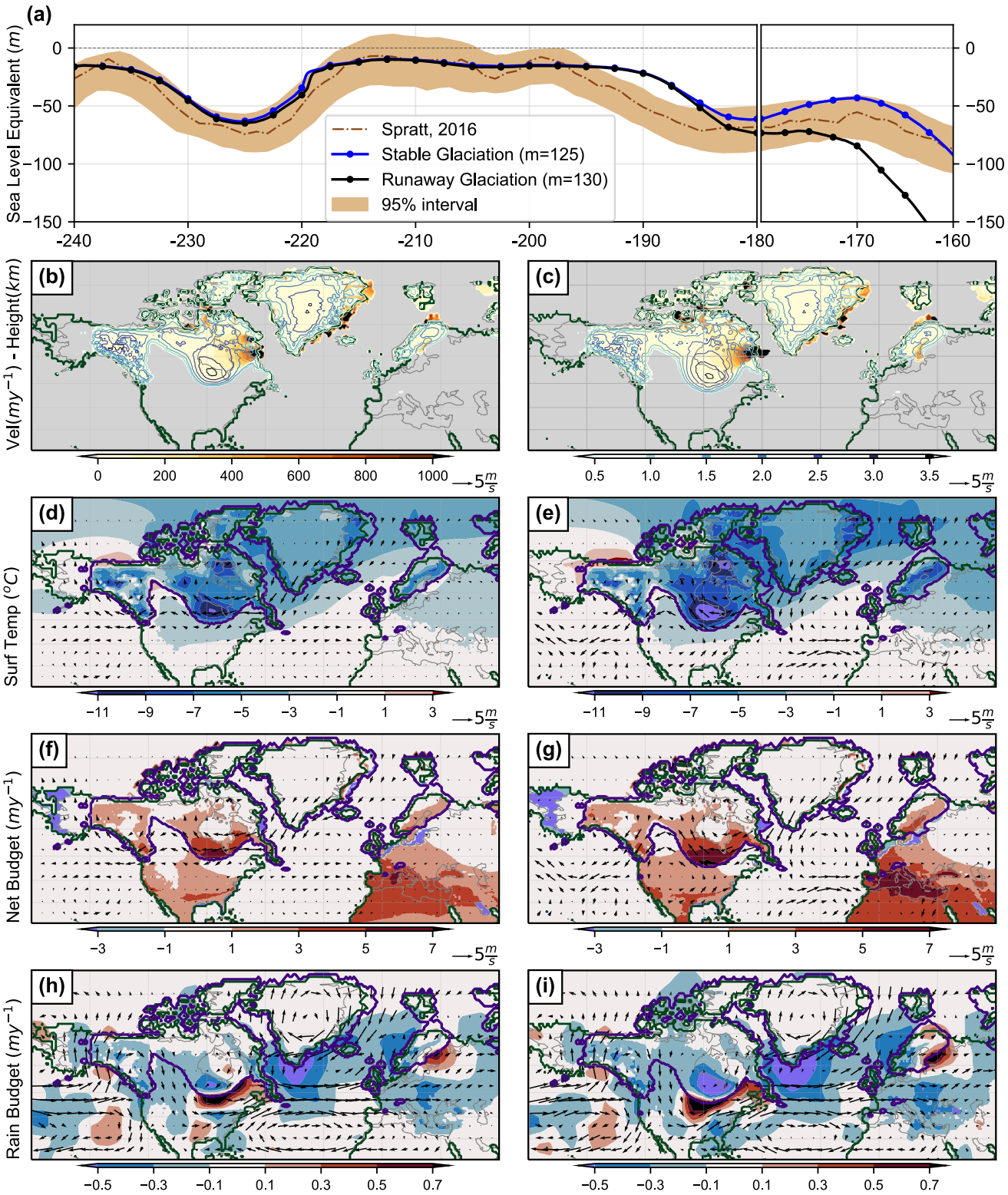

Figure 7: Bifurcation of the system at 180ka while transitioning into MIS 6 over Laurentide. (a) Sea level reconstruction (m) and 95% confidence interval of Spratt and Lisiecki (2016) (brown). Total ice volume (in terms of SLE, m) from two ensemble members of LOVECLIP, one that leads to a stable glacial inception (blue; α=2, m=125 Wm^{-2}) and another into a runaway glaciation (black; α=2, m=130 Wm^{-2}). Climate and ice sheet variables at 180ka from the stable glaciation on the left column (b, d, f and h) and runaway glaciation on the right (c, e, g and i). (b,c) Basal ice velocity (solid colors, my^{-1}) overlaid with ice thickness (colored contours, km) and the grounding line (solid green lines). (d,e) Surface temperature anomalies ($^\circ C$) overlaid with *anomalous* wind vectors at 800hPa (ms^{-1}). (f,g) Net mass balance anomalies (my^{-1}) overlaid with *anomalous* winds (ms^{-1}). (h,i) Rainfall anomalies (my^{-1}) overlaid with *absolute* winds (ms^{-1}). The purple contours in (d) to (i) mark the boundaries of the ice sheets from each run (stable for left and runaway for right). Anomalies here are with respect to the initial condition at 240ka. Anomalies over the Eurasian and Siberian ice sheets are small and not shown.

Fig. 7 I am sure that you can use a better colourbar for panel f to i. At least it can be white where there are small changes instead of yellow.

A. We now use a better color scheme for Figure 7, S8 and S9. For instance, see figure above.

Fig. 7 l675 purple contours are for which run (blue or black in panel a)?

A. The purple contours mark the boundaries of the ice sheets simulated in each experiment, the left one is from the blue line and the right one from the black line. We have now clarified this in the figure caption (see above).

Fig. S1 Panel b: since a multiplicative correction of 1 means no correction maybe it could have been better to have a neutral colour such as white around the value of 1.

A. Done.

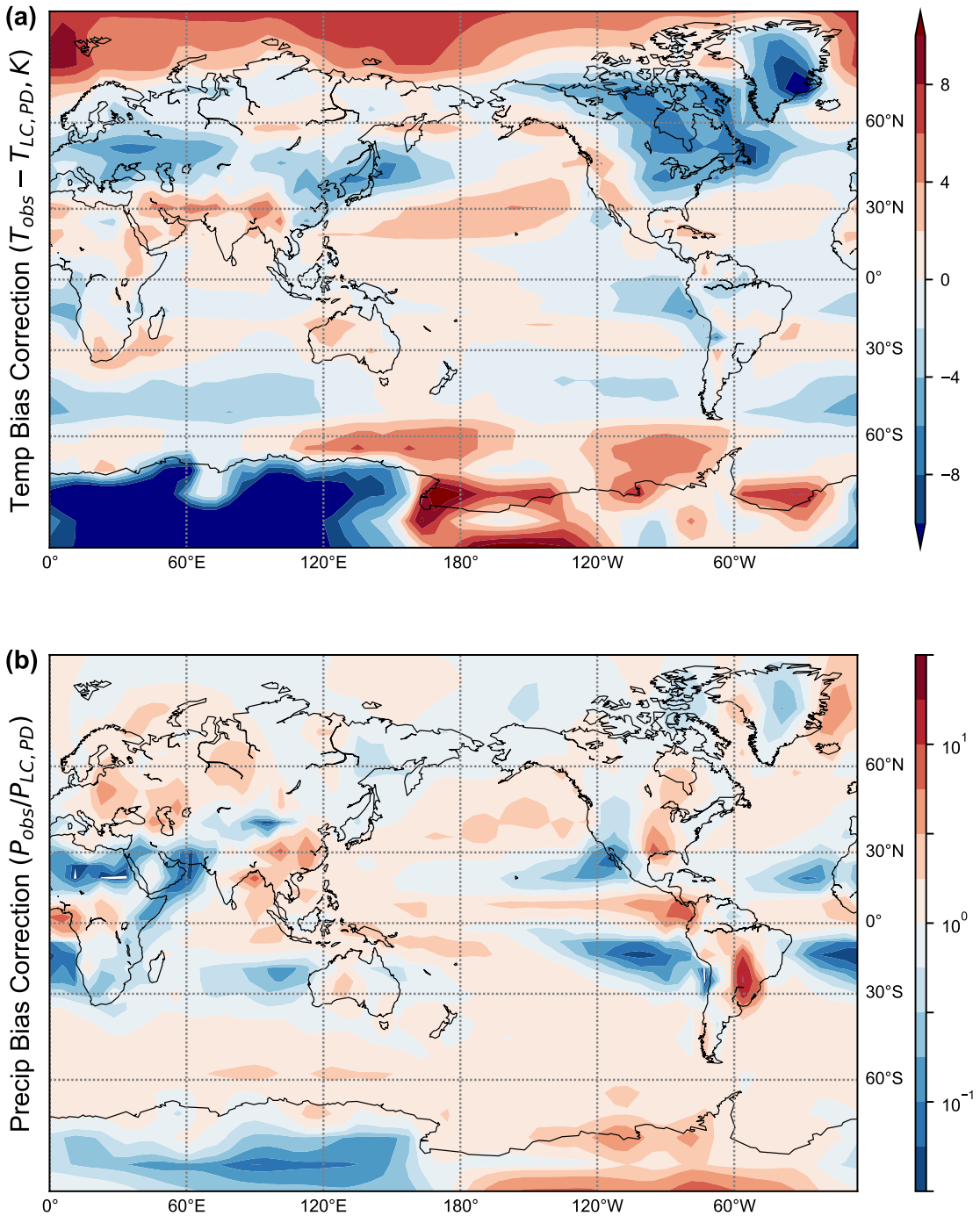

Figure S1: Bias correction used for LOVECLIM outputs. (a) Additive bias correction for annual mean surface temperature (K). (b) Multiplicative bias correction for annual mean precipitation. Colours are log normalised for the precipitation case.

Reviewer 2:

This submission presents the first asynchronously coupled ice sheet and LoveClim transient modelling results for the MIS 7 to 6d (240 to 170 ka) interval. It is therefore plenty novel and relevant for CP. Two of its main conclusions reflect those of another submission currently under CPD review examining last glacial inception (Bahadory et al, cp-2020-1, of which I'm a co-author): that 1) LoveClim appropriately coupled with an ice sheet model can within uncertainties capture major interglacial-glacial-interstadial transitions and 2) replicating such transitions can impose strong constraints on the coupled model. The third conclusion, that orbital forcing has more impact than GHG changes during glacial inception, is not surprising based on associated radiative forcings and chosen fixed forcing states but does not necessarily hold when one considers say the whole last glacial cycle (Tarasov and Peltier, JGR 1997, albeit with a much simpler 2D energy balance climate model and isothermal ice sheet model).

As to the quality and limitations of the scientific methods, aka model configuration and experimental design, the component PSU ice sheet model and LoveClim EMIC are well documented and well used models. They arguably remain near state-of-the-art for transient glacial contexts (though LoveClim is sorely in need of a replacement and ongoing work with transient GCM/ISM models are defining a new state of the art for very small ensembles). However, I do find some limitations that need to be made explicit in the manuscript. As shown in Bahadory et al, GMD 2018 (again from my group and curious why this paper is not cited), accounting for orographic forcing of precipitation in downscaling to the ice sheet grid and accounting for topographic changes in meltwater routing can each have significant impact on modelled ice sheet evolution. To be concrete, inclusion of the latter, for instance can, result in more than 15 m eustatic sealevel equivalent discrepancies within 4 kyr (IBID). The current submission is not even explicitly clear if the modelled surface freshwater routing changes during the glacial cycle (though it appears not to be the case). There are also a host of other sources of model uncertainty that are not mentioned, including: length of model spinup, topographic upscaling from ISM to LOVECLIM, the requirement of much higher ice sheet resolution or subgrid mass-balance accounting to adequately represent restricted glaciation over Alaska, and the dozens of poorly constrained parameters in both models that the modellers have chosen to not vary.

A. We share Lev's concern that there remains a number of parameters which are not well constrained. This is a general problem of climate-ice sheet models which are sufficiently computationally efficient to allow for simulations spanning multiple millennia, since such models cannot resolve many key processes and hence need to rely on parameterizations. On the other hand, there has been an extensive effort to constrain the parameters in the two LOVECLIP components separately, LOVECLIM and PSUIM, and sets of standard parameters have been developed, which are the default in our coupled modeling system. While it is generally possible to optimize parameter sets for a given period in time, these optimal parameter sets tend to depend on the period chosen. Presumably, this is related to model imperfections. We agree that including the processes described in Lev's comment do have the potential to reduce some of the model imperfections, however, they also come at the cost of new parameter values which need to be constrained. So, the general caveat of imperfect models and poorly constrained parameter values remains. Despite these caveats, the fact that our model is able to reproduce many transient features of past climate reconstructions gives us confidence that these models are sufficiently realistic to start using them to address questions related to physical processes and questions underlying ice sheet trajectories. As outlined below, we have revised the text to clarify the extent to which the processes above are included or not in our present model setup.

    a. Orographic forcing is not implemented in our setup. While the authors were aware of Bahadory and Tarasov (2018), it was an oversight on our part of not citing it since it was not applied to glacial simulations. We have clarified this in *Lines 244-248* in *Section 2.3*:

> Instead of using a fixed value of γ, both Roche et al. (2014) and Bahadory and Tarasov (2018) used a dynamic lapse rate, where γ is estimated locally for the ice model grids in each LOVECLIM grid. Moreover, the lapse rate also depends on the atmospheric CO_2 concentration. Such dynamic lapse rate corrections are not implemented in the current setup, and neither is the advective precipitation downscaling scheme of Bahadory and Tarasov (2018).

    b. The modelled freshwater in PSUIM is dynamically routed based on the actual topography. We have now clarified this in *Lines 263-266* in *Section 2.3*:

The total meltwater from basal melting and liquid runoff in PSUIM is dynamically routed based on PSUIM topography till it reaches the ocean or the domain edge, and then is routed to the nearest ocean grid point in LOVECLIM. The calving flux is channeled into CLIO's iceberg model (Schloesser et al., 2019;Jongma et al., 2009) in the Southern Hemisphere (SH) and as an iceberg melt flux (freshwater flux and heat flux) in the NH (Schloesser et al., 2019).

c. Our model was spun up for 10,000 years using orbital and GHG forcings of 240ka with the NH ice volume equilibrating to -20m SLE. This is mentioned in *Lines 282-286* in *Section 2.4*:

The LOVECLIP experiments are initialized using present day ice sheet conditions and spun up using orbital and greenhouse gas (GHG) forcings of 240 ka for a period of 10ky. The model equilibrates to an ice sheet distribution in the NH corresponding to -20m SLE, implying an open Bering Strait. Our initial ice sheet distribution at 240ka is shown in Fig. 4c and is in close agreement with that used by previous studies such as Colleoni and Liakka (2020) for 239ka and Colleoni et al. (2014) for 236ka.

d. The topography from PSUIM is upscaled to LOVECLIM using a simple weighted average. We have clarified this in *Lines 259-260* in *Section 2.3*:

LOVECLIM orography and surface ice mask are updated based on the evolution of ice sheets and bedrock elevation from PSUIM. The PSUIM topography is upscaled to LOVECLIM grid using simple weighted averaging.

e. The need for higher resolution to model mass balances and transport over regions with large sub-grid relief is a very valid concern, as mentioned in Le Morzadec et al. (2015). Coarse grid resolutions average out large sub-grid relief (tall peaks and low valleys) over some mountainous regions, such as parts of Alaska, and thus don't capture the non-linear combination of accumulation zones on the high peaks and ablations zones in the valleys. This is indeed a shortcoming of our modelling setup and we have now addressed this in *Lines 372-375* in *Section 3.2*:

Our modelling setup also does not account for sub-grid mass balances, which can be especially relevant over mountainous regions with large sub-grid relief such as Alaska (Le Morzadec et al., 2015). Coarse grids tend to average out such tall peaks and low valleys and thus don't capture the non-linear combination of accumulation zones on the high peaks and ablation zones in the valleys.

We have also added more discussion about discrepancies in the current study and further steps for model improvement in *Lines 543-577* in *Section 4*:

The simulated ice sheet volume is well within the range of reconstructions for a rather narrow range of parameters. Small changes in parameter values can produce strongly diverging trajectories, and the emergence of multiple equilibrium states may also suggest the model's dependence on initial conditions. This poses a challenge, as many ice sheet and climate model parameters remain poorly constrained. In this context, we note that parameterizations associated with hydrofracturing and cliff instability did not impact our ice sheet trajectories. These processes have provided substantial contributions to the rapid Antarctic ice sheet retreat simulated in response to future climate projections (DeConto and Pollard, 2016), and better constraining these parameterizations is important to reduce uncertainties related to future sea level trajectories (e.g., Edwards et al., 2019). Presumably, these processes did not play an important role in our present simulations, because the climate is generally too cold, suggesting that opportunities for constraining these parameters in glacial simulations may be limited. We further note that the parameter sets which allowed for the most realistic simulation of glacial inceptions during MIS 7-MIS 6 may not necessarily be optimal for other periods. That optimal parameter sets can depend on the period over which they are optimized, has recently been shown for a similar coupled climate ice sheet model (Bahadory et al., 2020).

Our present setup has difficulties in realistically simulating both Laurentide and Eurasian ice sheets simultaneously and generates a smaller Eurasian ice sheet compared to reconstructions, which could be a model dependent feature of LOVECLIM, given it is a T21 grid with only three levels in the atmosphere, and so could vary with the choice of the climate model used. Since we use an accelerated setup, we only conserve the freshwater flux from the ice model to LOVECLIM, which could lead to an underestimation of the oceanic circulation changes due to the lesser volume of net

freshwater being dumped into the ocean. Nevertheless, there is scope of further improving the current setup. For instance, we only implement temperature and precipitation bias corrections in the current setup, and including bias corrections for radiation and ocean temperature might improve our representation of ice sheets. Future research might further improve the current setup by including the advective precipitation downscaling scheme (Bahadory and Tarasov, 2018) to account for orographic forcing, which is not captured in LOVECLIM. We are also investigating the possibilities of using a dynamical, an altitude-dependent and a CO_2-dependent lapse rate corrections while downscaling temperature from LOVECLIM to PSUIM. This is because the atmospheric lapse rate depends on the atmospheric CO_2 concentration – an effect that has not been considered so far in glacial dynamics. Furthermore, improving our basal sliding coefficient map for the NH using information of sediment sizes, instead of simply using a binary coefficient map, has the potential of further improving the simulations.

Potentially more realistic results could be obtained if the simulations were unaccelerated (which would be computationally very expensive), and from using more complex climate models that include stratification-dependent mixing in the ocean for instance. Furthermore, Glacial Isostatic Adjustment (GIA) processes captured only in comprehensive full-Earth models such as forebulges are not simulated in the ice-sheet model used here. Nevertheless, we would like to reiterate that simulating a trajectory is more difficult than conducting timeslice experiments, as climate and ice sheet components work on totally different timescales and a fine interplay of parameters can add up to very different equilibrium states. And such coupled climate-ice sheet paleo-simulations offer great opportunities for constraining parameter sets for future simulations.

The other hole in the paper for me is pervasive in paleo ice sheet modelling: a very limited exploration of the impact of model uncertainties, given the small number of ensemble parameters and limited ensemble size. This is an exploratory work, and so arguably gets a pass with this limited ensemble, but I encourage the authors to expand their set of ensemble parameters and ensemble size in future work. And the paper needs a bit more attention to discussion of uncertainties that arise from the very limited ensemble size and the potential impact thereof.
The paper structure is logical. The abstract is concise and appropriate. The language is fluent, though there are instances where precision is lacking (eg "reasonably well", cf detailed commments below) as are some important (to me at least..) details about model setup.

A. We have now updated the table of experiments (Table 1) and added a figure in the supplementary showing all the experiments that were conducted as part of our ensemble (including those not discussed in the paper). We have also included discussions in the methods and results sections to further clarify the ensemble parameters, model uncertainties and future works. Answers to these questions are mentioned below as responses to the specific comments.

Specific comments:

For a range of model parameters, the simulations capture the reconstructed evolution of global ice volume reasonably well # What does "reasonably well" mean. Be precise

A. Reasonably well means within the uncertainty bounds of reconstructions. We have now replaced this in *Lines 18-19* in the *Abstract*:

For a range of model parameters, the simulations capture the evolution of global ice volume well within the range of reconstructions.

It is demonstrated that glacial inceptions are more sensitive to orbital variations, whereas terminations from deep glacial conditions need both orbital and greenhouse gas forcings to work in unison
 # this likely depends on your choice of fixed orbital configuration # cf Tarasov and Peltier, JGR 1997.

A. We have clarified this to be true for our time period of consideration. This is mentioned in *Lines 19-21* in the *Abstract*:

Over the MIS7-6 period, it is demonstrated that glacial inceptions are more sensitive to orbital variations, whereas terminations from deep glacial conditions need both orbital and greenhouse gas forcings to work in unison.

This poses a general challenge for transient coupled climate-ice sheet modeling.# on the flip side, it poses a strong constraint opportunity, cf# Bahadory et al, cp-2020-1.pdf in TCD

A. We agree and have added this in *Lines 24-26* in the *Abstract*:

This poses a general challenge for transient coupled climate-ice sheet modeling, with such coupled paleo-simulations providing opportunities to constrain such parameters.

which correspond to about 1.3 mm/year global sea level equivalent during the build-up phase.# that number is more than a factor too small for last glacial# inception if one goes by the cited LR04 stack

A. We have now modified this to clarify that this value is an average and the changes were much higher during the LGM. This is in *Lines 36-39* in the *Section 1*:

One of the main obstacles in simulating variability on orbital timescales is the fact that ice-sheets are slow integrators of small imbalances between ablation and accumulation, which correspond to an average of 1.3mm/year global sea level equivalent during the build-up phase but can exceed 10mm/year for instance during the Last Glacial Maximum (LGM, 21ka).

fig 3 captions # again mixing up ensemble with ensemble run. An ensemble is a collection # of model runs.
fig 3 # does this show all the model runs in the non-fixed forcing ensemble you # carried out? If so, please make this clear. including multi-ensemble simulations# do you mean mult-run or did you actually carry out multiple ensembles? # If so, how large was each ensemble?

A. We use only one ensemble of multiple runs in our simulations. We also updated Table 1 to show all the ensemble runs performed in this study. While we performed a total of 50 separate experiments, we reported only 15 of them in Figure 3 that best describe the parameter sensitivities. We have now clarified this in in *Lines 293-300* in *Section 2.4:*

Furthermore, sensitivity experiments with different GHG sensitivities (α, Sect. 2.1) and melt parameterizations (m, Sect. 2.2) are run with full forcing. Generally, higher α leads to a stronger sensitivity to CO_2 concentrations, and higher values of m strengthen buildup and weaken melting of ice during interglacial climates. These experiments are presented in the first row of Table 1 (1-15) and Fig. 3. Additional simulations with different combinations of acceleration (N_A), GHG sensitivity (α), melt parameter (m), basal sliding coefficient maps over the NH ($C(x,y)$) and higher ice model resolution ($0.5 \times 0.25°$ for NH, 20×20 km polar stereographic for Antarctica*)* have been performed (experiments 16-50 in Table 1). The whole ensemble of simulations is presented in Fig. S3. Although we note that these experiments do not present a systematic evaluation of the full parameter space, ice sheet trajectories are consistent with and thereby support the conclusions presented in this paper.

We have also updated the text throughout the manuscript to clarify that we do not run multiple ensembles but run multiple ensemble members.

We also updated the table of experiments (Table 1):

Expt Number	Orb Forced	GHG Forced	N_A	α	m (Wm^{-2})	C (myr^{-1}Pa^{-2})-NH
1 **(BLS)**	**Y**	**Y**	**5**	**2**	**125**	Binary distribution
2	**N**	**N**	5	2	125	
3	Y	**N**	5	2	125	**1.**Ocean:
4	**N**	Y	5	2	125	$C(x,y)$=10^{-6};
5	Y	Y	5	2	125	representing
6	Y	Y	5	**1.8**	125	deformable sediments

7	Y	Y	5	**2.2**	125	**2.**Land: $C(x,y)=10^{-10}$; representing non-deformable rock.
8	Y	Y	5	**2.5**	125	
9	Y	Y	5	**3**	125	
10	Y	Y	5	2	**80**	
11	Y	Y	5	2	**100**	
12	Y	Y	5	2	**120**	
13	Y	Y	5	2	**130**	
14	Y	Y	5	2	**140**	
15	Y	Y	5	2	**150**	
16-20	*Y*	*Y*	*5*	***1.5***	***120,125,130,140,150***	
21-24	*Y*	*Y*	*5*	***3.5***	***80,100,120,125***	
25-27	*Y*	*Y*	***1 (30ky run)***	*2*	***110,120,130***	
28-30	*Y*	*Y*	***2 (30ky run)***	*2*	***110,120,130***	*Binary*
31-33	*Y*	*Y*	***10***	*2*	***110,130,150***	
34-36	*Y*	*Y*	***10***	***2.5***	***110,120,130***	
37-38	*Y*	*Y*	***20***	***2.5, 3***	*125*	
39-41	*Y*	*Y*	*5*	*2*	*125*	*Tertiary* ***1.***Ocean: $C(x,y)=10^{-6}$; ***2.1*** Land (soft tills): $C(x,y)=$***10^{-7},10^{-8},10^{-9}*** *over northeastern North America* ***2.2*** Land (hard bed): $C(x,y)=10^{-10}$
42-44	*Y*	*Y*	*5*	*2*	***150***	
45-47	*Y*	*Y*	*5*	***2.5***	*125*	
High Resolution Runs: 0.5 × 0.25° *for NH*, 20 × 20 km *polar stereographic for Antarctica*						
48-50	*Y*	*Y*	*5*	*2*	***110,130,150***	*Binary*

Table 1: List of all ensemble runs performed for the study study (shown in Fig. S3). The first 15 experiments are discussed in Sect. 3.1 and shown in Fig. 3. Values in bold represent the difference from the baseline simulation (BLS, experiment number 1). N_A represents the PSUIM vs LOVECLIM acceleration factor (Sect 2.3). α represents the GHG sensitivity scaling factor (Eq. 1, Sect. 2.1) and m represents the constant parameter in the surface energy balance equation (Eq. 3, Sect. 2.2). C represents the basal sliding coefficient map used for the NH (Eq. 7, Sect. 2.2).

And added a figure in the supplementary, Fig. S3, showing all the ensemble runs used in our study:

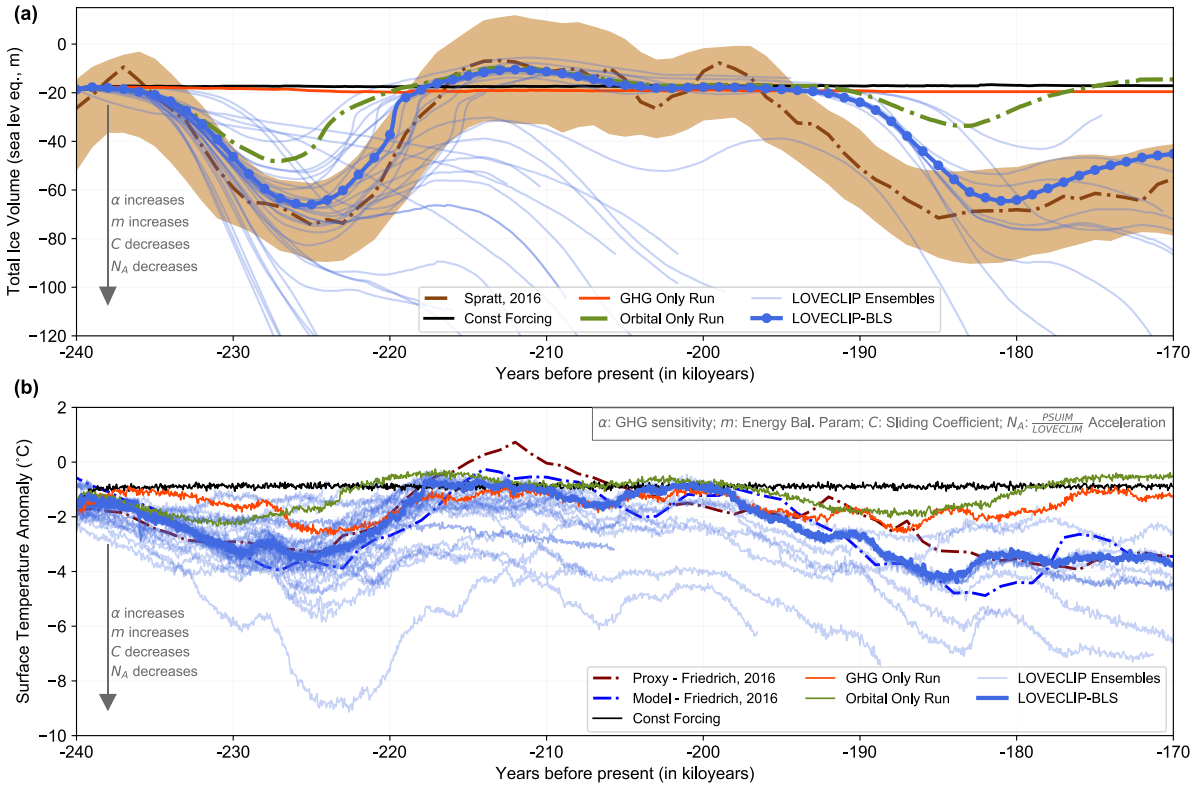

Figure S3: Transient LOVECLIP ensemble simulations over MIS7 with varying GHG sensitivities (α = 1.5-3.5), energy balance parameter (m = 80-150Wm^{-2}), basal sliding coefficient (C = 10^{-6}-10^{-8} myr^{-1}Pa^{-2}) and PSUIM-vs-LOVECLIM acceleration factor (N_A = 1,2,5,10,20). The best results are obtained for α=2, m=125 Wm^{-2}, binary sliding map (ocean: C=10^{-6} myr^{-1}Pa^{-2} and land: C=10^{-8} myr^{-1}Pa^{-2}) and N_A=5 (experiment 1 in Table 1, BLS).

The effect of CO2 variations with respect to the reference CO2 concentration (365ppm) on the longwave 120 radiation flux is scaled up by a factor α, to account for the low default sensitivity of ECBilt to changes in CO2 concentrations (Friedrich and Timmermann, 2020;Timmermann and Friedrich, 2016). α is determined based on transient past and future simulations.# Please provide the pCO2 ECR for alpha=2 with your setup. This would # let reader better judge how consistent this resultant sensitivity is# compared to that of IPCC grade GCMs. Also, it would be worthwhile# comparing your \alpha to that found based on 1D radiative-convective # modelling (Ramanathan et al, 1979 JGR).

A. Our ECS is 3.69K for CO_2 doubling for α=2, well within the ranges for LOVECLIM only simulation reported in Friedrich et al. (2016) and Friedrich and Timmermann (2020). We have now mentioned this in *Line 129* in the *Section 2.1*:

> For reference, the equilibrium climate sensitivity for CO_2 doubling is 3.69K for α of 2.

2.2 PSUIM surface mass balance description, eq 1 and 2 # on what timestep is this carried out? If longer than 1 hour # (presumably), what accounting is there for diurnal variations?

A. The surface mass balance is calculated at 3-hourly timesteps. The monthly data is interpolated to daily values using a weighted average of values across the adjacent months and then a sinusoidal cycle with max temperatures at 1400 and minimum at 0200, with peak-to-peak amplitude of 10˚C, is superimposed to account for daily variations.

We have now clarified this in *Lines 168-173* in the *Section 2.2*:

> This surface mass balance is calculated at timesteps of 3 hours. Monthly surface air temperature (T) and surface incoming shortwave radiation (Q) (obtained from LOVECLIM in the current setup, discussed further in Sect. 2.3) are interpolated into sub-daily values in two steps. Firstly, the monthly values are interpolated to daily values using a weighted averaging of the values across two adjacent months. Next, a sinusoidal cycle with max temperature at 1400 and minimum at 0200, with a peak-to-peak amplitude of 10˚C, is superimposed on the daily data to account for diurnal variations.

after eq 4 : with r = maxJ0, min[1, (T + 3)/3] = maxJ0, min[1, (T* + 3)/3]J0, min[1, (T* + 3)/3][1, (T* + 3)/3]* + 3)/3] # Based on my on examination of ice sheet model horizontal basal # temperature between along flow adjacent grid cells (which provides # logical upper bound for the transition range), 3 C is a wide # transition range for warm based sliding. How is this justified?*

A. The 3˚C range was chosen during model development of PSUIM to improve the realism of modern ice thicknesses and flow over certain regions of Antarctica, and avoid ubiquitous frozen beds over the Transantarctic for instance (Pollard and DeConto, 2012). Instead of using temperatures between adjacent along-flow grid cells as upper bounds, the authors use this 3˚C temperature range to represent the sub-grid variations in basal temperatures within a single grid cell, due to small-scale variations of bed properties, roughness and topography.

For the NH, a binary sliding coefficient map ... low sliding over present-day land (C(xJ0, min[1, (T + 3)/3], y) = ... representing non-deformable rock).) = ... representing non-deformable rock). # Much of Southern Canada and Northern USA (regions of glacial ice # cover) is covered by tills, not hard beds and this can significantly # influence ice sheet evolution (eg Tarasov and Peltier, 2004 # QSR). How do you justify making all this hard bedded?*

A. While we apply only a binary basal sliding coefficient map in the current study, we did try a tertiary map (with intermediate sliding over the northeastern North America) and the ice sheet evolutions were similar. Given this is the first study using this coupled setup, we presented results using the simple binary sliding coefficient map distribution. We are currently working on using an improved sliding map based on the sediment size data. We have added this as discussion of future work in in *Lines 567-569* in the *Section 4*:

Furthermore, improving our basal sliding coefficient map for the NH using information of sediment sizes, instead of simply using a binary coefficient map, has the potential of further improving the simulations.

Preliminary experiments (not shown) with different acceleration factors suggest that model results do not change significantly when N <= 5. # Please be more precise by what "significantly" means.

A. We wanted to convey that the simulated ice volume evolutions were similar over these low acceleration experiments. We have now replaced this in *Lines 215-217* in the *Section 2.3*:

Preliminary experiments (not shown) with different acceleration factors suggest that the simulated ice sheet evolution is relatively insensitive to N_A for $N_A \leq 5$. Therefore, $N_A = 5$ is used for the simulations presented in this paper, providing a good compromise between the objective to simulate realistic ice sheet evolution and computational efficiency.

Furthermore, for surface temperature T, a lapse-rate correction of 8 ℃ km−1 is applied to account for differences between LOVECLIM orography and PSUIM topography and precipitation is multiplied by a Clausius–Clapeyron factor of 2^.. with ΔT being the temperature lapse-rate correction, to account for the elevation desertification effect (DeConto and Pollard, 2016).# How do you justify using a lapse rate that is inconsistent with# the lapse rate LOVECLIM uses internally? For future work, I would # strongly advise inclusion of orographic forcing given the impact# thereof missed in a coarse grid EMIC (cf eg Bahadory# and Tarasov, GMD 2018)

A. Firstly, both the models LOVECLIM and PSUIM, and the parameterizations therein, were developed independently. Secondly, we use a higher lapse rate in PSUIM because we are more interested over the high latitudes in terms of ice sheet evolution. These regions are also drier and would have a higher lapse rate compared to the environmental lapse rate used in LOVECLIM. We are currently investigating the possibilities of using a dynamic lapse rate following Roche et al. (2014) and Bahadory and Tarasov (2018), an altitude dependent lapse rate as in Colleoni and Liakka (2020), and a CO_2 dependent lapse rate. We have added more discussion around this in *Lines 219-248* in *Section 2.3*:

PSUIM uses surface air temperature (T), precipitation (P), solar radiation (Q), and ocean temperature at 400m depth (T_o) as inputs from LOVECLIM. These are downscaled using a bilinear interpolation approach. The surface temperature and precipitation outputs from LOVECLIM which are used for the PSUIM surface mass balance are bias-corrected in the coupler, following Pollard and DeConto (2012), Heinemann et al. (2014) and Tigchelaar et al. (2018).

$$T(t) = T_{LC}(t) + T_{obs} - T_{LC,PD} \quad (8)$$

$$P(t) = P_{LC}(t) \times P_{obs}/P_{LC,PD} \quad (9)$$

where T is monthly surface air temperature and P is monthly precipitation forcing from LOVECLIM at timestep t. Subscripts 'LC', 'obs' and 'LC, PD' refer to LOVECLIM chunk output, observed present day climatology, and LOVECLIM present day control run, respectively. The observed present day climatology is obtained from the European Centre for Medium-Range Weather Forecasts reanalysis dataset, ERA-40 (Uppala et al., 2005). These LOVECLIM biases are calculated for PD simulations using an LGM bathymetry. We did compare the biases between using a PD or LGM bathymetry, and while there were regional differences, the large-scale structure was found to be similar (not shown). The annual mean of the monthly mean bias correction terms $T_{obs} - T_{LC,PD}$ and $P_{obs}/P_{LC,PD}$ are presented in Fig. S1. Temperature biases in LOVECLIM for boreal summer (JJA) and austral summer (DJF) are shown in Fig. S2 for reference, since summer temperatures are more crucial for ice sheet growth and decay. Furthermore, a lapse-rate correction of 8˚C km^{-1} is applied to account for differences between LOVECLIM orography and PSUIM topography for the interpolated temperature, $T(t)$, and precipitation is multiplied by a Clausius–Clapeyron factor of $2^{\frac{-\gamma.\Delta H}{10^{\circ}C}}$, with $\gamma.\Delta H$ being the temperature lapse-rate correction, to account for the elevation desertification effect (DeConto and Pollard, 2016):

$$T_{PSUIM}(t) = T_{interp}(t) - \gamma.\Delta H \quad (10)$$

$$P_{PSUIM}(t) = P_{interp}(t) \times 2^{\frac{-\gamma.\Delta H}{10^{\circ}C}} \quad (11)$$

where T_{PSUIM} and P_{PSUIM} are the final temperature and precipitation inputs for PSUIM, T_{interp} and P_{interp} are bias corrected LOVECLIM temperature (T, Eq. 8) and precipitation (P, Eq. 9) interpolated to PSUIM resolution, γ is the lapse

rate (8˚C km^{-1}), and ΔH is the altitude difference between PSUIM grids and the corresponding LOVECLIM grid. Colleoni and Liakka (2020) used a similar fixed atmospheric lapse rate correction during downscaling temperature to their ice model, GRISLI, with γ as 3.3˚C km^{-1} for annual mean and 4.1˚C km^{-1} for summer mean. And they reported slightly smaller ice sheets on using an elevation dependent lapse rate, going all the way up to 7.9˚C km^{-1}. Instead of using a fixed value of γ, both Roche et al. (2014) and Bahadory and Tarasov (2018) used a dynamic lapse rate, where γ is estimated locally for the ice model grids in each LOVECLIM grid. Moreover, the lapse rate also depends on the atmospheric CO_2 concentration. Such dynamic lapse rate corrections are not implemented in the current setup, and neither is the advective precipitation downscaling scheme of Bahadory and Tarasov (2018).

And have added these as possibilities of further improvement in *Lines 561-569* in *Section 4*:

. Nevertheless, there is scope of further improving the current setup. For instance, we only implement temperature and precipitation bias corrections in the current setup, and including bias corrections for radiation and ocean temperature might improve our representation of ice sheets. Future research might further improve the current setup by including the advective precipitation downscaling scheme (Bahadory and Tarasov, 2018) to account for orographic forcing, which is not captured in LOVECLIM. We are also investigating the possibilities of using a dynamical, an altitude-dependent and a CO_2-dependent lapse rate corrections while downscaling temperature from LOVECLIM to PSUIM. This is because the atmospheric lapse rate depends on the atmospheric CO_2 concentration – an effect that has not been considered so far in glacial dynamics. Furthermore, improving our basal sliding coefficient map for the NH using information of sediment sizes, instead of simply using a binary coefficient map, has the potential of further improving the simulations.

Basal melting and liquid runoff from PSUIM is discharged via LOVECLIM's runoff masks in both hemispheres; # do these masks account for changing topography? And if so, what # accounting is there for critical subgrid gateways for southern # drainage from the NA North American) ice complex (cf eg Tarasov and # Peltier, QSR 2006).

A. The net meltwater in PSUIM is dynamically routed based on the actual topography. The current setup does not account for the subgrid pathways needed for southward drainage from the North American ice sheets. We have clarified this in *Lines 263-266* in *Section 2.3*:

The total meltwater from basal melting and liquid runoff in PSUIM is dynamically routed based on PSUIM topography till it reaches the ocean or the domain edge, and then is dumped into the nearest ocean grid point in LOVECLIM. The calving flux is channeled into CLIO's iceberg model (Schloesser et al., 2019;Jongma et al., 2009) in the Southern Hemisphere (SH) and as an iceberg melt flux (freshwater flux and heat flux) in the NH (Schloesser et al., 2019).

Increasing the value of m (Eq. (1)) # as a reader, it is a pain to flip back 5 pages to find out what m # is, please add a few descriptive words (surface energy offset term # or some such) ditto for \alpha

A. Done.

3.2 Ice sheet evolution # this section would be strengthened with more contact with the # (albeit limited) glacial geological litterature. The key relevant # data are Late Pleistocene glacial limits. Does your model respect # them everywhere? If not, what are the main discrepancies? The only # regions I see that could be at issue are your Alaskan incursion and # Northern Siberia.

A. While we could not find many reconstructions over this period, we have now added discussions comparing our simulations with other modelling and reconstruction studies. Some excerpts of these are mentioned under from *Lines 344-376* in *Section 3.2*:

In the context of previous modelling studies and geological records over this MIS 7-6 period, our ice sheet distribution at MIS 7c (212ka, Fig. 4g and 219.5ka, Fig. S7) is very similar to that reported in Colleoni and Liakka (2020). However, we simulate a stronger inception compared to that of Colleoni et al. (2014) over the corresponding 236-230ka period. They also reported a bifurcated but connected North American ice sheet at MIS 6 (157ka) from both their control (100km) and

high resolution (40km) experiments. Our simulation results in separate Laurentide and Cordilleran ice sheets but generates neither a Eurasian nor a Siberian ice sheet, albeit at 170ka. On a side note, our North American ice sheet distribution at 180ka (Fig. 7) is closer to that of Colleoni and Liakka (2020) at 157ka. Studies of NH reconstructions during MIS 6 such as Svendsen et al. (2004), over 160-140ka, Rohling et al. (2017), around 140ka, and Batchelor et al. (2019), over 190-132ka, have all reported glacial geological records to indicate a larger extent of the Eurasian ice sheet at MIS 6 glacial maximum compared to the LGM, while our simulations only show a persistent Fenno-Scandian ice sheet and a relatively small Eurasian ice sheet at 170ka. More recently, Zhang et al. (2020) reported the existence of a Northeast Siberia-Beringian ice sheet at MIS 6e (190-180ka) using NorESM-PISM simulations validated by North Pacific geological records. However, our model does not simulate any ice over Alaska, Beringia and northeast Siberia over MIS 7-6.

Our model's difficulty in simulating the Eurasian ice sheet can be attributed to the competition between Laurentide and Eurasian ice sheet growth, which makes it arduous to realistically simulate them simultaneously alongside generating the right atmospheric patterns. Some previous studies have suggested that teleconnections from stationary wave patterns induced by a large Laurentide ice sheet could lead to warming over Europe and influence Eurasian ice sheet evolution (Roe and Lindzen, 2001;Ullman et al., 2014). The Laurentide building up first in our simulations could have changed the storm tracks and dried out Eurasia. It is also worth reiterating that LOVECLIM has a coarse T21 grid with a simple 3-layered atmosphere. While the circulation changes reported here maybe model dependent, Lofverstrom and Liakka (2018) reported that at least a T42 grid was needed in their atmospheric model (CAM3) to generate a Eurasian ice sheet using SICOPOLIS, albeit for the LGM. They attribute this discrepancy to lapse rate induced warming due to reduced and smoother topography and higher cloudiness leading to increased re-emitted longwave radiation towards the surface. These teleconnection patterns are further discussed in Sect. 3.6. Our LOVECLIM setup also uses a fixed lapse rate for downscaling LOVECLIM surface temperatures (Eq. 10 and 11), while both Roche et al. (2014) and Bahadory and Tarasov (2018) used a dynamic lapse rate, which is estimated locally for the ice model grids in each LOVECLIM grid. Bahadory and Tarasov (2018) reported ice thickness differences up to 1km on using the dynamic lapse rate scheme compared to a fixed 6.5°Ckm^{-1}. Nevertheless, for runaway trajectories, our model can build up a Eurasian ice sheet for ice volumes greater than -200m SLE once the Laurentide growth slows down (not shown). Our modelling setup also does not account for sub-grid mass balances, which can be especially relevant over mountainous regions with large sub-grid relief such as Alaska (Le Morzadec et al., 2015). Coarse grids tend to average out tall peaks and low valleys and thus don't capture the non-linear combination of accumulation zones on the high peaks and ablation zones in the valleys. These shortcomings could explain the lack of Eurasian, Siberian and Beringian ice sheets in our simulations.

the glaciation 235 into MIS 6 is delayed by ~3ky (191ka instead of 194ka). # Do you really believe that temporaly uncertainty in inferred# sealevel is < 3 kyr that far back?

A. We agree with Lev on this and have now added this to our discussion of results in *Lines 309-313* in *Section 3.1*:

The model captures the overall trajectory of ice volume evolution reasonably well. Specifically, the model stays within the uncertainty range for the extreme glaciation-deglaciation event of MIS 7e-7d-7c. Larger differences only exist as the glaciation into MIS 6 is delayed by ~3ky in the simulation (191ka instead of 194ka). A possible explanation for this discrepancy may be related to the temporal uncertainty in reconstructions themselves, since a similar lag occurs in other modeling studies (e.g., Ganopolski and Calov (2011); Ganopolski and Brovkin (2017).

After a relatively stable interglacial state till MIS 7a, the system moves into the next glacial and reaches a glacial equilibrium state. # This description does not accurately reflect your figure 3, I see no # sign of a "glacial equilibrium"
...Batchelor et al. (2019), have suggested a larger Eurasian ice sheet over the MIS 6 period (160-140ka), # "suggested" does not accurately nor precisely reflect the # inferences. Be more accurate: eg glacial geological record indicates # that the asynchronous maximal MIS 6 ice margins are outside of MIS 2 # ice margins.

A. We have now removed the phrase about "glacial equilibrium" and have clarified MIS 6 ice sheet reconstructions in *Lines 350-356* in *Section 3.2*:

Studies of NH reconstructions during MIS 6 such as Svendsen et al. (2004), over 160-140ka, Rohling et al. (2017), around 140ka, and Batchelor et al. (2019), over 190-132ka, have all reported glacial geological records to indicate a larger extent

of the Eurasian ice sheet at MIS 6 glacial maximum compared to the LGM, while our simulations only show a persistent Fenno-Scandian ice sheet and a relatively small Eurasian ice sheet at 170ka. More recently, Zhang et al. (2020) reported the existence of a Northeast Siberia-Beringian ice sheet at MIS 6e (190-180ka) using NorESM-PISM simulations validated by North Pacific geological records. However, our model does not simulate any ice over Alaska, Beringia and northeast Siberia over MIS 7-6.

 # leading to temperatures low enough (Fig. 6d) to avoid ablation even if # the Laurentide extends equatorward There is always seasonal ablation on an northern ice sheet. Be more precise.

A. We have now rephrased these in *Lines 440-442* in *Section 3.4*:

This can be attributed to the low CO_2 value (<200ppmv) leading to lower temperatures (Fig. 6d) and reduced ablation even if the Laurentide extends equatorward (Fig. 6g). Furthermore, the southern extent of the Laurentide can lead to changes in circulation patterns that can alter the SMB (discussed in Sect. 3.6).

Figure 7: # makes it a lot easier for the reader if subplots have descriptive # headings on the plot. Having to visually jump between each subplot and a large # caption disrupts reader assimilation of the plots.

A. Done.

Fig 7 caption two ensembles of # do you mean two ensemble members?

A. Yes. We have updated ensembles to ensemble members throughout the study.

Fig 7f-I # I find the colour scheme has insufficient and distorting colour range. Eg # for 7h the 0.3:0.5 colour is just a shade darker than the -0.3:-0.1 range # colour. Furthermore, it makes no sense that the plot has regions where # these colour border each other without any intermediate ranges showing.

A. We have now used a better colormap to plot negatives in blue and positives in red throughout the manuscript.

Fig 7: # I am a bit confused why there is such limited glaciation east of the # Canadian Cordillera, given the northwesterly (and therefore relatively colder) # absolute winds and rainfall anomalies that match (within the colour # scheme) other sectors with significant ice cover. Is this due to # the temperature bias correction or limited rainful or ? On that note, # a short discussion on the impact of the bias correction would aid # interpretation of its role in your results.

A. We suspect the reduced glaciation east of the Canadian Cordillera because of low net precipitation (not anomalies). The precipitation bias over this region is almost 1 (Fig. S1). While Fig. 7 shows the *anomalies* in mass balance terms with reference to those at 240ka, the figure underneath (Fig. R5) shows the *absolute* values of these mass balance terms. Fig. R5 (h) and (i) show that the precipitation just east of the Cordilleran is very low. To make these patterns clearer, we have now added a figure in the supplementary showing the initial patterns of the mass balance variables at 240ka for comparison (Fig. S8 now) with the anomalies presented in Fig. 7 and Fig. S9.

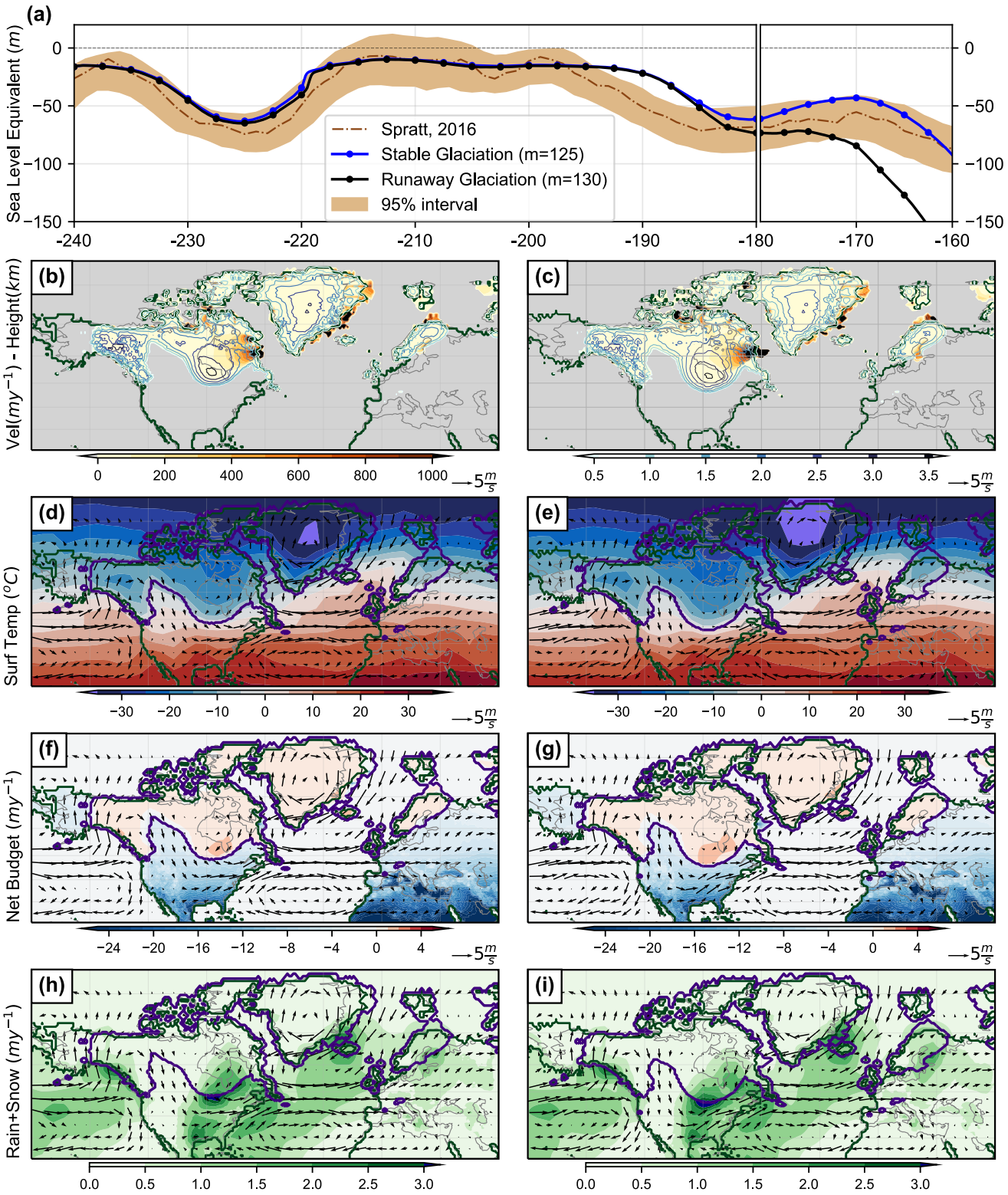

Figure R5: Bifurcation of the system at 180ka while transitioning into MIS 6 over Laurentide. (a) Sea level reconstruction (m) and 95% confidence interval of Spratt and Lisiecki (2016) (brown). Total ice volume (in terms of SLE, m) from two ensemble members of LOVECLIP, one that leads to a stable glacial inception (blue; α=2, m=125 Wm^{-2}) and another into a runaway glaciation (black; α=2, m=130 Wm^{-2}). Climate and ice sheet variables at 180ka from the stable glaciation on the left column (b, d, f and h) and runaway glaciation on the right (c, e, g and i). (b,c) Basal ice velocity (solid colors, my^{-1}) overlaid with ice thickness (colored contours, km) and the grounding line (solid green lines). (d,e) Surface temperature ($^{\circ}C$) overlaid with wind vectors at 800hPa (ms^{-1}). (f,g) Net mass balance (my^{-1}) overlaid with winds (ms^{-1}). (h,i) Net accumulation (my^{-1}) overlaid with winds (ms^{-1}). The purple contours in (d) to (i) mark the boundaries of the ice sheets from each run (stable for left and runaway for right).

this behavior is reminiscent of a saddle node bifurcation

We find that small changes in the Laurentide's ice distribution for similar total ice volumes can lead to a saddle node 400 bifurcation of the system # which is correct? Have you shown this to be a saddle node bifurcation # or is this reminiscent of a saddle node bifurcation?

A. We apologize for this confusion. We see small differences in ice sheet distributions reminiscent of a saddle node bifurcation. We have now updated this in the text in *Lines 536-538* in *Section 4*:

> We find that small changes in the Laurentide's ice distribution for similar total ice volumes reminiscent of a saddle node bifurcation, which in turn determines whether the coupled trajectory will follow a deglaciation or a runaway glaciation pathway in response to the combination of forcings.

Also, the stationary wave feedback reported here 410 could be a model dependent feature of LOVECLIM, given it has only three atmospheric levels # and LOVECLIM is run at a relatively coarse T21, while the
 # litterature indicates that at least T42 is needed to avoid major # resolution sensitivity of the eddy driven jet (eg Lofverstrom and # Liakka, 2018).

A. We thank Lev for this suggestion. We have now discussed and expanded on this in *Lines 358-368* in *Section 3.2*:

> Our model's difficulty in simulating the Eurasian ice sheet can be attributed to the competition between Laurentide and Eurasian ice sheet growth, which makes it arduous to realistically simulate them simultaneously alongside generating the right atmospheric patterns. Some previous studies have suggested that teleconnections from stationary wave patterns induced by a large Laurentide ice sheet could lead to warming over Europe and influence Eurasian ice sheet evolution (Roe and Lindzen, 2001;Ullman et al., 2014). The Laurentide building up first in our simulations could have changed the storm tracks and dried out Eurasia. It is also worth reiterating that LOVECLIM has a coarse T21 grid with a simple 3-layered atmosphere. While the circulation changes reported here maybe model dependent, Lofverstrom and Liakka (2018) reported that at least a T42 grid was needed in their atmospheric model (CAM3) to generate a Eurasian ice sheet using SICOPOLIS, albeit for the LGM. They attribute this discrepancy to lapse rate induced warming due to reduced and smoother topography and higher cloudiness leading to increased re-emitted longwave radiation towards the surface. These teleconnection patterns are further discussed in Sect. 3.6.

And in *Lines 520-522* in *Section 3.6*:

> As mentioned earlier in Sect. 3.2, it is important to acknowledge the low horizontal and vertical resolutions of LOVECLIM's atmosphere, which could mean the circulation changes reported here to be model dependent.

Results also suggest that our coupled simulations are realistic over a narrow range of parameters # what does "realistic" mean? Again, be precise

A. We meant 'realistic' simulations to have good agreement with the reconstructions. We have clarified this in *Lines 543-545* in *Section 4*:

> The simulated ice sheet volume is well within the range of reconstructions for a rather narrow range of parameters. Small changes in parameter values can produce strongly diverging trajectories, and the emergence of multiple equilibrium states may also suggest the model's dependence on initial conditions.

is more difficult than conducting timeslice experiments # I would say much more difficult and therefore offers much more # self-constraint

A. Agreed. We have added in *Lines 574-577* in *Section 4*:

> Nevertheless, we would like to reiterate that simulating a trajectory is more difficult than conducting timeslice experiments, as climate and ice sheet components work on totally different timescales and a fine interplay of parameters can add up to

very different equilibrium states. And such coupled climate-ice sheet paleo-simulations offer great opportunities for constraining parameter sets for future simulations.

Fig S1 # summer (JJA for NH and DJF for SH) temperature is much more critical # for ice sheet growth than mean annual temperature, given surface mass-balance # dependencies, so please add these plots.

A. We have now added the summer temperature biases in Fig. S2 in the supplementary.

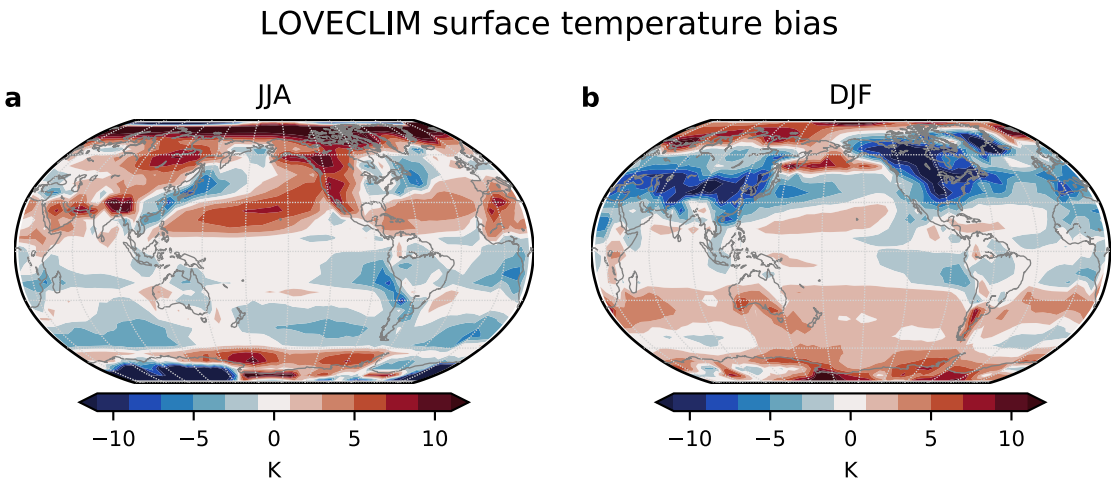

Figure S2: Seasonal biases in surface temperature (K) from LOVECLIM for (a) JJA, and (b) DJF.

References:

Bahadory, T., and Tarasov, L.: LCice 1.0 – a generalized Ice Sheet System Model coupler for LOVECLIM version 1.3: description, sensitivities, and validation with the Glacial Systems Model (GSM version D2017.aug17), Geoscientific Model Development, 11, 3883-3902, 10.5194/gmd-11-3883-2018, 2018.

Bahadory, T., Tarasov, L., and Andres, H.: The phase space of last glacial inception for the Northern Hemisphere from coupled ice and climate modelling, Clim. Past Discuss., 2020, 1-30, 10.5194/cp-2020-1, 2020.

Batchelor, C. L., Margold, M., Krapp, M., Murton, D. K., Dalton, A. S., Gibbard, P. L., Stokes, C. R., Murton, J. B., and Manica, A.: The configuration of Northern Hemisphere ice sheets through the Quaternary, Nature communications, 10, 1-10, 2019.

Clark, P. U., He, F., Golledge, N. R., Mitrovica, J. X., Dutton, A., Hoffman, J. S., and Dendy, S.: Oceanic forcing of penultimate deglacial and last interglacial sea-level rise, Nature, 577, 660-664, 2020.

Colleoni, F., Masina, S., Cherchi, A., Navarra, A., Ritz, C., Peyaud, V., and Otto-Bliesner, B.: Modeling Northern Hemisphere ice-sheet distribution during MIS 5 and MIS 7 glacial inceptions, Climate of the Past, 10, 269-291, 10.5194/cp-10-269-2014, 2014.

Colleoni, F., and Liakka, J.: Transient simulations of the Eurasian ice sheet during the Saalian glacial cycle, SVENSK KÄRNBRÄNSLEHANTERING AB, StockholmSKB TR-19-17, 2020.

DeConto, R. M., and Pollard, D.: Contribution of Antarctica to past and future sea-level rise, Nature, 531, 591-591, 2016.

Edwards, T. L., Brandon, M. A., Durand, G., Edwards, N. R., Golledge, N. R., Holden, P. B., Nias, I. J., Payne, A. J., Ritz, C., and Wernecke, A.: Revisiting Antarctic ice loss due to marine ice-cliff instability, Nature, 566, 58-64, 10.1038/s41586-019-0901-4, 2019.

Friedrich, T., Timmermann, A., Tigchelaar, M., Timm, O. E., and Ganopolski, A.: Nonlinear climate sensitivity and its implications for future greenhouse warming, Science Advances, 2, e1501923-e1501923, 2016.

Friedrich, T., and Timmermann, A.: Using Late Pleistocene sea surface temperature reconstructions to constrain future greenhouse warming, Earth and Planetary Science Letters, 530, 115911, 2020.

Ganopolski, A., and Calov, R.: The role of orbital forcing, carbon dioxide and regolith in 100 kyr glacial cycles, Climate of the Past, 7, 1415-1425, 2011.

Ganopolski, A., and Brovkin, V.: Simulation of climate, ice sheets and CO2; evolution during the last four glacial cycles with an Earth system model of intermediate complexity, Climate of the Past Discussions, 1-38, 2017.

Heinemann, M., Timmermann, A., Elison Timm, O., Saito, F., and Abe-Ouchi, A.: Deglacial ice sheet meltdown: orbital pacemaking and CO 2 effects, Climate of the Past, 10, 2014.

Jongma, J. I., Driesschaert, E., Fichefet, T., Goosse, H., and Renssen, H.: The effect of dynamic–thermodynamic icebergs on the Southern Ocean climate in a three-dimensional model, Ocean Modelling, 26, 104-113, 2009.

Laskar, J., Robutel, P., Joutel, F., Gastineau, M., Correia, A., and Levrard, B.: A long-term numerical solution for the insolation quantities of the Earth, Astronomy & Astrophysics, 428, 261-285, 2004.

Le Morzadec, K., Tarasov, L., Morlighem, M., and Seroussi, H.: A new sub-grid surface mass balance and flux model for continental-scale ice sheet modelling: testing and last glacial cycle, Geoscientific Model Development, 8, 3199, 2015.

Liu, Z., Otto-Bliesner, B., He, F., Brady, E., Tomas, R., Clark, P., Carlson, A., Lynch-Stieglitz, J., Curry, W., and Brook, E.: Transient simulation of last deglaciation with a new mechanism for Bølling-Allerød warming, Science, 325, 310-314, 2009.

Locarnini, R. A., Mishonov, A. V., Antonov, J. I., Boyer, T. P., Garcia, H. E., Baranova, O. K., Zweng, M. M., Paver, C. R., Reagan, J. R., and Johnson, D. R.: World ocean atlas 2013. Volume 1, Temperature, 2013.

Lofverstrom, M., and Liakka, J.: The influence of atmospheric grid resolution in a climate model-forced ice sheet simulation, Cryosphere, 12, 2018.

Lüthi, D., Le Floch, M., Bereiter, B., Blunier, T., Barnola, J.-M., Siegenthaler, U., Raynaud, D., Jouzel, J., Fischer, H., Kawamura, K., and others: High-resolution carbon dioxide concentration record 650,000-800,000 years before present, Nature, 453, 379-379, 2008.

Pollard, D., and DeConto, R. M.: Description of a hybrid ice sheet-shelf model, and application to Antarctica, Geoscientific Model Development, 5, 1273-1295, 10.5194/gmd-5-1273-2012, 2012.

Pollard, D., DeConto, R. M., and Alley, R. B.: Potential Antarctic Ice Sheet retreat driven by hydrofracturing and ice cliff failure, Earth and Planetary Science Letters, 412, 112-121, 10.1016/j.epsl.2014.12.035, 2015.

Roche, D. M., Dumas, C., Bügelmayer, M., Charbit, S., and Ritz, C.: Adding a dynamical cryosphere to iLOVECLIM (version 1.0): coupling with the GRISLI ice-sheet model, Geoscientific Model Development, 7, 1377-1394, 10.5194/gmd-7-1377-2014, 2014.

Roe, G. H., and Lindzen, R. S.: The mutual interaction between continental-scale ice sheets and atmospheric stationary waves, Journal of Climate, 14, 1450-1465, 2001.

Rohling, E. J., Hibbert, F. D., Williams, F. H., Grant, K. M., Marino, G., Foster, G. L., Hennekam, R., De Lange, G. J., Roberts, A. P., and Yu, J.: Differences between the last two glacial maxima and implications for ice-sheet, δ18O, and sea-level reconstructions, Quaternary Science Reviews, 176, 1-28, 2017.
Schloesser, F., Friedrich, T., Timmermann, A., DeConto, R. M., and Pollard, D.: Antarctic iceberg impacts on future Southern Hemisphere climate, Nature Climate Change, 9, 672-677, 2019.
Spratt, R. M., and Lisiecki, L. E.: A Late Pleistocene sea level stack, Climate of the Past, 12, 1079-1092, 2016.
Svendsen, J. I., Alexanderson, H., Astakhov, V. I., Demidov, I., Dowdeswell, J. A., Funder, S., Gataullin, V., Henriksen, M., Hjort, C., and Houmark-Nielsen, M.: Late Quaternary ice sheet history of northern Eurasia, Quaternary Science Reviews, 23, 1229-1271, 2004.
Tigchelaar, M., Timmermann, A., Pollard, D., Friedrich, T., and Heinemann, M.: Local insolation changes enhance Antarctic interglacials: Insights from an 800,000-year ice sheet simulation with transient climate forcing, Earth and Planetary Science Letters, 495, 69-78, 10.1016/j.epsl.2018.05.004, 2018.
Timm, O., and Timmermann, A.: Simulation of the last 21 000 years using accelerated transient boundary conditions, Journal of Climate, 20, 4377-4401, 2007.
Timm, O., Köhler, P., Timmermann, A., and Menviel, L.: Mechanisms for the onset of the African Humid Period and Sahara Greening 14.5–11 ka BP, Journal of Climate, 23, 2612-2633, 2010.
Timmermann, A., and Friedrich, T.: Late Pleistocene climate drivers of early human migration, Nature, 538, 92-95, 10.1038/nature19365, 2016.
Ullman, D., LeGrande, A., Carlson, A. E., Anslow, F., and Licciardi, J.: Assessing the impact of Laurentide Ice-Sheet topography on glacial climate, 2014.
Uppala, S. M., Kållberg, P., Simmons, A., Andrae, U., Bechtold, V. D. C., Fiorino, M., Gibson, J., Haseler, J., Hernandez, A., and Kelly, G.: The ERA-40 re-analysis, Quarterly Journal of the Royal Meteorological Society: A journal of the atmospheric sciences, applied meteorology and physical oceanography, 131, 2961-3012, 2005.
Zhang, Z., Yan, Q., Zhang, R., Colleoni, F., Ramstein, G., Dai, G., Jakobsson, M., O'Regan, M., Liess, S., Rousseau, D. D., Wu, N., Farmer, E. J., Contoux, C., Guo, C., Tan, N., and Guo, Z.: Rapid waxing and waning of Beringian ice sheet reconcile glacial climate records from around North Pacific, Clim. Past Discuss., 2020, 1-25, 10.5194/cp-2020-38, 2020.

Simulating Marine Isotope Stage 7 with a coupled climate-ice sheet model

Dipayan Choudhury[1,2], Axel Timmermann[1,2], Fabian Schloesser[3], Malte Heinemann[4] and David Pollard[5]

[1]Center for Climate Physics, Institute for Basic Science (IBS), Busan 46241, South Korea
[2]Pusan National University, Busan 46241, South Korea
[3]International Pacific Research Center, University of Hawaii at Manoa, Honolulu, HI 96822, USA
[4]Institute of Geosciences, Kiel University, 24118, Kiel, Germany
[5]Earth and Environmental Systems Institute, Pennsylvania State University, Pennsylvania 16802, USA

Correspondence to: Dipayan Choudhury (dipayanc@pusan.ac.kr)

Abstract. It is widely accepted that orbital variations are responsible for the generation of glacial cycles during the late Pleistocene. However, the relative contributions of the orbital forcing compared to CO_2 variations and other feedback mechanisms causing the waxing and waning of ice-sheets have not been fully understood. Testing theories of ice-ages beyond statistical inferences, requires numerical modeling experiments that capture key features of glacial transitions. Here, we focus on the glacial build-up from Marine Isotope Stage (MIS) 7 to 6 covering the period from 240-170 ka (thousand years before present). This transition from interglacial to glacial conditions includes one of the fastest Pleistocene glaciation/deglaciation events which occurred during MIS 7e-7d-7c (236-218ka). Using a newly developed three-dimensional coupled atmosphere-ocean-vegetation-ice-sheet model (LOVECLIP), we simulate the transient evolution of northern and southern hemisphere ice-sheets during the MIS 7-6 period in response to orbital and greenhouse-gas forcing. For a range of model parameters, the simulations capture the evolution of global ice volume well within the range of reconstructions. Over the MIS 7-6 period, it is demonstrated that glacial inceptions are more sensitive to orbital variations, whereas terminations from deep glacial conditions need both orbital and greenhouse gas forcings to work in unison. For some parameter values, the coupled model also exhibits a critical North American ice sheet configuration, beyond which a stationary wave – ice-sheet topography feedback can trigger an unabated and unrealistic ice-sheet growth. The strong parameter sensitivity found in this study originates from the fact that delicate mass imbalances, as well as errors, are integrated during a transient simulation for thousands of years. This poses a general challenge for transient coupled climate-ice sheet modeling, with such coupled paleo-simulations providing opportunities to constrain such parameters.

Deleted: reconstructed

Deleted: reasonably

Deleted: . It

1 Introduction

Earth's climate over the past one million years (Late Quaternary) is characterized by glacial/interglacial cycles representing cold/warm periods, transitioning in timescales of around 80,000-120,000 years. These transitions correspond to global sea level changes of up to 130m (Fig. 1b) (Waelbroeck et al., 2002;Lisiecki and Raymo, 2005;Bintanja et al., 2005). Simulating these massive reorganizations of earth's climate using earth system models of varying complexity is an active area of research. By comparing such simulations with paleoclimate data, we can evaluate the fidelity of these climate models, as well as refine our understanding of the underlying sensitivities and feedbacks to a variety of forcings. One of the main obstacles in simulating variability on orbital timescales is the fact that ice-sheets are slow integrators of small imbalances between ablation and accumulation, which correspond to an average of 1.3mm/year global sea level equivalent during the build-up phase but can exceed 10mm/year for instance during the Last Glacial Maximum (LGM, 21ka). In order to simulate an entire glacial/interglacial cycle, model errors can accumulate for thousands of years and potential multiple equilibria of the fully coupled system can create further complications. Simulating a transient climate "trajectory" realistically is an even bigger modeling and computational challenge than simulating climate snapshots realistically, such as for the LGM (Yoshimori et al., 2002;Lunt et al., 2013;Colleoni et al., 2014a;Rachmayani et al., 2016).

Most efforts so far, with the notable exception of Ziemen et al. (2019), have used earth system models of intermediate complexity, EMICs, (Ganopolski and Brovkin, 2017;Ganopolski et al., 2010;Stap et al., 2014;Vizcaino et al., 2015;Calov et al., 2005;Heinemann et al., 2014;Willeit et al., 2019) or ice-sheet models (ISMs) coupled to statistical relationships, based on a set of coupled general circulation model (CGCM) timeslice runs (Abe-Ouchi et al., 2013;Colleoni et al., 2014b) to simulate the transient evolution of the coupled atmosphere-ocean-ice-sheet system. Bi-directional coupling between climate components and the ice-sheets, typically not captured in offline ice-sheet simulations (Born et al., 2010;Dolan et al., 2015;Koenig et al., 2015), is crucial in representing important feedbacks such as the ice albedo (Abe-Ouchi et al., 2013), elevation-desertification (Yamagishi et al., 2005) and the stationary wave – ice-sheet (Roe and Lindzen, 2001) feedbacks. Furthermore, it has been argued that the interaction between ice-sheets and ocean circulation (Timmermann et al., 2010;Rahmstorf, 2002;Knutti et al., 2004), and the resulting effects on the marine carbon cycle (Gildor and Tziperman, 2000;Menviel et al., 2012;Stein et al., 2020) can play a first-order role in shaping the climate evolution of the Quaternary on millennial and orbital timescales.

Glacial inceptions from warm mean states (interglacials) to cold mean states (glacials) over relatively short periods represent a bifurcation of the climate system and climate models have been shown to struggle in realistically simulating them (Calov and Ganopolski, 2005;Colleoni et al., 2014b). The glacial inception that has been studied most extensively is the one starting from the end of Last Interglacial (LIG, 125ka), corresponding to MIS 5a (Calov et al., 2005;Capron et al., 2017;Clark and Huybers, 2009;Crucifix and Loutre, 2002;Kubatzki et al., 2000;Nikolova et al., 2013;Otto-Bleisner et al., 2017;Pedersen et al., 2017). To our knowledge the penultimate interglacial, MIS 7 (240ka-170ka), has not received as much attention in ice-sheet modeling (Fig. 1). MIS 7 (Fig.1c and 1d) is the coldest interglacial occurring after the Mid Brunhes Event (MBE, ~430k) (Colleoni and Masina, 2014) with an intensity comparable to typical pre-MBE interglacials (Pages, 2016). Furthermore, CO_2 concentrations were lower than 260 ppmv for most of MIS 7. Contrary to the classic sawtooth pattern of the Earth's glacial cycle (gradual buildup and fast termination of ice sheets within 80,000-120,000 years) (Clark et al., 2009;Hays et al., 1976), the global ice volume during MIS 7e-7c increased rapidly and then decreased rapidly by around 60 m of global sea level equivalent (SLE, relative to present day) within a period of 20 ky (thousand years) (Cheng et al. (2016), Fig. 1). This is the

Deleted: about
Deleted: 3 mm
Deleted: .
Deleted: Last Glacial Maximum (
Deleted:)
Deleted: .

fastest such glaciation and deglaciation transition during the last 800 ky (Waelbroeck et al., 2002;Lisiecki and Raymo, 2005;Bintanja et al., 2005) although the last deglaciation had a sea level rise of ~100m in 10ky, which makes it an interesting test-case for coupled climate-ice-sheet models. Subsequently, the system stayed in a relatively stable interglacial state and descended into the next glacial state at the end of MIS 7a (~190ka) into MIS 6e. In this paper, we follow the lettering convention of MIS substages as suggested by Railsback et al. (2015). In summary, the climate system started from an interglacial and went into a glacial state for both MIS 7e-7d (235-225ka) and MIS 7a-6e (190-180ka) transitions, but bounced back to the interglacial state only for the MIS 7d-7c (225-215ka) state and not for MIS 6e-6d (180-170ka) (Fig. 1). The drivers of this unique phasing and amplitude of sea level high stands during MIS 7 still remain elusive. Both periods of pre-inception (MIS 7e-7d and 7a-6e) have similar orbital forcings and so do the periods post-inception (MIS 7d-7c and 6e-6d). But the CO_2 values differ by ~40ppmv. Although the CO_2 trends are similar over pre-inception, they differ in the post-inception times (Fig. 4a, Lüthi et al. (2008)). The CO_2 values rise steeply over MIS 7d-7c but stay low during MIS 6e-6d.

Most simulations struggle in realistically simulating the whole of MIS 7. Previous studies focusing on the MIS 7 have modeled MIS 7e and MIS 7a-7c as separate interglacials. For instance, Yin and Berger (2012) and Colleoni et al. (2014a) have simulated the climate during MIS 7e using LOVECLIM (Goosse et al., 2010) and CESM (Gent et al., 2011) respectively, and compared it to that during MIS 5. While Yin and Berger (2012) report the insolation-induced cooling during MIS 7e to be the primary reason for it being a cold interglacial, Colleoni et al. (2014a) suggest that 70% of the cooling over the Northern Hemisphere (NH) in MIS 7e compared to MIS 5 can be explained by CO_2 forcings. Further, Colleoni et al. (2014b) used CESM output to force an offline 3-D ice-sheet model (ISM), Grenoble Ice Shelf and Land Ice model (Ritz et al., 2001), and they were not able to produce as realistic results for MIS 7 as they could for MIS 5. Ganopolski and Brovkin (2017) simulated the last 400ky using the CLIMBER-2 EMIC (Petoukhov et al., 2000) coupled with the SICOPOLIS ISM (Greve, 1997). When forced with both orbital and CO_2 variations, they reported an exaggerated inception at MIS 6e (~180ka) followed by an overshoot to interglacial levels at MIS 6d (~160ka), while forcing with just orbital variations led to a much weaker glacial inception at MIS 6e. More recently, Willeit et al. (2019) performed transient simulations using the previous setup (CLIMBER-SICOPOLIS) forced with orbital, regolith removal and volcanic outgassing and also showed an overshoot to interglacial levels after the glacial inception of MIS 6e.

Our study presents transient simulations over the MIS 7-6 period which use a novel bidirectionally coupled 3-dimensional EMIC-ISM framework (LOVECLIM-PSUIM) with interactive ice sheets in both hemispheres. Using multiple ensemble runs, we test the sensitivity of the simulation to different forcing and model parameters. By comparing the MIS 7e-7c and MIS 7a-6d transitions, we investigate the relative role of orbital and CO_2 forcings on glacial inceptions and terminations. We also look at different climate-ice sheet feedbacks and local processes that induce a bifurcation in the system and can show abrupt changes in the climate-cryosphere system such as those in the Atlantic Meridional Overturning Circulation (AMOC).

In Sect. 2, the individual components of our coupled model and the coupling framework are described, along with a list of the experiments. Next, the main results are presented in Sect. 3, including multi-parameter ensemble simulations of ice sheet evolution, effects of orbital and CO_2 forcings pre and post glacial inception, abrupt changes in the climate-cryosphere system and the existence of multiple ice sheet equilibrium states. We conclude with a discussion of the key results and their implications for other glacial cycles along with key deficiencies in the current setup and possible solutions for future simulations.

Deleted: outputs

Deleted: ensembles

2 Methods

We perform a series of transient glacial inception simulations covering the period from 240-170 ka using the bi-directionally coupled LOVECLIM-PSUIM system, henceforth called *LOVECLIP*. Both LOVECLIM (Friedrich et al., 2016;Nikolova et al., 2013;Timmermann and Friedrich, 2016;Timmermann et al., 2014;Yin and Berger, 2012) and the Penn State University Ice sheet Model, PSUIM (DeConto and Pollard, 2016;Gasson et al., 2018;Pollard et al., 2015;Tigchelaar et al., 2018), have been extensively used for simulating past and future climate. The individual components of the modelling framework as well as their coupling strategy are described below.

2.1 LOVECLIM

LOVECLIM is a three-dimensional Earth System Model of Intermediate Complexity with atmosphere, ocean, sea ice and vegetation models coupled together (Goosse et al., 2010). The atmospheric component of LOVECLIM, ECBilt (Opsteegh et al., 1998), is a spectral T21 (5.625° × 5.625°) quasi-geostrophic model with three vertical levels including a parameterization of ageostrophic terms. The effect of CO_2 variations with respect to the reference CO_2 concentration (356 ppm) on the longwave radiation flux is scaled up by a factor α (Eq. 1), to account for the low default sensitivity of ECBilt to changes in CO_2 concentrations (Friedrich and Timmermann, 2020;Timmermann and Friedrich, 2016;Timm et al., 2010). The effect of CO_2 on the longwave radiation is given as:

$$LWR = \alpha . a(\lambda, \phi, p, t_{season}) . \log\left[\frac{CO_2(t)}{CO_2^{ref}}\right] \quad (1)$$

where LWR is the longwave radiation flux from CO_2; α is our scaling factor for the transfer coefficient, a, which is a function of longitude, latitude, height and season; CO_2^{ref} is the reference CO_2 value set at 356 ppm. α changes the sensitivity of our model. For reference, the equilibrium climate sensitivity for CO_2 doubling is 3.69K for α of 2. Climate sensitivity is a non-trivial measure that can be changed in many different ways. For instance, changing the cloud parameterization or surface parameters would change both the longwave and shortwave forcings. Adjusting multiple parameters may not necessarily lead to more realistic simulations. While it is possible that the climate sensitivity to some of the other forcings are also weak (Timm and Timmermann, 2007), we use a simple alpha (α) parameter to change only the longwave sensitivity to CO_2, and not to other greenhouse gases. α is determined based on transient past and future simulations.

The ocean component, CLIO (Goosse and Fichefet, 1999), is a free-surface primitive-equation ocean general circulation model with 3° × 3° horizontal resolution and 20 vertical levels; which is further coupled to a thermodynamic-dynamic sea ice model. Additionally, an iceberg model is employed that integrates iceberg trajectories (based on Coriolis force, air-water-sea ice drag, horizontal pressure gradient and wave radiation) and melt (depending on basal plus lateral melt and wave erosion along individual iceberg pathways) (Schloesser et al., 2019;Bigg et al., 1997). The atmosphere-ocean coupling is based on the freshwater, heat and momentum flux exchanges. The Bering Strait is opened and closed interactively depending on global mean sea level height. Specifically, its parameterized transport is multiplied with a constant that is zero for sea levels lower than – 50 m meters and linearly increases to 1 as global sea level rises to -25 m relative to present day. The terrestrial biosphere component of LOVECLIM, VECODE (Brovkin et al., 1997), estimates the evolution of vegetation cover (fraction of grass, trees and desert) over each land grid cell not covered by ice.

2.2 PSUIM

PSUIM is a hybrid ice-sheet-ice-shelf model that combines the scaled shallow ice and shallow shelf approximations (Pollard and DeConto, 2012b). It has been shown to reasonably capture both slow and fast flowing grounded ice regimes as well as floating ice shelves while being simpler and more computationally efficient than Full-Stokes or Higher-Order models. The

Deleted: 365ppm

Deleted: . α is determined based on transient past and future simulations. …

Deleted: (

model also accounts for free grounding-line migration based on a sub-grid parameterization that calculates ice fluxes at the grounding line based on Schoof (2007). The ice is determined to be grounded or floating based on buoyancy, as per:

$$\left.\begin{array}{l} \rho_w(S-h_b) < \rho_i h; \text{ and } h_s = h + h_b; \text{ for grounded ice (ice sheet)} \\ \rho_w(S-h_b) > \rho_i h; \text{ and } h_s = S + h\left(1-\frac{\rho_i}{\rho_w}\right); \text{ for floating ice (ice shelves)} \end{array}\right\} \quad (2)$$

where $\rho_w = 1028 kgm^{-3}$ is the density of ocean water; $\rho_i = 910 kgm^{-3}$ is the ice density; S is the sea level (m); h_b is the bedrock elevation (m); h is the ice thickness (m); and h_s is the ice surface elevation (m).

PSUIM calculates the surface energy and mass balances, by including the temperature and radiation contributions, to solve for surface melting and freezing (Robinson et al., 2010;Van Den Berg et al., 2008). Specifically, the energy flux available for melting ($dE > 0$) or refreezing ($dE < 0$) is given by:

$$dE = b(T - T_o) + (1-a)Q - m, \quad (3)$$

where constant $b = 10\, Wm^{-2}K^{-1}$, T is the surface air temperature, T_o the freezing point, a the albedo, Q the surface incoming short wave radiation, and parameter m a constant (see Sect.2.3). The albedo is linearly interpolated between values for no snow ($a_{ns} = 0.5$), wet snow ($a_{ws} = 0.6$), and dry snow ($a_{ds} = 0.8$),

$$a = (1 - r_s)a_{ns} + r_s[r_l a_{ws} + (1 - r_l)a_{ds}], \quad (4)$$

where r_s is the snow covered area fraction and r_l the ratio between liquid water contained in the snow mass and the maximum embedded liquid capacity. The parameter 'm' in Eq. (3) represents net upwards infrared radiation from a solid surface at temperature T_o to the atmosphere, plus a constant correction for other simplifications in Eq. (3) and has units of Wm^{-2}.The surface mass balance is then calculated based on snow fall (which is calculated locally based on total precipitation and temperature) and melting/refreezing based on dE. This surface mass balance is calculated at timesteps of 3 hours. Monthly surface air temperature (T) and surface incoming shortwave radiation (Q) (obtained from LOVECLIM in the current setup, discussed further in Sect. 2.3) are interpolated into sub-daily values in two steps. Firstly, the monthly values are interpolated to daily values using a weighted averaging of the values across two adjacent months. Next, a sinusoidal cycle with max temperature at 1400 and minimum at 0200, with a peak-to-peak amplitude of 10˚C, is superimposed on the daily data to account for diurnal variations.

The sub-ice-shelf ocean melting is calculated as per Pollard et al. (2015) using ocean temperature at 400m depth (T_o) from LOVECLIM as follows:

$$OM = \frac{KK_T\rho_w c_w}{\rho_i L_f}|T_{oc} - T_f|(T_{oc} - T_f) \quad (5)$$

where OM is the subshelf ocean melting rate (myr^{-1}), T_{oc} is the LOVECLIM ocean temperature at 400m depth (°C), T_f is the ocean freezing temperature at depth z (m) calculated as $T_f = 0.0939 - 0.057 \times 34.5 - 0.000764 \times z$, $K_T = 15.77 myr^{-1}K^{-1}$ is a coefficient; K is a non-dimensional factor of order 1, $K = 3$; $c_w = 4218 Jkg^{-1}K^{-1}$ is the specific heat of ocean water; and $L_f = 0.335 \times 10^6 Jkg^{-1}$ is the latent heat of fusion.

Calving is primarily parameterized depending on the ice shelf flow divergence. The model also includes parameterizations for surface meltwater and rainfall-driven hydrofracturing and the structural failure of tall sub-aerial ice cliffs, which produce strong ice retreat in Antarctic marine basins needed to explain past high sea level stands suggested by geologic data (DeConto and Pollard, 2016;Pollard et al., 2015). The sea level dependence is implemented by the formulation of boundary processes, such as calving, flotation of ice, grounding line dynamics and sub-grid pinning by bedrock bumps, which also affects the grounding line flux (Schoof, 2007). PSUIM is used to simulate ice sheets in both hemispheres. The bedrock deformation is

Deleted: 1
Deleted: 2
Deleted: appears
Deleted: 1
Deleted: 1
Deleted: the

calculated by an ELRA (Elastic Lithosphere Relaxing Asthenosphere) model, assuming a bedrock density of 3370 kgm^{-3} and an isostatic asthenospheric relaxation time of 3000 years (Pollard and DeConto, 2012b). The basal sliding velocity is defined as in Pollard and DeConto (2012b) and depends on the basal sliding coefficient:

$$u_b = C'|\tau_b|^{\mu-1}\tau_b \,, \quad (6)$$

where u_b is the basal sliding velocity, τ_b is the basal stress; μ is the basal sliding exponent (=2); C' is the basal sliding coefficient which is a function of the basal homologous temperature:

$$C' = (1-r)C_{froz} + rC(x,y) \,, \quad (7)$$

with $r = max[0, min[1, (T_b + 3)/3]]$; where T_b(°C) is the basal homologous temperature relative to the pressure melting point ($T_m = -0.000866h$, h being the ice thickness in m); and $C_{froz} = 10^{-20}$m yr^{-1}Pa^{-2} (which cannot be zero to avoid numerical inconsistencies but is small enough to allow essentially no sliding). For Antarctica, the sliding coefficient $C(x,y)$ is deduced from the inverse modelling approach of Pollard and DeConto (2012a). For the NH, a binary sliding coefficient map is used with higher sliding over present-day oceans ($C(x,y) = 10^{-6}$m yr^{-1}Pa^{-2} representing deformable sediments), and low sliding over present-day land ($C(x,y) = 10^{-10}$m yr^{-1}Pa^{-2} representing non-deformable rock).The model was tested at two resolutions for each hemisphere; for the NH, a longitude-latitude grid is used at either 1 × 0.5° or 0.5 × 0.25°, and for Antarctica, a polar stereographic grid is used at either 40 × 40 km or 20 × 20 km. No significant differences in the results using the two resolutions were noticed for either hemisphere. All the results presented in this paper use 1 × 0.5° for the NH and 40 × 40 km for Antarctica.

2.3 LOVECLIP

Figure 2 shows the coupling algorithm employed in the current setup to exchange information across LOVECLIM and PSUIM, between alternating climate model and ice sheet runs (chunks). LOVECLIM chunks of length T_L alternate with PSUIM chunks of length T_P ($\geq T_L$). Here we define the acceleration factor $N_A = T_P/T_L$. An earlier version of this coupling algorithm was used by Heinemann et al. (2014) for a different ISM (Ice sheet model for Integrated Earth system Studies (Saito and Abe-Ouchi, 2004) that was active only in the NH and did not include ice shelf-dynamics. The coupling strategy has the advantage of using asynchronous coupling to speed up climate simulations at millennial to orbital timescales (Friedrich et al., 2016;Tigchelaar et al., 2018;Timm and Timmermann, 2007;Timmermann and Friedrich, 2016). The fidelity of using the acceleration factor depends on how quickly the variables of interest equilibrate to the slowly evolving external boundary conditions. Preliminary experiments (not shown) with different acceleration factors suggest that the simulated ice sheet evolution is relatively insensitive to N_A for $N_A \leq 5$. Therefore, $N_A = 5$ is used for the simulations presented in this paper, providing a good compromise between the objective to simulate realistic ice sheet evolution and computational efficiency.

PSUIM uses surface air temperature (T), precipitation (P), solar radiation (Q), and ocean temperature at 400m depth (T_o) as inputs from LOVECLIM. These are downscaled using a bilinear interpolation approach. The surface temperature and precipitation outputs from LOVECLIM which are used for the PSUIM surface mass balance are bias-corrected in the coupler, following Pollard and DeConto (2012b), Heinemann et al. (2014) and Tigchelaar et al. (2018).

$$T(t) = T_{LC}(t) + T_{obs} - T_{LC,PD} \quad (8)$$

$$P(t) = P_{LC}(t) \times P_{obs}/P_{LC,PD} \quad (9)$$

where T is monthly surface air temperature and P is monthly precipitation forcing from LOVECLIM at timestep t. Subscripts 'LC', 'obs' and 'LC, PD' refer to LOVECLIM chunk output, observed present day climatology, and LOVECLIM present day control run, respectively. The observed present day climatology is obtained from the European Centre for Medium-Range Weather Forecasts reanalysis dataset, ERA-40 (Uppala et al., 2005). These LOVECLIM biases are calculated for PD

Deleted: 3
Deleted: 4
Deleted: model results do not change significantly when $N_A \leq 5$
Deleted: ,
Deleted: ,
Deleted: ,
Deleted: and
Deleted: .
Deleted: 5
Deleted: 6

simulations using an LGM bathymetry. We did compare the biases between using a PD or LGM bathymetry, and while there were regional differences, the large-scale structure was found to be similar (not shown). The annual mean of the monthly mean bias correction terms $T_{obs} - T_{LC,PD}$ and $P_{obs}/P_{LC,PD}$ are presented in Fig. S1. Temperature biases in LOVECLIM for boreal summer (JJA) and austral summer (DJF) are shown in Fig. S2 for reference, since summer temperatures are more crucial for ice sheet growth and decay. Furthermore, a lapse-rate correction of 8°C km^{-1} is applied to account for differences between LOVECLIM orography and PSUIM topography for the interpolated temperature, $T(t)$, and precipitation is multiplied by a Clausius–Clapeyron factor of $2^{\frac{-\gamma.\Delta H}{10°C}}$, with $\gamma.\Delta H$ being the temperature lapse-rate correction, to account for the elevation desertification effect (DeConto and Pollard, 2016):

$$T_{PSUIM}(t) = T_{interp}(t) - \gamma.\Delta H \quad (10)$$

$$P_{PSUIM}(t) = P_{interp}(t) \times 2^{\frac{-\gamma.\Delta H}{10°C}} \quad (11)$$

where T_{PSUIM} and P_{PSUIM} are the final temperature and precipitation inputs for PSUIM, T_{interp} and P_{interp} are bias corrected LOVECLIM temperature (T, Eq. 8) and precipitation (P, Eq. 9) interpolated to PSUIM resolution, γ is the lapse rate (8°C km^{-1}), and ΔH is the altitude difference between PSUIM grids and the corresponding LOVECLIM grid. Colleoni and Liakka (2020) used a similar fixed atmospheric lapse rate correction during downscaling temperature to their ice model, GRISLI, with γ as 3.3°C km^{-1} for annual mean and 4.1°C km^{-1} for summer mean. And they reported slightly smaller ice sheets on using an elevation dependent lapse rate, going all the way up to 7.9°C km^{-1}. Instead of using a fixed value of γ, both Roche et al. (2014) and Bahadory and Tarasov (2018) used a dynamic lapse rate, where γ is estimated locally for the ice model grids in each LOVECLIM grid. Moreover, the lapse rate also depends on the atmospheric CO_2 concentration. Such dynamic lapse rate corrections are not implemented in the current setup, and neither is the advective precipitation downscaling scheme of Bahadory and Tarasov (2018).

Surface incoming shortwave radiation from LOVECLIM (Q, Eq. (3)) is bilinearly interpolated to PSUIM grid and then used to calculate the surface mass balance. PSUIM calculates albedo using snow covered fraction (r_s) and the ratio between liquid water contained in the snow mass and the maximum embedded liquid capacity (r_l) from the last year of its previous chunk. This provides a more realistic estimate of the albedo than downscaling from LOVECLIM. T_{oc}, used in calculating the ocean sub-ice-shelf melting (Eq. 5) is interpolated to PSUIM grid using conservative remapping. For some of the floating ice (shelves) in PSUIM (Eq. 2), the ocean points underneath may not get an ocean temperature assigned on interpolation from LOVECLIM, since the land-sea mask in LOVECLIM is kept constant. For each of such grid points, the algorithm averages over the neighboring eight PSUIM grid points and this process is repeated until all PSUIM ocean points get ocean temperatures.

LOVECLIM orography and surface ice mask are updated based on the evolution of ice sheets and bedrock elevation from PSUIM. The PSUIM topography is upscaled to LOVECLIM grid using simple weighted averaging. Each grid cell of ECBilt and VECODE is defined as either ice-free or ice-covered (not fractionally covered); it is ice-covered if more than half of the cell has more than 10 m of ice in the finer PSUIM cells that lie within the LOVECLIM cell, thus changing the ground albedo to ice albedo. The total meltwater from basal melting and liquid runoff in PSUIM is dynamically routed based on PSUIM topography till it reaches the ocean or the domain edge, and then is routed to the nearest ocean grid point in LOVECLIM. The calving flux is channeled into CLIO's iceberg model (Schloesser et al., 2019;Jongma et al., 2009) in the Southern Hemisphere (SH) and as an iceberg melt flux (freshwater flux and heat flux) in the NH (Schloesser et al., 2019). While both freshwater flux and freshwater volume cannot be simultaneously conserved in an accelerated run (Heinemann et al., 2014), we conserve freshwater flux in the current setup. The primary rational for this being that surface freshwater and meltwater fluxes are balanced by the convergence of ocean salt fluxes in equilibrium states, and adjustments of the ocean circulation are thought to occur rapidly compared to those of ice sheets. PSUIM is forced by LOVECLIM precipitation and LOVECLIM by PSUIM

Deleted: Figure

Deleted: , for surface temperature T

Deleted: $2^{\frac{\Delta T}{10°C}}$

Deleted: ΔT

Deleted: .

Deleted: Basal

Deleted: from

Deleted: discharged via LOVECLIM's runoff masks in both hemispheres; while

runoff. During a glacial inception (termination), the runoff from PSUIM into LOVECLIM reduces (increases) as ice sheets grow. This reduction (increase) in runoff into the ocean, relative to the evaporation, increases (decreases) the salinity of the ocean. This salinity change is spatially resolved.

The contributions of the ice sheets to global sea level changes are calculated independently for the two hemispheres in PSUIM, and the net sea level change is used for the next chunk of ice model run. Note, however, that LOVECLIM does not see the change in sea level, and the ocean bathymetry and land-sea mask (with the exception of the Bering Strait opening and closing) are not updated in the coupling framework. Our coupled simulations use the LGM bathymetry and land-sea mask throughout the entire transient simulation.

2.4 Experiments

The LOVECLIP experiments are initialized using present day ice sheet conditions and spun up using orbital and greenhouse gas (GHG) forcings of 240 ka for a period of 10ky. The model equilibrates to an ice sheet distribution in the NH corresponding to -20m SLE, implying an open Bering Strait. Our initial ice sheet distribution at 240ka is shown in Fig. 4c and is in close agreement with that used by previous studies such as Colleoni and Liakka (2020) for 239ka and Colleoni et al. (2014b) for 236ka. From these initial conditions, LOVECLIP is run forward with two transient forcings: Orbitally induced solar insolation variations following Berger (1978); and time-varying atmospheric GHG concentrations measured from the European Project for Ice Coring in Antarctica Dome C ice core (Loulergue et al., 2008;Lüthi et al., 2008;Schilt et al., 2010). Two additional sets of experiments are run to discern the independent effects of the two primary forcings: (1) Time varying orbital forcing with constant GHG concentration (set at its value for 240 ka), and (2) Constant orbital forcing (set at the orbit for 240 ka) and time varying GHG concentrations.

Furthermore, sensitivity experiments with different GHG sensitivities (α, Sect. 2.1) and melt parameterizations (m, Sect. 2.2) are run with full forcing. Generally, higher α leads to a stronger sensitivity to CO_2 concentrations, and higher values of m strengthen buildup and weaken melting of ice during interglacial climates. These experiments are presented in the first row of Table 1 (1-15) and Fig. 3. Additional simulations with different combinations of acceleration (N_A), GHG sensitivity (α), melt parameter (m), basal sliding coefficient maps over the NH ($C_{(x,y)}$) and higher ice model resolution ($0.5 \times 0.25°$ for NH, 20×20 km polar stereographic for Antarctica) have been performed (experiments 16-50 in Table 1). The whole ensemble of simulations is presented in Fig. S3. Although we note that these experiments do not present a systematic evaluation of the full parameter space, ice sheet trajectories are consistent with and thereby support the conclusions presented in this paper. For benchmarking purposes, our model throughputs ~1200 years per day on one node at the University of Southern California Center for High-Performance Computing, so for an acceleration (N_A) of 5, we simulate 6000 years per day in real time.

Deleted: All the experiments presented in the paper are conducted with an acceleration factor $N_A = 5$. Ensembles of the full forcing experiments …

Deleted: also

Deleted: to test the sensitivity of the model to different sets of parameters. Higher

Deleted: larger response of ice to changes in

Deleted: . And generally speaking,

Deleted: lead to stronger

Deleted: weaker

Deleted: All of the

Deleted: listed in Table 1.

3 Results

3.1 Overview of multi-parameter ensemble coupled simulations

Figure 3 shows the simulated ice volume in SLE (m) from experiments that best describe parameter sensitivities, while the complete ensemble of simulations is presented in Fig. S3. Figure 3a shows the most realistic simulation (referred to as baseline simulation BLS, experiment 1 in Table 1) in comparison to the sea level reconstructions of Spratt and Lisiecki (2016). Parameter sensitivities will be further discussed below. The model captures the overall trajectory of ice volume evolution reasonably well. Specifically, the model stays within the uncertainty range for the extreme glaciation-deglaciation event of

Deleted:).

Deleted: Although

MIS 7e-7d-7c. Larger differences only exist as the glaciation into MIS 6 is delayed by ~3ky in the simulation (191ka instead of 194ka). A possible explanation for this discrepancy may be related to the temporal uncertainty in reconstructions themselves, since a similar lag occurs in other modeling studies (e.g., Ganopolski and Calov (2011); Ganopolski and Brovkin (2017). Higher climate sensitivity (α) leads to a faster and stronger glacial inception and termination at the MIS 7e-7d-7c transition, in response to the time-varying orbital forcing and CO_2 changes (Fig. 3b). Increasing the value of the melt parameter, m (Eq. (3), leads to a deeper inception and much weaker termination (Fig. 3c). The most realistic simulation is obtained for $\alpha = 2$ and $m = 125$ Wm^{-2}. Unless otherwise mentioned, all results presented in this study are from this particular ensemble member (labelled BLS). When the climate sensitivity (α) or the parameter in the linear energy balance model (m) exceed certain thresholds, our model simulates an unrealistic runaway glaciation. The model physics underlying this feature will be described further below. Following the concerns raised in Edwards et al. (2019), we ran a BLS simulation with hydrofracturing and cliff instability inactive and found no differences in the ice evolutions. This finding illustrates the complexity of the task to better constrain associated parameters in comparison of paleo climate simulations and data.

Deleted: is very well simulated,
Deleted: This
Deleted: can be also found
Deleted: such as and
Deleted: and
Deleted: , and we could not identify a reason for this discrepancy between simulations and reconstructions. Only a selection of ensembles is shown here that depict the sensitivity of the model to physical and model parameters in a representative way. Higher climate sensitivity (α) leads to a much
Deleted: 1))
Deleted: Clearly, if either
Deleted: The underlying model physics involved in this feature will be described further below.

3.2 Ice sheet evolution

The rapid waxing and waning of ice sheets during the MIS 7e-7d-7c transition is presented in terms of maps of ice height and basal velocities in Fig. 4. In our simulations, the primary contribution to the ice volume evolution during MIS 7-6 comes from the NH (blue line in Fig. 4b). SH only contributes around 10m SLE during the interstadial of MIS 7c (red line in Fig. 4b). During the short transition (~10ky) from MIS 7e (235ka, Fig. 4c) to MIS 7d (226ka, Fig. 4e), ~4km thick Laurentide and ~3km thick Cordilleran ice sheets are built up over the NH. The Eurasian ice sheet grows substantially slower in our simulations during this period. Although the contribution of Antarctica during MIS 7d is less than 5m, the Filchner-Ronne ice shelf spreads further out into the Weddell Sea (Fig. 4f, ice shelves do not directly contribute to sea level change). This quick glaciation event coincides with decreasing NH summer insolation and CO_2 forcings. Although NH insolation reaches a minimum at ~230ka and starts rising again, CO_2 stays higher than 220ppm till ~227ka and drops only just before MIS 7d (~226ka, Fig. 4a). Subsequently, a rapid deglaciation event occurs, associated with a steep increase in both orbital and GHG forcings over MIS 7d to 7c. Our model successfully simulates ice sheet retreat similar to a saddle collapse of Laurentide and Cordilleran splitting (Gregoire et al., 2012). While some studies have suggested the sea level peak at MIS 7c to be lower (Dutton et al., 2009) than those at MIS 7e and 7a, our model simulates MIS 7c to be the highest peak in MIS 7 with marked deglaciation of the Laurentide and Cordilleran, reduced Innuitian, Greenland, and small Icelandic and Norwegian ice sheets (Fig. 4g), along with a reduced West Antarctic ice sheet (Fig. 4h). The highest contribution of SH to MIS 7 of ~10m (Fig. 4b and 4h) occurs during MIS 7c. After a relatively stable interglacial state till MIS 7a, the system moves into a glacial state. At the end of the simulation, our model simulates a bigger Laurentide and relatively smaller and detached Cordilleran as the model glaciates into MIS 6 (Fig. 4i).

Deleted: Our
Deleted: suggest that
Deleted: came
Deleted: In
Deleted: Our simulation shows the
Deleted: builds up much less
Deleted: Next, there is
Deleted: corresponding to the
Deleted: by the
Deleted: the next glacial and reaches
Deleted: equilibrium
Deleted: Although studies of NH reconstructions

In the context of previous modelling studies and geological records over this MIS 7-6 period, our ice sheet distribution at MIS 7c (212ka, Fig. 4g and 219.5ka, Fig. S7) is very similar to that reported in Colleoni and Liakka (2020). However, we simulate a stronger inception compared to that of Colleoni et al. (2014b) over the corresponding 236-230ka period. They also reported a bifurcated but connected North American ice sheet at MIS 6 (157ka) from both their control (100km) and high resolution (40km) experiments. Our simulation results in separate Laurentide and Cordilleran ice sheets but generates neither a Eurasian nor a Siberian ice sheet, albeit at 170ka. On a side note, our North American ice sheet distribution at 180ka (Fig. 7) is closer to that of Colleoni and Liakka (2020) at 157ka. Studies of NH reconstructions during MIS 6 such as Svendsen et al. (2004), over 160-140ka, Rohling et al. (2017), around 140ka, and Batchelor et al. (2019), over 190-132ka, have all reported glacial geological records to indicate a larger extent of the Eurasian ice sheet at MIS 6 glacial maximum compared to the LGM, while

Deleted: and more recently,
Deleted: , have suggested a larger Eurasian ice sheet over the MIS 6 period (160-140ka), our simulations show a persistent Fenno-Scandian ice sheet and a relatively small Eurasian ice sheet at 170ka

our simulations only show a persistent Fenno-Scandian ice sheet and a relatively small Eurasian ice sheet at 170ka. More recently, Zhang et al. (2020) reported the existence of a Northeast Siberia-Beringian ice sheet at MIS 6e (190-180ka) using NorESM-PISM simulations validated by North Pacific geological records. However, our model does not simulate any ice over Alaska, Beringia and northeast Siberia over MIS 7-6.

Our model's difficulty in simulating the Eurasian ice sheet can be attributed to the competition between Laurentide and Eurasian ice sheet growth, which makes it arduous to realistically simulate them simultaneously alongside generating the right atmospheric patterns. Some previous studies have suggested that teleconnections from stationary wave patterns induced by a large Laurentide ice sheet could lead to warming over Europe and influence Eurasian ice sheet evolution (Roe and Lindzen, 2001;Ullman et al., 2014). The Laurentide building up first in our simulations could have changed the storm tracks and dried out Eurasia. It is also worth reiterating that LOVECLIM has a coarse T21 grid with a simple 3-layered atmosphere. While the circulation changes reported here maybe model dependent, Lofverstrom and Liakka (2018) reported that at least a T42 grid was needed in their atmospheric model (CAM3) to generate a Eurasian ice sheet using SICOPOLIS, albeit for the LGM. They attribute this discrepancy to lapse rate induced warming due to reduced and smoother topography and higher cloudiness leading to increased re-emitted longwave radiation towards the surface. These teleconnection patterns are further discussed in Sect. 3.6. Our LOVECLIM setup also uses a fixed lapse rate for downscaling LOVECLIM surface temperatures (Eq. 10 and 11), while both Roche et al. (2014) and Bahadory and Tarasov (2018) used a dynamic lapse rate, which is estimated locally for the ice model grids in each LOVECLIM grid. Bahadory and Tarasov (2018) reported ice thickness differences up to 1km on using the dynamic lapse rate scheme compared to a fixed 6.5°Ckm^{-1}. Nevertheless, for runaway trajectories, our model can build up a Eurasian ice sheet for ice volumes greater than -200m SLE once the Laurentide growth slows down (not shown). Our modelling setup also does not account for sub-grid mass balances, which can be especially relevant over mountainous regions with large sub-grid relief such as Alaska (Le Morzadec et al., 2015). Coarse grids tend to average out tall peaks and low valleys and thus don't capture the non-linear combination of accumulation zones on the high peaks and ablation zones in the valleys. These shortcomings could explain the lack of Eurasian, Siberian and Beringian ice sheets in our simulations.

3.3 Effects of orbital and GHG forcings

Figure 5 shows the effects of the individual orbital and GHG forcings on the simulated ice volume. As expected, keeping both orbital and GHG forcings fixed at 240ka values leads to no change in the ice volume (control run, dashed line). Forcing with only GHG variations alone (red line) leads to a small cooling trend compared to the control run but does not simulate any glacial inceptions. On the other hand, forcing with orbital variations only (blue line) does simulate glacial inceptions, albeit only half of the magnitude over MIS 7e-7d-7c, and the system does not glaciate completely at MIS 6 (170ka). This can be attributed to the fact that the NH summer insolation at 170ka is relatively strong at almost interglacial levels (Fig. 1a and 4a) and that the MIS 6 inception might have been controlled by the low GHG values. We also performed orbital only runs with different background CO_2 values of 180,200,220,240,260 and 280 ppmv, instead of keeping CO_2 constant at 240ka values (~245 ppmv); and found the model to still simulate the inception over MIS 7e-7d (not shown). Our orbital-only simulation is also very similar to the run of Ganopolski and Brovkin (2017) which was forced with orbital variations only with a constant CO_2 concentration of 240ppm (ONE_240 experiment, green line in their Fig. 8). Although they simulated the 7e-7d-7c transition well, their orbital-only run did not glaciate successfully into MIS 6. This suggests that glacial inceptions, at least over the MIS 7-6 period, are primarily controlled by orbital forcings, discussed further in the next Sect. 3.4, supporting previous studies of Ganopolski and Brovkin (2017), Yin and Berger (2012) and Ganopolski and Calov (2011). However, it is imperative to restate that orbital forcings alone cannot force the system into the MIS 6 glacial, and low GHG values over 180-170ka are crucial for the MIS 6 inception. Please note that all four runs in Fig. 5 were conducted with GHG sensitivity (α) = 2 and melt

parameter (m) = 125 Wm^{-2}, and different values of the parameters might have led to different ice sheet evolutions and different sensitivities with respect to orbital and greenhouse gas forcing.

3.4 Effects of forcings pre and post inception

In Figures 4a and 4b we highlight two 20ky periods in shading (235-215ka and 190-170ka) in dark and light grey colors. The dark grey periods (235-225ka and 190-180ka) are characterized by minimum values of NH summer insolation and the buildup of ice volume. The light grey marked periods (225-215ka and 180-170ka) correspond to peak summer insolation. In case of MIS 7d-7c, we observe a glacial termination, whereas the MIS 6e-6d period is characterized only by small changes in ice volume. By compositing the climate evolution over the NH for these two periods, we can further explore the reasons for the varying ice sheet responses during the MIS 7d-7c and the MIS 6e-6d periods (Figure 6). MIS 7e-7d-7c (MIS 7a-6e-6d) data are marked by dashed (solid) lines. Figure 6a shows the similarity of the orbital forcings during both periods. In contrast, their respective CO_2 evolutions are very different (Figure 6b). Even though the CO_2 values are markedly different in the first part (10ky) of the two periods (Fig. 6b), the simulated total NH ice volume evolution is quite similar (Fig. 6c). This highlights the relevance of orbital forcing during glacial inceptions. In spite of orbital forcing being similar over the second half of the composite figure, model trajectories diverge markedly. The successful glacial termination coincides with increasing CO_2 concentrations (dashed line), whereas the aborted termination during MIS 6e-6d (180-170ka, solid line) is associated with flat-lined glacial CO_2 values (Fig. 6a-6c). Although the insolation maximum is weaker for the later period (MIS 7a-6e-6d) compared to the earlier period (MIS 7e-7d-7c), we argue the full inception of the later period to be primarily driven by changes in CO_2. This is further supported by the orbital-only run showing a substantially weaker inception and subsequent termination over MIS 7a-6e-6d compared to MIS 7e-7d-7c (Figure 5), suggesting that the latter full inception could not be attributed only to an insolation threshold. Likewise, the global average surface temperature evolution is similar for the pre-inception case but different for the post-inception cases (Fig. 6d).

For both periods the Atlantic Meridional Overturning Circulation (AMOC) is strongest during the inception phase, and weaker during termination (Fig. 6e). The AMOC weakening is substantially more pronounced in the earlier period, following the successful termination. In both periods, the AMOC recovers almost to its full interglacial state. The reduced AMOC (Fig. 6e) could lead to increased subsurface warming (Liu et al., 2009;Clark et al., 2020) causing the higher subsurface melting in Fig. 6i. Figure 6 also shows the evolution of the different mass balance terms for both the pre-inception and post-inception cases. Accumulation and ablation depend on the surface temperature over and the extent of the ice sheets (Fig. 6f and 6g). As ice sheets grow further equatorward, they come in contact with warmer moist air leading to a positive feedback on the ice growth because of higher moisture carrying ability of warm air. But higher temperatures also lead to higher ablation because of increased surface melting. Furthermore, as the ice sheet grows in height, accumulation decreases because of the elevation desertification effect (DeConto and Pollard, 2016), while ablation reduces due to the lapse rate. Although accumulation and ablation can change both in and out of phase, the delicate interplay of leads and lags between them governs the sign of the net surface mass balance (Fig. 6h). For the pre-inception cases, accumulation leads ablation producing a net positive surface mass balance (SMB) till it reaches peak glaciation for both time periods. Subsequently, the SMB turns negative only for the second half of the 7e-7d-7c period and not the 7a-6e-6d period (Fig. 6e-g). The deglaciation is initiated by increased ablation around 4ky after the inception at MIS 7d (~221ka, dashed line in Fig. 6g), corresponding to the increasing CO_2 (dashed line in Fig. 6b), followed by a decrease in accumulation (dashed line in Fig. 6f) that can be attributed to the ice sheets retreating further north. Also, the ablation over 7d-7c (225-215ka, Fig. 6g) contains an additional saddle collapse (Gregoire et al., 2012) contribution when the Laurentide and Cordilleran ice sheets separate (Fig. 4e) leading to higher surface melting followed by rapid melting of both ice sheets. This shows up as the sharp spike in ablation around 15ky of the 7e-7d-7c transition (~220ka,

Deleted: However, in

Deleted: and in spite of similar orbital forcing, we see a very different behavior, with one

Deleted: , due to

Deleted: and an

Deleted:), due to

Deleted: 6a-6c).

Deleted: Any difference in the patterns within the two time periods of pre-inception and those of post-inception periods can be attributed to the difference in CO_2 evolution.

Deleted: However, unlike ice volume and surface temperature evolutions, the time evolution of the Atlantic Meridional Overturning Circulation (AMOC) is very similar for both periods (Fig. 6e). Even over the 180-170 ka period in the post-inception case of high NH ice volume, the AMOC recovers almost to its full interglacial state.

Fig. 6g) and amounts to the steep negative SMB in Fig. 6h. Together with the negative subshelf melting spike in Fig. 6i, this leads to a ~10m rapid increase in SLE around 219.5ka in Fig. 6c and Fig. 4b. Such abrupt changes are discussed further in Sect. 3.5. Although the Laurentide and Cordilleran ice sheets separate during the period 180-170ka, the net SMB does not exhibit a negative trend. This can be attributed to the low CO_2 value (<200ppmv) leading to lower temperatures (Fig. 6d) and reduced ablation even if the Laurentide extends equatorward (Fig. 6g). Furthermore, the southern extent of the Laurentide can lead to changes in circulation patterns that can alter the SMB (discussed in Sect. 3.6).

Deleted: low enough

Deleted: to avoid

3.5 Abrupt changes in the coupled climate-cryosphere system

One advantage of using a fully coupled framework is that feedbacks in the climate-ice-sheet system can be simulated and understood. Here we focus on the feedbacks that lead to exceptionally fast ice loss around 220ka during the MIS 7d-7e transition; with anomalies of different climate variables during this transition for 220.5ka, 220ka and 219.5ka shown in Fig. S4, S5 and S7 respectively. A 3˚C anomalous subsurface warming over Baffin Bay at 220.5k (Fig. S4b) causes the Laurentide ice-sheet to melt from the east (Fig. S4a, S4d and S4f). At the same time, as the very western margin of the Laurentide starts thinning, it becomes a floating ice shelf instead of being grounded, as can be seen by the grounding line and ice velocities in Fig. S4a. This is because as the ice-sheet retreats, land areas below sea-level become exposed, which are connected to ocean points. PSUIM then assumes that the points will become ocean points and therefore the thinning western Laurentide changes from a grounded ice sheet to an ice shelf (grounding line in Fig. S4a). This shelf on the western margin has a surface temperature relatively warmer than the rest of Laurentide (Fig. S4c) and shows a weakly positive to negative SMB anomaly (Fig. S4d and S4f). The surface melting in the ice free region between Laurentide and Cordilleran ice sheets leads to an expanded surface ablation zone (Fig. S4d) and accelerated mass balance-elevation feedbacks (Weertman, 1961). This sort of accelerated melting due to the saddle effect has previously been documented by Gregoire et al. (2012) for the Meltwater Pulse events. These anomalies over the western Laurentide amplify over the next 500 years. Alongside warmer temperatures over the eastern Laurentide, the western Laurentide also shows anomalies up to +2˚C during 220ka (Fig. S5c). Not only the floating shelves, but also grounded regions of the western Laurentide show negative SMB anomalies (Fig. S5d) and basal sliding (Fig. S5a). Further, relatively warm subsurface ocean water (>-1˚C) seeps along the west bank of Hudson Bay leading to a more pronounced negative mass balance (Fig. S5d). This shows up as a spike in the subsurface ocean melt values in Fig. 6i. Temporal snapshots every 0.1ky in the vicinity of the spikes in ablation (Fig. 6g), SMB (Fig. 6h) and ocean melting (Fig. 6i) are shown in Figure S6. It shows that the spikes in ablation and SMB predominantly come from a small area in the southern end of the Laurentide, while the spike in subshelf melting results only from the western part of the Laurentide with a receding grounding line. Although our model simulates sub shelf melting along the western Hudson Bay, we did not find any geologic evidence of such subsurface melting around 219.5ka. It is also worth mentioning that our setup does not simulate forebulges or other specific mechanisms modelled by more comprehensive full-Earth models. But Tigchelaar et al. (2018) have reported such changes in mass balance arising due to changing of ice sheets to ice shelves near the grounding line. The spike in subshelf melting (Fig. 6i) as well as surface ablation (Fig. 6g) during this period lead to an increase of the freshwater flux into the ocean. This could explain the synchronization with the AMOC slowdown seen during this period in Fig. 6e. However, since our model is run at an acceleration ($N_A = 5$) and we conserve the freshwater flux (Sec. 2.3), the total freshwater volume dumped into the ocean is being underestimated, which may distort the LOVECLIM response. These surface and sub-surface melting processes of the Laurentide trigger a rapid retreat of the ice-sheet within the next 0.5ky (Fig. S7), accounting for the ~10m SLE rise in 0.5ky (Fig. 6c and 4b). Such relatively ice-free conditions at 219.5ka (Fig. S7) were also reported by Colleoni and Liakka (2020) in both their control (100km) and high resolution (40km) simulations.

Deleted: The

Deleted: S2, S3

Deleted: S4

Deleted: S2b

Deleted: S2a, S2d

Deleted: S2f

Deleted: S2a

Deleted: S2a

Deleted: S2c

Deleted: S2d

Deleted: S2f

Deleted: S2d

Deleted: S3c

Deleted: anomaly

Deleted: S3d

Deleted: S3a

Deleted: waters

Deleted: S3d

Deleted: the

Deleted: These surface and sub-surface melting processes of the Laurentide trigger a rapid retreat of the ice-sheet within the next 0.5ky (Fig. S4), accounting for the ~10m SLE rise in 0.5ky (Fig. 6c and 4b).

3.6 Climate-ice sheet bifurcations and multiple equilibria

Figure 3 indicates a strong sensitivity of the simulated ice-sheet evolution to the melt parameter (m). Experiments with values in the range of $120\ Wm^2 \leq m \leq 130\ Wm^2$ and other parameters as in BLS produce a realistic glacial inception and termination over MIS 7e-7d-7c. Lower m values lead to a reduced magnitude of glaciation, while higher values cause a rapid glacial build-up and a run-away effect with unrealistic, unabated growth of ice-sheets. Even though we did not run steady-state experiments, this behavior is reminiscent of a saddle node bifurcation. Bifurcations in the climate-cryosphere system in response to astronomical forcings have been previously documented by studies such as Paillard (1998), Calov et al. (2005), Ashwin and Ditlevsen (2015) and Ganopolski et al. (2016). While previous studies have used empirical models or coupled ice sheet models to understand such bifurcations based solely on forcing and ice volume thresholds, here we investigate the changes in climate teleconnections and stationary wave patterns that can arise from slightly different ice sheet distributions, to explain the inherent mechanisms of the simulated bifurcation. Roe and Lindzen (2001) suggested that the topography of an ice sheet such as the Laurentide induces a high-pressure anticyclonic circulation over the western end of the ice sheet. The associated cooling and upslope flow lead to enhanced rainfall over the western and southwestern ends of Laurentide. However, the prevailing cold northerlies downslope cause a reduction in rainfall over the ice sheet. This interplay between cooling associated with anticyclonic circulations alongside enhanced rainfall over western Laurentide and the reduction in rainfall over most of the ice sheet due to cold northerlies, can lead to an equilibrium ice sheet configuration or ice sheet growth/decay. Figure 7 shows the ice volume evolutions and anomalies in climate and ice sheet variables at 180ka with respect to 240ka. The initial values of these variables at 240ka is shown in Fig. S8.

Figure 7a shows two simulations that have a very similar evolution and capture the 7e-7d-7c transition realistically but show very different trajectories after the inception at MIS 6. Both ensemble members were run with the same GHG sensitivity, α=2, but different melt parameters, m=125 Wm^{-2} and m=130 Wm^{-2}. While one leads to a stable inception into MIS 6 (blue, m=125 Wm^{-2}), the other leads to a runaway glaciation (black, m=130 Wm^{-2}) with a total ice volume of 180 m SLE at 160ka (Fig. 7a). We assume that the bifurcation of the trajectories happens around 180ka, where the difference in ice volume between the two ensemble runs is only 10m SLE. Although the Cordilleran looks very similar, the Laurentide is slightly bigger and has a higher and wider dome at the southern tip in the runaway simulation (Fig. 7c compared to 7b). Also, the Laurentide and Cordilleran are connected further south and this bridge is also higher in the runaway simulation (Fig. 7e). This higher bridge and Laurentide ice sheet locally lead to a surface cooling and thus to a net positive surface mass balance (Fig. 7f and 7g). Also, an anomalous cyclonic circulation develops south of the Laurentide in the runaway case leading to a positive net budget just south of the Laurentide (Fig. 7g), while the positive budget is much further away from the Laurentide in the stable run (Fig. 7f). Westerly storm tracks veered further south by a weaker Aleutian Low and a stronger North Pacific High, as reported by Oster et al. (2015) for the LGM, bring in moisture towards the southern end of the Laurentide. The shape of the Laurentide and the saddle in the stable run cause this jet stream to meander around and precipitate on the southeastern tip of the Laurentide (Francis and Vavrus, 2012) (Fig. 7h). These winds might also cause the moisture laden air from the Gulf of Mexico to precipitate just north of the Gulf of Mexico (Fig. 7h). But in the runaway run, the jet stream is more northerly and precipitates over the southwestern tip of Laurentide (Fig. 7i). The Laurentide ice-sheet extending further south causes the moist air from the Gulf of Mexico to also precipitate over the southwestern end of the Laurentide alongside the moist air from the jet stream intensifying further southwestward growth of the Laurentide. This southwestward growth of Laurentide in turn enhances the poleward moisture transport. While these stationary wave feedbacks are similar to the ones described by Roe and Lindzen (2001) and they suggested these patterns to be robust for a range of parameters, it is possible that such circulation patterns could change when using a more realistic atmospheric model or by the presence of a Eurasian ice sheet. The atmospheric patterns strengthen over the next 10ky and the runaway run simulates ~30m SLE greater ice volume than the stable run (Fig. S9). The difference between the two runs at 180ka and 170ka are presented in Fig. S10. As mentioned earlier in Sect. 3.2, it is important to

Deleted: In
Deleted: we found
Deleted: energy balance
Deleted: lead to a
Deleted: Values lower than this do not simulate the full
Deleted: values
Deleted: than this threshold
Deleted: ensembles
Deleted: ensembles
Deleted: These
Deleted: .
Deleted: S5
Deleted: S6.

acknowledge the low horizontal and vertical resolutions of LOVECLIM's atmosphere, which could mean the circulation changes reported here to be model dependent.

4 Summary and Discussion

Modeling glacial cycles remains a key challenge, especially because of the two-way interactions between ice sheets and climate and the emerging possibility for multiple equilibrium states. The ice-volume evolution originates from a time-integration of small net mass balance terms (e.g. Fig. 6h), which themselves originate from the difference of large accumulation and ablation terms. Long-term orbital-scale integrations of such delicate net surface mass balances can further lead to an accrual of errors. Here we focused on the penultimate interglacial, MIS 7-MIS 6 which is characterized by intervals with both in-phase and out-of-phase orbital and GHG variations. This interesting period involves one of the fastest glacial build-ups and terminations, with SLE variations of up to ±60m within a period of 20ky. Due to the rapid response of the ice sheets to orbital and CO_2 forcings, this period serves as an excellent benchmark for coupled climate-ice sheet simulations. Our bidirectionally coupled three-dimensional climate-ice sheet model simulations with ice sheets and ice shelves represented in both hemispheres suggest that glacial inceptions are more sensitive to orbital variations, whereas terminations from deep glacial conditions need both orbital and CO_2 forcing to work in tandem over a narrow ablation zone at the southern margins of northern hemispheric ice sheets. We find that small changes in the Laurentide's ice distribution for similar total ice volumes reminiscent of a saddle node bifurcation, which in turn determines whether the coupled trajectory will follow a deglaciation or a runaway glaciation pathway in response to the combination of forcings. This runaway glaciation can be explained in terms of a positive stationary-wave-ice sheet feedback in which ice topography-driven moisture transport from westerly storm tracks, a cold high-pressure anticyclonic circulation and moisture-laden winds from the Gulf of Mexico lead to enhanced rainfall accumulation over the southern tip of the Laurentide, making it grow further southwestward.

The simulated ice sheet volume is well within the range of reconstructions for a rather narrow range of parameters. Small changes in parameter values can produce strongly diverging trajectories, and the emergence of multiple equilibrium states may also suggest the model's dependence on initial conditions. This poses a challenge, as many ice sheet and climate model parameters remain poorly constrained. In this context, we note that parameterizations associated with hydrofracturing and cliff instability did not impact our ice sheet trajectories. These processes have provided substantial contributions to the rapid Antarctic ice sheet retreat simulated in response to future climate projections (DeConto and Pollard, 2016), and better constraining these parameterizations is important to reduce uncertainties related to future sea level trajectories (e.g., Edwards et al., 2019). Presumably, these processes did not play an important role in our present simulations, because the climate is generally too cold, suggesting that opportunities for constraining these parameters in glacial simulations may be limited. We further note that the parameter sets which allowed for the most realistic simulation of glacial inceptions during MIS 7-MIS 6 may not necessarily be optimal for other periods. That optimal parameter sets can depend on the period over which they are optimized, has recently been shown for a similar coupled climate ice sheet model (Bahadory et al., 2020).

Our present setup has difficulties in realistically simulating both Laurentide and Eurasian ice sheets simultaneously and generates a smaller Eurasian ice sheet compared to reconstructions, which could be a model dependent feature of LOVECLIM, given it is a T21 grid with only three levels in the atmosphere, and so could vary with the choice of the climate model used. Since we use an accelerated setup, we only conserve the freshwater flux from the ice model to LOVECLIM, which could lead to an underestimation of the oceanic circulation changes due to the lesser volume of net freshwater being dumped into the ocean. Nevertheless, there is scope of further improving the current setup. For instance, we only implement temperature and precipitation bias corrections in the current setup, and including bias corrections for radiation and ocean temperature might

Deleted: can lead to

Deleted: of the system

Deleted: leads

Deleted: Results also suggest that our coupled simulations are realistic over a narrow range of parameters, and are very sensitive to changes in parameter values that can produce starkly different trajectories.

improve our representation of ice sheets. Future research might further improve the current setup by including the advective precipitation downscaling scheme (Bahadory and Tarasov, 2018) to account for orographic forcing, which is not captured in LOVECLIM. We are also investigating the possibilities of using a dynamical, an altitude-dependent and a CO_2-dependent lapse rate corrections while downscaling temperature from LOVECLIM to PSUIM. This is because the atmospheric lapse rate depends on the atmospheric CO_2 concentration – an effect that has not been considered so far in glacial dynamics. Furthermore, improving our basal sliding coefficient map for the NH using information of sediment sizes, instead of simply using a binary coefficient map, has the potential of further improving the simulations.

Potentially more realistic results could be obtained if the simulations were unaccelerated (which would be computationally very expensive), and from using more complex climate models that include stratification-dependent mixing in the ocean for instance. Furthermore, Glacial Isostatic Adjustment (GIA) processes captured only in comprehensive full-Earth models such as forebulges are not simulated in the ice-sheet model used here. Nevertheless, we would like to reiterate that simulating a trajectory is more difficult than conducting timeslice experiments, as climate and ice sheet components work on totally different timescales and a fine interplay of parameters can add up to very different equilibrium states. And such coupled climate-ice sheet paleo-simulations offer great opportunities for constraining parameter sets for future simulations.

Deleted: Also, the stationary wave feedback reported here could be a model dependent feature of LOVECLIM, given it has only three atmospheric levels, and so could vary with the choice of the climate model used.

Data Availability

The data that support the findings of this study are available from the corresponding author on request.

Author contributions

AT and DC designed the research. DC, FS, MH and DP developed the model code. DC conducted the model simulations and analyzed the data. DC and AT prepared the manuscript with contributions from all the co-authors.

Competing interests

Deleted: ¶

The authors declare no competing interests.

Acknowledgements

This research is supported by the Institute for Basic Science, South Korea (Grant No: IBS-R028-D1) and NSF Grant # 1903197. The simulations were conducted at the Center for High-Performance Computing at the University of Southern California. We would like to thank Lev Tarasov and another anonymous reviewer for their constructive comments, which have definitely helped improve the quality of the manuscript. DC would also like to acknowledge the many helpful discussions at the Advanced Climate Dynamics Course (ACDC) summer school in 2018 and the ACDC 10-year alumni conference in 2019.

References

Abe-Ouchi, A., Saito, F., Kawamura, K., Raymo, M. E., Okuno, J. i., Takahashi, K., and Blatter, H.: Insolation-driven 100,000-year glacial cycles and hysteresis of ice-sheet volume, nature, 500, 190-193, 2013.

Ashwin, P., and Ditlevsen, P.: The middle Pleistocene transition as a generic bifurcation on a slow manifold, Climate dynamics, 45, 2683-2695, 2015.

Bahadory, T., and Tarasov, L.: LCice 1.0 – a generalized Ice Sheet System Model coupler for LOVECLIM version 1.3: description, sensitivities, and validation with the Glacial Systems Model (GSM version D2017.aug17), Geoscientific Model Development, 11, 3883-3902, 10.5194/gmd-11-3883-2018, 2018.

Bahadory, T., Tarasov, L., and Andres, H.: The phase space of last glacial inception for the Northern Hemisphere from coupled ice and climate modelling, Clim. Past Discuss., 2020, 1-30, 10.5194/cp-2020-1, 2020.

Batchelor, C. L., Margold, M., Krapp, M., Murton, D. K., Dalton, A. S., Gibbard, P. L., Stokes, C. R., Murton, J. B., and Manica, A.: The configuration of Northern Hemisphere ice sheets through the Quaternary, Nature communications, 10, 1-10, 2019.

Berger, A.: Long-term variations of daily insolation and Quaternary climatic changes, Journal of the Atmospheric Sciences, 35, 2362-2367, 1978.

Bigg, G. R., Wadley, M. R., Stevens, D. P., and Johnson, J. A.: Modelling the dynamics and thermodynamics of icebergs, Cold Regions Science and Technology, 26, 113-135, 1997.

Bintanja, R., van de Wal, R. S. W., and Oerlemans, J.: Modelled atmospheric temperatures and global sea levels over the past million years, Nature, 437, 125-125, 2005.

Born, A., Kageyama, M., and Nisancioglu, K. H.: Warm Nordic Seas delayed glacial inception in Scandinavia, Climate of the Past, 6, 817-826, 2010.

Brovkin, V., Ganopolski, A., and Svirezhev, Y.: A continuous climate-vegetation classification for use in climate-biosphere studies, Ecological Modelling, 101, 251-261, 1997.

Calov, R., and Ganopolski, A.: Multistability and hysteresis in the climate-cryosphere system under orbital forcing, Geophysical Research Letters, 32, 10.1029/2005gl024518, 2005.

Calov, R., Ganopolski, A., Claussen, M., Petoukhov, V., and Greve, R.: Transient simulation of the last glacial inception. Part I: glacial inception as a bifurcation in the climate system, Climate Dynamics, 24, 545-561, 10.1007/s00382-005-0007-6, 2005.

Capron, E., Govin, A., Feng, R., Otto-Bliesner, B. L., and Wolff, E. W.: Critical evaluation of climate syntheses to benchmark CMIP6/PMIP4 127 ka Last Interglacial simulations in the high-latitude regions, Quaternary Science Reviews, 168, 137-150, 2017.

Cheng, H., Edwards, R. L., Sinha, A., Spotl, C., Yi, L., Chen, S., Kelly, M., Kathayat, G., Wang, X., Li, X., Kong, X., Wang, Y., Ning, Y., and Zhang, H.: The Asian monsoon over the past 640,000 years and ice age terminations, Nature, 534, 640-646, 10.1038/nature18591, 2016.

Clark, P. U., Dyke, A. S., Shakun, J. D., Carlson, A. E., Clark, J., Wohlfarth, B., Mitrovica, J. X., Hostetler, S. W., and McCabe, A. M.: The last glacial maximum, science, 325, 710-714, 2009.

Clark, P. U., and Huybers, P.: Global change: Interglacial and future sea level, Nature, 462, 856-856, 2009.

Clark, P. U., He, F., Golledge, N. R., Mitrovica, J. X., Dutton, A., Hoffman, J. S., and Dendy, S.: Oceanic forcing of penultimate deglacial and last interglacial sea-level rise, Nature, 577, 660-664, 2020.

Colleoni, F., and Masina, S.: Impact of greenhouse gases and insolation on the threshold of glacial inception, Annual Conference of the Societá Italiana per le Scienze del Clima, 2014,

Colleoni, F., Masina, S., Cherchi, A., and Iovino, D.: Impact of Orbital Parameters and Greenhouse Gas on the Climate of MIS 7 and MIS 5 Glacial Inceptions, Journal of Climate, 27, 8918-8933, 2014a.

Colleoni, F., Masina, S., Cherchi, A., Navarra, A., Ritz, C., Peyaud, V., and Otto-Bliesner, B.: Modeling Northern Hemisphere ice-sheet distribution during MIS 5 and MIS 7 glacial inceptions, Climate of the Past, 10, 269-291, 10.5194/cp-10-269-2014, 2014b.

Colleoni, F., and Liakka, J.: Transient simulations of the Eurasian ice sheet during the Saalian glacial cycle, SVENSK KÄRNBRÄNSLEHANTERING AB, StockholmSKB TR-19-17, 2020.

Crucifix, M., and Loutre, F. M.: Transient simulations over the last interglacial period (126--115 kyr BP): feedback and forcing analysis, Climate Dynamics, 19, 417-433, 2002.

DeConto, R. M., and Pollard, D.: Contribution of Antarctica to past and future sea-level rise, Nature, 531, 591-591, 2016.

Dolan, A. M., Hunter, S. J., Hill, D. J., Haywood, A. M., Koenig, S. J., Otto-Bliesner, B. L., Abe-Ouchi, A., Bragg, F., Chan, W. L., Chandler, M. A., and others: Using results from the PlioMIP ensemble to investigate the Greenland Ice Sheet during the mid-Pliocene Warm Period, Climate of the Past Discussions, 11, 403-424, 2015.

Dutton, A., Bard, E., Antonioli, F., Esat, T. M., Lambeck, K., and McCulloch, M. T.: Phasing and amplitude of sea-level and climate change during the penultimate interglacial, Nature Geoscience, 2, 355-355, 2009.

Edwards, T. L., Brandon, M. A., Durand, G., Edwards, N. R., Golledge, N. R., Holden, P. B., Nias, I. J., Payne, A. J., Ritz, C., and Wernecke, A.: Revisiting Antarctic ice loss due to marine ice-cliff instability, Nature, 566, 58-64, 10.1038/s41586-019-0901-4, 2019.

Francis, J. A., and Vavrus, S. J.: Evidence linking Arctic amplification to extreme weather in mid-latitudes, Geophysical Research Letters, 39, 2012.

Friedrich, T., Timmermann, A., Tigchelaar, M., Timm, O. E., and Ganopolski, A.: Nonlinear climate sensitivity and its implications for future greenhouse warming, Science Advances, 2, e1501923-e1501923, 2016.

Friedrich, T., and Timmermann, A.: Using Late Pleistocene sea surface temperature reconstructions to constrain future greenhouse warming, Earth and Planetary Science Letters, 530, 115911, 2020.

Ganopolski, A., Calov, R., and Claussen, M.: Simulation of the last glacial cycle with a coupled climate ice-sheet model of intermediate complexity, Climate of the Past, 6, 229-244, 2010.

Ganopolski, A., and Calov, R.: The role of orbital forcing, carbon dioxide and regolith in 100 kyr glacial cycles, Climate of the Past, 7, 1415-1425, 2011.

Ganopolski, A., Winkelmann, R., and Schellnhuber, H. J.: Critical insolation–CO_2 relation for diagnosing past and future glacial inception, Nature, 529, 200, 2016.

Ganopolski, A., and Brovkin, V.: Simulation of climate, ice sheets and CO_2; evolution during the last four glacial cycles with an Earth system model of intermediate complexity, Climate of the Past Discussions, 1-38, 2017.

Gasson, E. G. W., DeConto, R. M., Pollard, D., and Clark, C. D.: Numerical simulations of a kilometre-thick Arctic ice shelf consistent with ice grounding observations, Nature communications, 9, 1510-1510, 2018.
Gent, P. R., Danabasoglu, G., Donner, L. J., Holland, M. M., Hunke, E. C., Jayne, S. R., Lawrence, D. M., Neale, R. B., Rasch, P. J., Vertenstein, M., and others: The community climate system model version 4, Journal of Climate, 24, 4973-4991, 2011.
Gildor, H., and Tziperman, E.: Sea ice as the glacial cycles' climate switch: Role of seasonal and orbital forcing, Paleoceanography and Paleoclimatology, 15, 605-615, 2000.
Goosse, H., and Fichefet, T.: Importance of ice-ocean interactions for the global ocean circulation: A model study, Journal of Geophysical Research: Oceans, 104, 23337-23355, 1999.
Goosse, H., Brovkin, V., Fichefet, T., Haarsma, R., Huybrechts, P., Jongma, J., Mouchet, A., Selten, F., Barriat, P. Y., Campin, J. M., Deleersnijder, E., Driesschaert, E., Goelzer, H., Janssens, I., Loutre, M. F., Morales Maqueda, M. A., Opsteegh, T., Mathieu, P. P., Munhoven, G., Pettersson, E. J., Renssen, H., Roche, D. M., Schaeffer, M., Tartinville, B., Timmermann, A., and Weber, S. L.: Description of the Earth system model of intermediate complexity LOVECLIM version 1.2, Geoscientific Model Development, 3, 603-633, 10.5194/gmd-3-603-2010, 2010.
Gregoire, L. J., Payne, A. J., and Valdes, P. J.: Deglacial rapid sea level rises caused by ice-sheet saddle collapses, Nature, 487, 219, 2012.
Greve, R.: A continuum-mechanical formulation for shallow polythermal ice sheets, Philosophical Transactions of the Royal Society of London A: Mathematical, Physical and Engineering Sciences, 355, 921-974, 1997.
Hays, J. D., Imbrie, J., and Shackleton, N. J.: Variations in the Earth's orbit: pacemaker of the ice ages, Science, 194, 1121-1132, 1976.
Heinemann, M., Timmermann, A., Elison Timm, O., Saito, F., and Abe-Ouchi, A.: Deglacial ice sheet meltdown: orbital pacemaking and CO_2 effects, Climate of the Past, 10, 2014.
Jongma, J. I., Driesschaert, E., Fichefet, T., Goosse, H., and Renssen, H.: The effect of dynamic–thermodynamic icebergs on the Southern Ocean climate in a three-dimensional model, Ocean Modelling, 26, 104-113, 2009.
Jouzel, J., Masson-Delmotte, V., Cattani, O., Dreyfus, G., Falourd, S., Hoffmann, G., Minster, B., Nouet, J., Barnola, J.-M., and Chappellaz, J.: Orbital and millennial Antarctic climate variability over the past 800,000 years, science, 317, 793-796, 2007.
Knutti, R., Flückiger, J., Stocker, T., and Timmermann, A.: Strong hemispheric coupling of glacial climate through freshwater discharge and ocean circulation, Nature, 430, 851-856, 2004.
Koenig, S. J., Dolan, A. M., De Boer, B., Stone, E. J., Hill, D. J., DeConto, R. M., Abe-Ouchi, A., Lunt, D. J., Pollard, D., Quiquet, A., and others: Ice sheet model dependency of the simulated Greenland Ice Sheet in the mid-Pliocene, Climate of the Past, 11, 369-381, 2015.
Kubatzki, C., Montoya, M., Rahmstorf, S., Ganopolski, A., and Claussen, M.: Comparison of the last interglacial climate simulated by a coupled global model of intermediate complexity and an AOGCM, Climate Dynamics, 16, 799-814, 2000.
Laskar, J., Robutel, P., Joutel, F., Gastineau, M., Correia, A., and Levrard, B.: A long-term numerical solution for the insolation quantities of the Earth, Astronomy & Astrophysics, 428, 261-285, 2004.
Le Morzadec, K., Tarasov, L., Morlighem, M., and Seroussi, H.: A new sub-grid surface mass balance and flux model for continental-scale ice sheet modelling: testing and last glacial cycle, Geoscientific Model Development, 8, 3199, 2015.
Lisiecki, L. E., and Raymo, M. E.: A Pliocene-Pleistocene stack of 57 globally distributed benthic δ18O records, Paleoceanography, 20, 2005.
Liu, Z., Otto-Bliesner, B., He, F., Brady, E., Tomas, R., Clark, P., Carlson, A., Lynch-Stieglitz, J., Curry, W., and Brook, E.: Transient simulation of last deglaciation with a new mechanism for Bølling-Allerød warming, Science, 325, 310-314, 2009.
Lofverstrom, M., and Liakka, J.: The influence of atmospheric grid resolution in a climate model-forced ice sheet simulation, Cryosphere, 12, 2018.
Loulergue, L., Schilt, A., Spahni, R., Masson-Delmotte, V., Blunier, T., Lemieux, B., Barnola, J.-M., Raynaud, D., Stocker, T. F., and Chappellaz, J.: Orbital and millennial-scale features of atmospheric CH 4 over the past 800,000 years, Nature, 453, 383-383, 2008.
Lunt, D. J., Abe-Ouchi, A., Bakker, P., Berger, A., Braconnot, P., Charbit, S., Fischer, N., Herold, N., Jungclaus, J. H., Khon, V. C., and others: A multi-model assessment of last interglacial temperatures, Climate of the Past, 9, 699-717, 2013.
Lüthi, D., Le Floch, M., Bereiter, B., Blunier, T., Barnola, J.-M., Siegenthaler, U., Raynaud, D., Jouzel, J., Fischer, H., Kawamura, K., and others: High-resolution carbon dioxide concentration record 650,000–800,000 years before present, Nature, 453, 379-379, 2008.
Menviel, L., Joos, F., and Ritz, S.: Simulating atmospheric CO_2, ^{13}C and the marine carbon cycle during the Last Glacial–Interglacial cycle: possible role for a deepening of the mean remineralization depth and an increase in the oceanic nutrient inventory, Quaternary Science Reviews, 56, 46-68, 2012.
Nikolova, I., Yin, Q., Berger, A., Singh, U. K., and Karami, M. P.: The last interglacial (Eemian) climate simulated by LOVECLIM and CCSM3, Climate of the Past, 9, 1789-1806, 2013.
Opsteegh, J. D., Haarsma, R. J., Selten, F. M., and Kattenberg, A.: ECBILT: A dynamic alternative to mixed boundary conditions in ocean models, Tellus A: Dynamic Meteorology and Oceanography, 50, 348-367, 1998.
Oster, J. L., Ibarra, D. E., Winnick, M. J., and Maher, K.: Steering of westerly storms over western North America at the Last Glacial Maximum, Nature Geoscience, 8, 201, 2015.
Otto-Bleisner, B. L., Braconnot, P., Harrison, S. P., Lunt, D. J., Abe-Ouchi, A., Albani, S., Bartlein, P. J., Capron, E., Carlson, A. E., Dutton, A., and others: The PMIP4 contribution to CMIP6–Part 2: Two interglacials, scientific objective and experimental design for Holocene and Last Interglacial simulations, Geoscientific Model Development, 10, 3979-4003, 2017.
Pages, P. I. W. G. o.: Interglacials of the last 800,000 years, Reviews of Geophysics, 54, 162-219, 2016.
Paillard, D.: The timing of Pleistocene glaciations from a simple multiple-state climate model, Nature, 391, 378, 1998.
Pedersen, R. A., Langen, P. L., and Vinther, B. M.: The last interglacial climate: comparing direct and indirect impacts of insolation changes, Climate Dynamics, 48, 3391-3407, 2017.
Petoukhov, V., Ganopolski, A., Brovkin, V., Claussen, M., Eliseev, A., Kubatzki, C., and Rahmstorf, S.: CLIMBER-2: a climate system model of intermediate complexity. Part I: model description and performance for present climate, Climate dynamics, 16, 1-17, 2000.
Pollard, D., and DeConto, R. M.: A simple inverse method for the distribution of basal sliding coefficients under ice sheets, applied to Antarctica, The Cryosphere, 6, 953-971, 10.5194/tc-6-953-2012, 2012a.
Pollard, D., and DeConto, R. M.: Description of a hybrid ice sheet-shelf model, and application to Antarctica, Geoscientific Model Development, 5, 1273-1295, 10.5194/gmd-5-1273-2012, 2012b.
Pollard, D., DeConto, R. M., and Alley, R. B.: Potential Antarctic Ice Sheet retreat driven by hydrofracturing and ice cliff failure, Earth and Planetary Science Letters, 412, 112-121, 2015.
Rachmayani, R., Prange, M., and Schulz, M.: Intra-interglacial climate variability: model simulations of Marine Isotope Stages 1, 5, 11, 13, and 15, Climate of the Past, 12, 677-695, 10.5194/cp-12-677-2016, 2016.
Rahmstorf, S.: Ocean circulation and climate during the past 120,000 years, Nature, 419, 207-214, 2002.

Deleted: --

Deleted: CO 2

Deleted: --

Deleted: --

Railsback, L. B., Gibbard, P. L., Head, M. J., Voarintsoa, N. R. G., and Toucanne, S.: An optimized scheme of lettered marine isotope substages for the last 1.0 million years, and the climatostratigraphic nature of isotope stages and substages, Quaternary Science Reviews, 111, 94-106, 2015.
Ritz, C., Rommelaere, V., and Dumas, C.: Modeling the evolution of Antarctic ice sheet over the last 420,000 years: Implications for altitude changes in the Vostok region, Journal of Geophysical Research: Atmospheres, 106, 31943-31964, 2001.
Robinson, A., Calov, R., and Ganopolski, A.: An efficient regional energy-moisture balance model for simulation of the Greenland Ice Sheet response to climate change, 2010.
Roche, D. M., Dumas, C., Bügelmayer, M., Charbit, S., and Ritz, C.: Adding a dynamical cryosphere to iLOVECLIM (version 1.0): coupling with the GRISLI ice-sheet model, Geoscientific Model Development, 7, 1377-1394, 10.5194/gmd-7-1377-2014, 2014.
Roe, G. H., and Lindzen, R. S.: The mutual interaction between continental-scale ice sheets and atmospheric stationary waves, Journal of Climate, 14, 1450-1465, 2001.
Rohling, E. J., Hibbert, F. D., Williams, F. H., Grant, K. M., Marino, G., Foster, G. L., Hennekam, R., De Lange, G. J., Roberts, A. P., and Yu, J.: Differences between the last two glacial maxima and implications for ice-sheet, δ18O, and sea-level reconstructions, Quaternary Science Reviews, 176, 1-28, 2017.
Saito, F., and Abe-Ouchi, A.: Thermal structure of Dome Fuji and east Dronning Maud Land, Antarctica, simulated by a three-dimensional ice-sheet model, Annals of Glaciology, 39, 433-438, 2004.
Schilt, A., Baumgartner, M., Blunier, T., Schwander, J., Spahni, R., Fischer, H., and Stocker, T. F.: Glacial--interglacial and millennial-scale variations in the atmospheric nitrous oxide concentration during the last 800,000 years, Quaternary Science Reviews, 29, 182-192, 2010.
Schloesser, F., Friedrich, T., Timmermann, A., DeConto, R. M., and Pollard, D.: Antarctic iceberg impacts on future Southern Hemisphere climate, Nature Climate Change, 9, 672-677, 2019.
Schoof, C.: Ice sheet grounding line dynamics: Steady states, stability, and hysteresis, Journal of Geophysical Research: Earth Surface, 112, 2007.
Spratt, R. M., and Lisiecki, L. E.: A Late Pleistocene sea level stack, Climate of the Past, 12, 1079-1092, 2016.
Stap, L. B., Van de Wal, R. S. W., De Boer, B., Bintanja, R., and Lourens, L. J.: Interaction of ice sheets and climate during the past 800 000 years, Climate of the Past, 10, 2135-2152, 2014.
Stein, K., Timmermann, A., Kwon, E. Y., and Friedrich, T.: Timing and magnitude of Southern Ocean sea ice/carbon cycle feedbacks, Proceedings of the National Academy of Sciences, 2020.
Svendsen, J. I., Alexanderson, H., Astakhov, V. I., Demidov, I., Dowdeswell, J. A., Funder, S., Gataullin, V., Henriksen, M., Hjort, C., and Houmark-Nielsen, M.: Late Quaternary ice sheet history of northern Eurasia, Quaternary Science Reviews, 23, 1229-1271, 2004.
Tigchelaar, M., Timmermann, A., Pollard, D., Friedrich, T., and Heinemann, M.: Local insolation changes enhance Antarctic interglacials: Insights from an 800,000-year ice sheet simulation with transient climate forcing, Earth and Planetary Science Letters, 495, 69-78, 10.1016/j.epsl.2018.05.004, 2018.
Timm, O., and Timmermann, A.: Simulation of the last 21 000 years using accelerated transient boundary conditions, Journal of Climate, 20, 4377-4401, 2007.
Timm, O., Köhler, P., Timmermann, A., and Menviel, L.: Mechanisms for the onset of the African Humid Period and Sahara Greening 14.5–11 ka BP, Journal of Climate, 23, 2612-2633, 2010.
Timmermann, A., Knies, J., Timm, O. E., Abe-Ouchi, A., and Friedrich, T.: Promotion of glacial ice sheet buildup 60–115 kyr BP by precessionally paced Northern Hemispheric meltwater pulses, Paleoceanography, 25, 2010.
Timmermann, A., Sachs, J., and Timm, O. E.: Assessing divergent SST behavior during the last 21 ka derived from alkenones andG. ruber-Mg/Ca in the equatorial Pacific, Paleoceanography, 29, 680-696, 2014.
Timmermann, A., and Friedrich, T.: Late Pleistocene climate drivers of early human migration, Nature, 538, 92-95, 10.1038/nature19365, 2016.
Ullman, D., LeGrande, A., Carlson, A. E., Anslow, F., and Licciardi, J.: Assessing the impact of Laurentide Ice-Sheet topography on glacial climate, 2014.
Uppala, S. M., Kållberg, P., Simmons, A., Andrae, U., Bechtold, V. D. C., Fiorino, M., Gibson, J., Haseler, J., Hernandez, A., and Kelly, G.: The ERA-40 re-analysis, Quarterly Journal of the Royal Meteorological Society: A journal of the atmospheric sciences, applied meteorology and physical oceanography, 131, 2961-3012, 2005.
Van Den Berg, J., van de Wal, R., and Oerlemans, H.: A mass balance model for the Eurasian Ice Sheet for the last 120,000 years, Global and Planetary Change, 61, 194-208, 2008.
Vizcaino, M., Mikolajewicz, U., Ziemen, F., Rodehacke, C. B., Greve, R., and Van Den Broeke, M. R.: Coupled simulations of Greenland Ice Sheet and climate change up to AD 2300, Geophysical Research Letters, 42, 3927-3935, 2015.
Waelbroeck, C., Labeyrie, L., Michel, E., Duplessy, J. C., McManus, J. F., Lambeck, K., Balbon, E., and Labracherie, M.: Sea-level and deep water temperature changes derived from benthic foraminifera isotopic records, Quaternary Science Reviews, 21, 295-305, 2002.
Weertman, J.: Stability of ice-age ice sheets, Journal of Geophysical Research, 66, 3783-3792, 1961.
Willeit, M., Ganopolski, A., Calov, R., and Brovkin, V.: Mid-Pleistocene transition in glacial cycles explained by declining CO2 and regolith removal, Science Advances, 5, eaav7337, 2019.
Yamagishi, T., Abe-Ouchi, A., Saito, F., Segawa, T., and Nishimura, T.: Re-evaluation of paleo-accumulation parameterization over Northern Hemisphere ice sheets during the ice age examined with a high-resolution AGCM and a 3-D ice-sheet model, Annals of Glaciology, 42, 433-440, 2005.
Yin, Q. Z., and Berger, A.: Individual contribution of insolation and CO_2 to the interglacial climates of the past 800,000 years, Climate Dynamics, 38, 709-724, 2012.
Yoshimori, M., Reader, M., Weaver, A., and McFarlane, N.: On the causes of glacial inception at 116 kaBP, Climate Dynamics, 18, 383-402, 2002.
Zhang, Z., Yan, Q., Zhang, R., Colleoni, F., Ramstein, G., Dai, G., Jakobsson, M., O'Regan, M., Liess, S., Rousseau, D. D., Wu, N., Farmer, E. J., Contoux, C., Guo, C., Tan, N., and Guo, Z.: Rapid waxing and waning of Beringian ice sheet reconcile glacial climate records from around North Pacific, Clim. Past Discuss., 2020, 1-25, 10.5194/cp-2020-38, 2020.
Ziemen, F., Kapsch, M.-L., Klockmann, M., and Mikolajewicz, U.: Heinrich events show two-stage climate response in transient glacial simulations, Climate of the Past, 15, 153-168, 2019.

Expt Number	Orb Forced	GHG Forced	N_A	α	m (Wm^{-2})	C (myr^{-1}Pa^{-2})-NH
1 **(BLS)**	**Y**	**Y**	**5**	**2**	**125**	
2	**N**	**N**	5	2	125	
3	Y	**N**	5	2	125	
4	**N**	Y	5	2	125	Binary distribution
5	Y	Y	5	2	125	
6	Y	Y	5	**1.8**	125	**1.**Ocean:
7	Y	Y	5	**2.2**	125	$C(x,y)$=10^{-6};
8	Y	Y	5	**2.5**	125	representing
9	Y	Y	5	**3**	125	deformable sediments
10	Y	Y	5	2	**80**	**2.**Land:
11	Y	Y	5	2	**100**	$C(x,y)$=10^{-10};
12	Y	Y	5	2	**120**	representing non-
13	Y	Y	5	2	**130**	deformable rock.
14	Y	Y	5	2	**140**	
15	Y	Y	5	2	**150**	
16-20	*Y*	*Y*	*5*	***1.5***	***120,125,130,140,150***	
21-24	*Y*	*Y*	*5*	***3.5***	***80,100,120,125***	
25-27	*Y*	*Y*	***1 (30ky run)***	*2*	***110,120,130***	
28-30	*Y*	*Y*	***2 (30ky run)***	*2*	***110,120,130***	*Binary*
31-33	*Y*	*Y*	***10***	*2*	***110,130,150***	
34-36	*Y*	*Y*	***10***	***2.5***	***110,120,130***	
37-38	*Y*	*Y*	***20***	***2.5, 3***	*125*	
39-41	*Y*	*Y*	*5*	*2*	*125*	*Tertiary* ***1.****Ocean:* $C(x,y)$=10^{-6}; ***2.1*** *Land (soft tills):* $C(x,y)$=$\mathbf{10^{-7},10^{-8},10^{-9}}$ *over northeastern North America* ***2.2*** *Land (hard bed):* $C(x,y)$=10^{-10}
42-44	*Y*	*Y*	*5*	*2*	***150***	
45-47	*Y*	*Y*	*5*	***2.5***	*125*	
High Resolution Runs: 0.5 × 0.25° *for NH,* 20 × 20 km *polar stereographic for Antarctica*						
48-50	*Y*	*Y*	*5*	*2*	***110,130,150***	*Binary*

Table 1: List of all ensemble runs performed for the study (shown in Fig. S3). The first 15 experiments are discussed in Sect. 3.1 and shown in Fig. 3. Values in bold represent the difference from the baseline simulation (BLS, experiment number 1). N_A represents the PSUIM vs LOVECLIM acceleration factor (Sect 2.3). α represents the GHG sensitivity scaling factor (Eq. 1, Sect. 2.1) and m represents the constant parameter in the surface energy balance equation (Eq. 3, Sect. 2.2). C represents the basal sliding coefficient map used for the NH (Eq. 7, Sect. 2.2).

Deleted: Experiment

Deleted: Orbitally

Inserted Cells

Deleted: Equation 1

Deleted: All experiments are run at 1 × 0.5° resolution

Deleted: Northern Hemisphere and 40 × 40 km polar stereographic resolution for Antarctica.

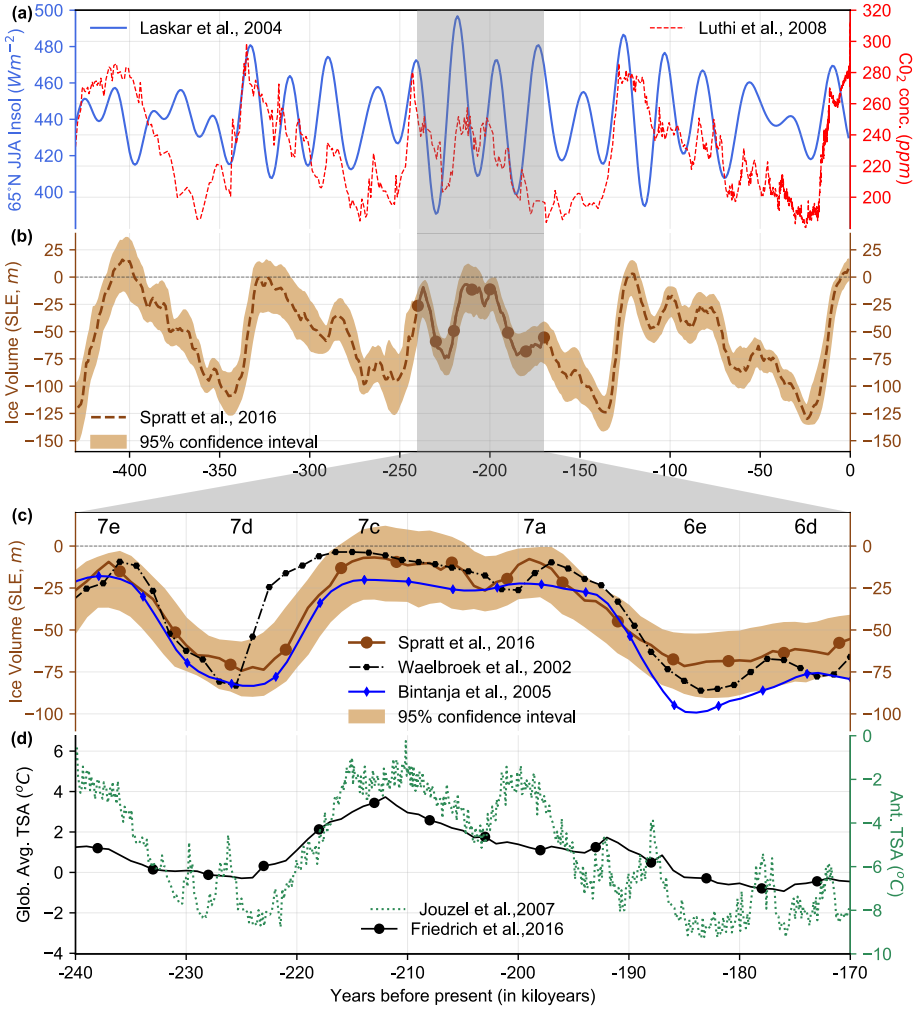

970

Figure 1: Overview of the forcings and reconstructions relevant to this study. From top to bottom: (a) summer insolation at 65°N (Wm^{-2}, blue (Laskar et al., 2004)) and CO_2 concentration (ppm, red (Lüthi et al., 2008)) over the last 430ka; (b) Sea level reconstructions (m) along with 95% confidence limits from Spratt and Lisiecki (2016) (brown) since the Mid Brunhes event. Notice the relatively cold MIS 7; (c) Sea level reconstructions (m) from Spratt and Lisiecki (2016) (brown), Waelbroeck et al. (2002) (black)
975 **and Bintanja et al. (2005) (blue) over MIS 7 (240-170ka); (d) Global average surface air temperature anomaly reconstructed from proxies (°C, black (Friedrich et al., 2016)) and Antarctic temperature anomaly relative to present day (°C, green (Jouzel et al., 2007)). The lettering convention of MIS substages as suggested by Railsback et al. (2015).**

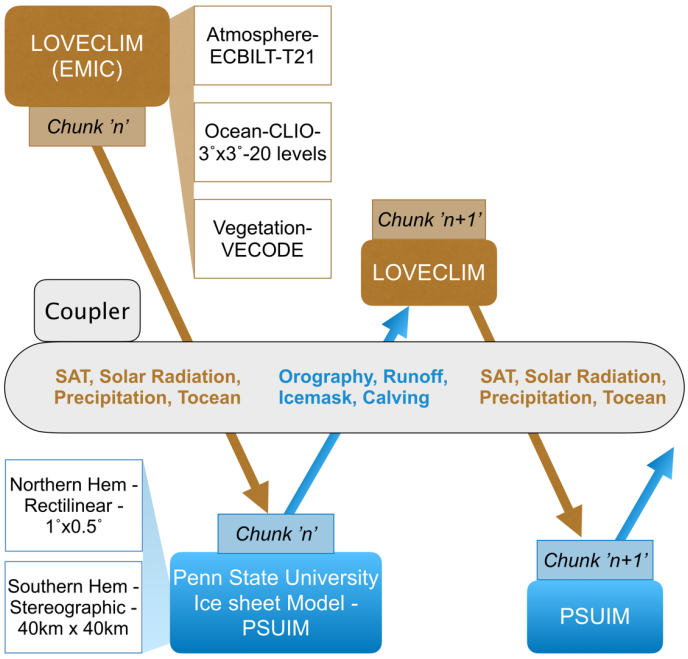

Deleted:

Figure 2: Schematic of the coupling between LOVECLIM and PSUIM. SAT is the surface air temperature and Tocean is the ocean temperature at a depth of 400m. Refer to Sect. 2.3 for details.

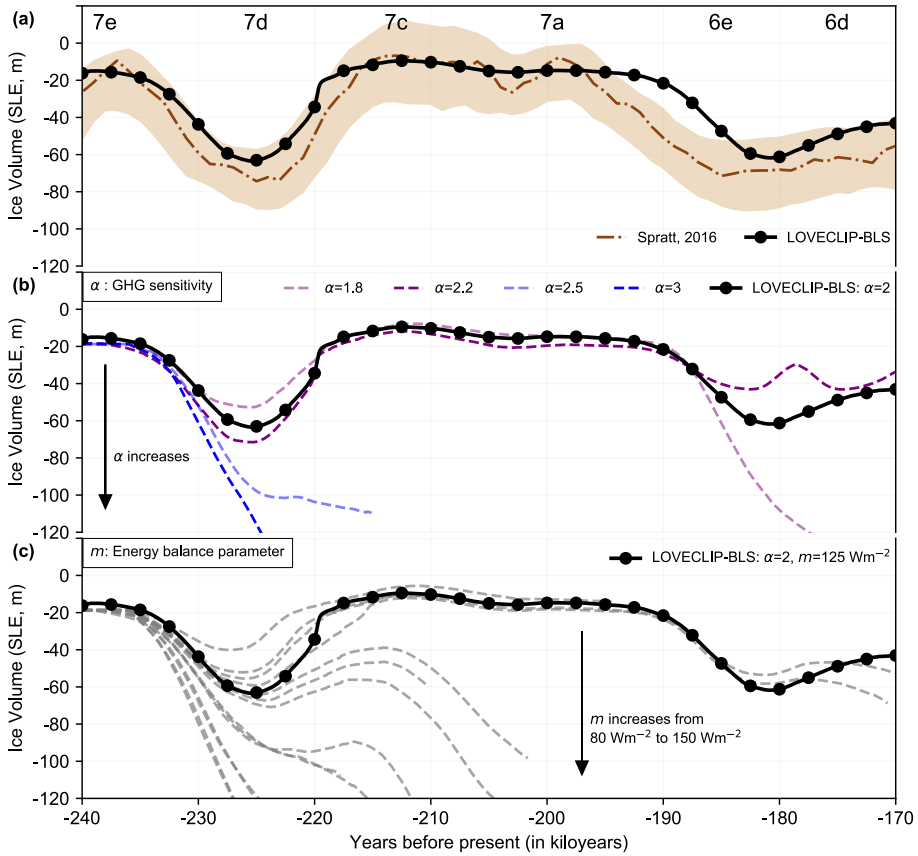

985 **Figure 3: Transient simulation and parameter sensitivity over MIS 7. (a) Sea level reconstruction (m) of Spratt and Lisiecki (2016) (brown) and total ice volume (in terms of SLE, m) from LOVECLIP baseline simulation (BLS, Experiment 1 in Table 1 using α=2 and *m*=125 Wm^{-2}). (b) LOVECLIP ensemble runs with varying GHG sensitivities (α, Eq. (1)) and a melt parameter value (*m*, Eq. (3)) of 125 Wm^{-2}. The best results are obtained for an α of 2. (c) LOVECLIP ensemble runs with α of 2 and different values of the melt parameter (*m*, Wm^{-2}). The best results are obtained for an *m* of 125 Wm^{-2} (BLS).**

990

Deleted: ensembles

Deleted:)

Deleted: ensembles

Deleted: energy balance

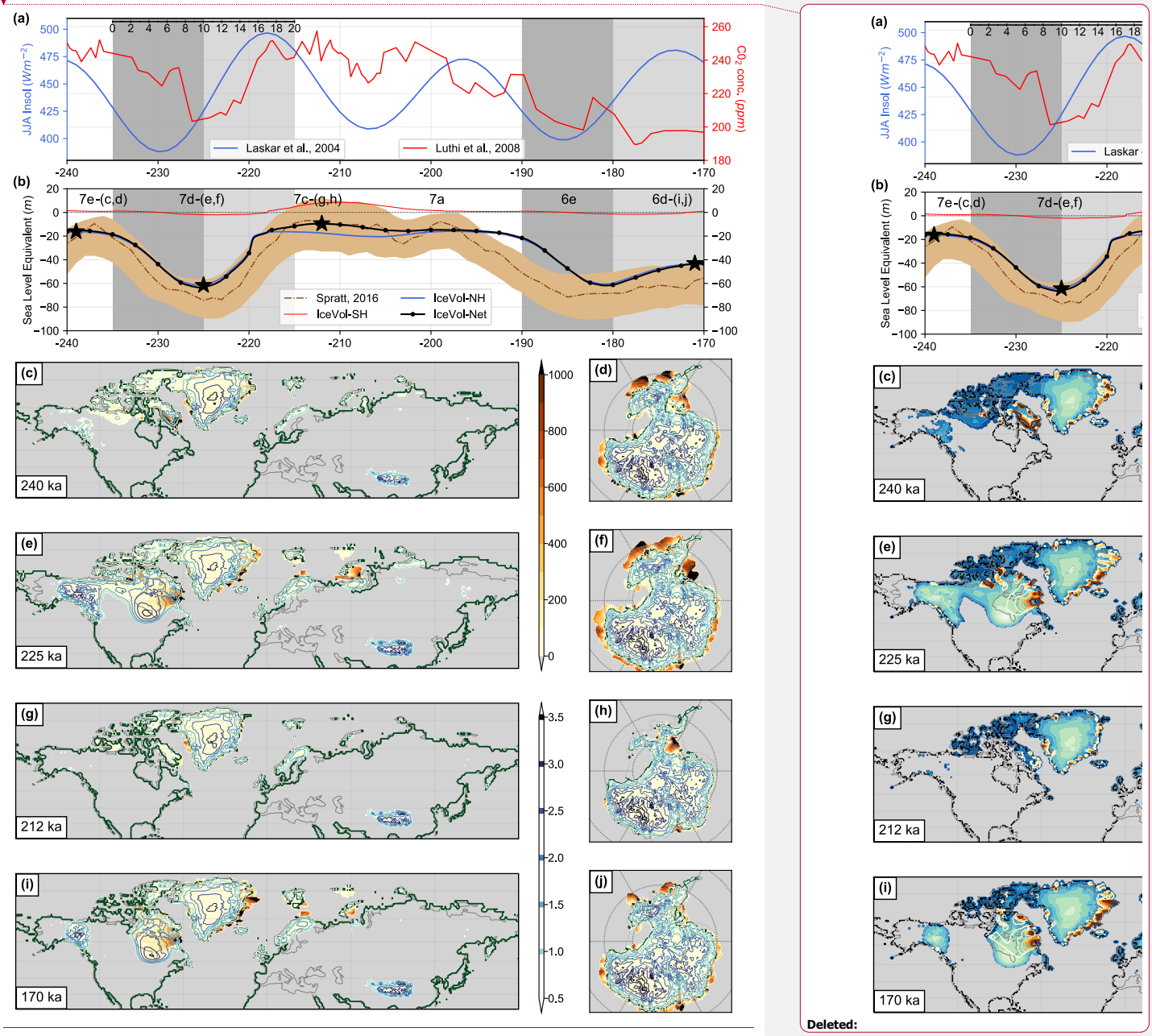

Figure 4: Maps of ice height and ice velocity from our transient coupled climate-ice sheet simulation over MIS 7. (a) JJA mean insolation at 65°N (Wm^{-2}, blue, *(Laskar et al., 2004)*) and CO_2 concentration (ppm, red *(Lüthi et al., 2008)*). The dark grey and light grey patches in the backgrounds of (a) and (b) refer to two 20ky periods leading into a glacial inception (10ky) and immediately after a glacial inception (10ky). The duration of these periods (20ky) is marked by a small scale on the top left and used in Figure 6. (b) Global sea level estimates (m) from *Spratt and Lisiecki (2016)* (brown) and sea level equivalent of ice volume from SH (red), NH

Deleted:

(blue) and total (black) from our transient simulation. The marked stars on the simulated SLE represent four instances corresponding to MIS 7e (240ka), MIS 7d (225ka), MIS 7c (212ka) and MIS 6 (170ka). (c) Basal ice velocity (solid colors, my^{-1}); ice thickness (colored contours, km) and the grounding line (solid green lines) for the Northern Hemisphere at 240ka, initial condition. (d) Same as (c) but for the southern hemisphere. (e) & (f) Same as (c) and (d), but for 225 ka. (g) & (h) Same as (c) and (d), but for 212 ka. (i) & (j) Same as (c) and (d), but for 170 ka.

Deleted: Ice thickness (solid colors, km); basal

Deleted: my^{-1}

Deleted: thick black

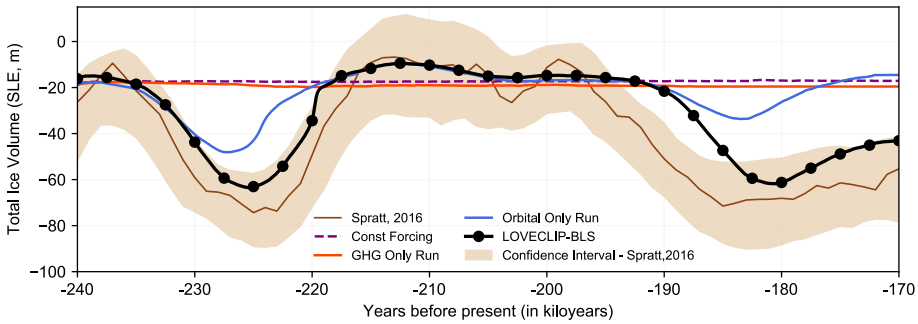

Figure 5: Effects of orbital and GHG forcings on simulated ice volumes during MIS 7. Sea level reconstruction (m) and 95% confidence interval of Spratt and Lisiecki (2016) (brown). Total ice volume (in terms of SLE, m) from transient LOVECLIP simulations with: (i) constant orbital and GHG values set at 240ka (dashed purple line); (ii) orbital values set at 240ka but time varying GHG values (red); (iii) time varying orbital values with GHG values set at 240ka (blue); and (iv) time varying orbital and GHG values (black marked, BLS). All experiments are conducted with an α value of 2 and *m* of 125 Wm^{-2}.

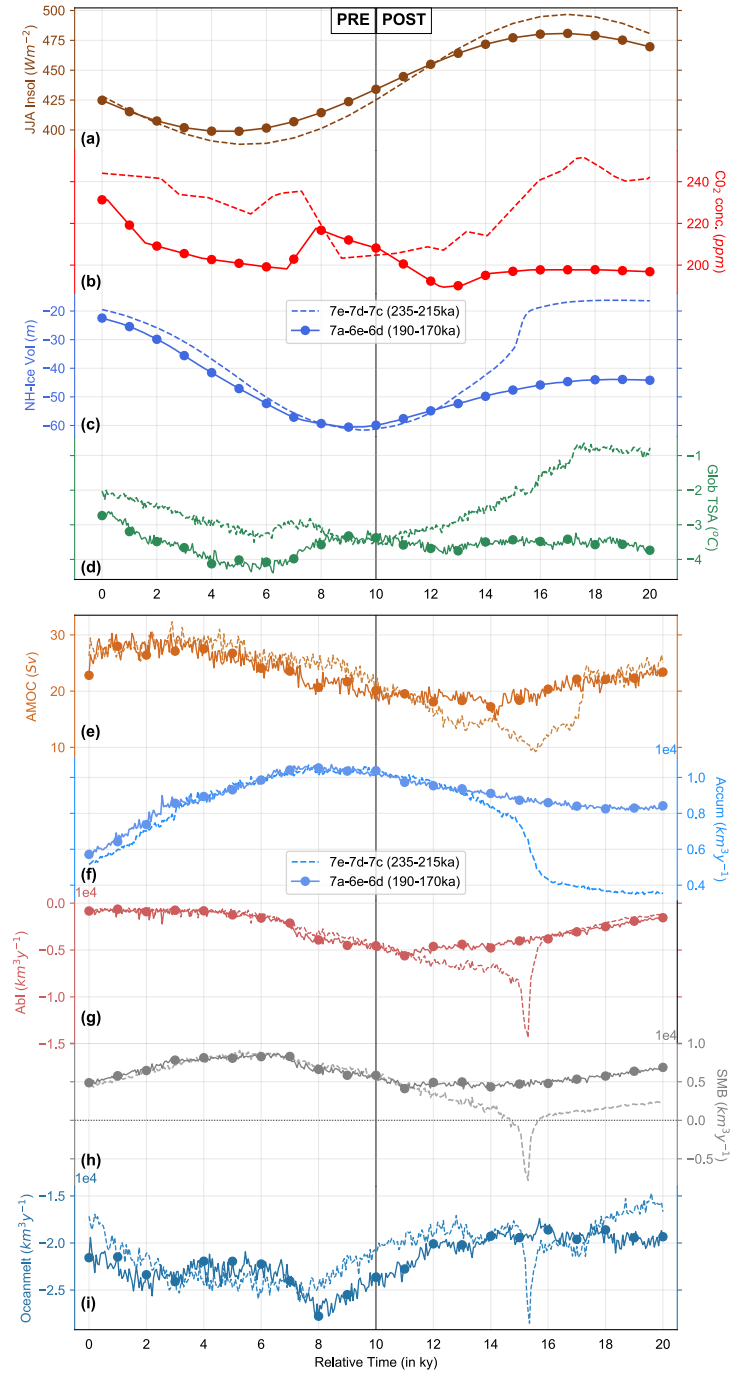
PRE
POST
JJA Insol (Wm^{-2})
(a)
CO_2 conc. (ppm)
(b)
7e-7d-7c (235-215ka)
7a-6e-6d (190-170ka)
NH-Ice Vol (m)
(c)
Glob TSA (°C)
(d)
AMOC (Sv)
(e)
1e4
Accum (km^3y^{-1})
(f)
Abl (km^3y^{-1})
(g)
SMB (km^3y^{-1})
(h)
Oceanmelt (km^3y^{-1})
(i)
Relative Time (in ky)

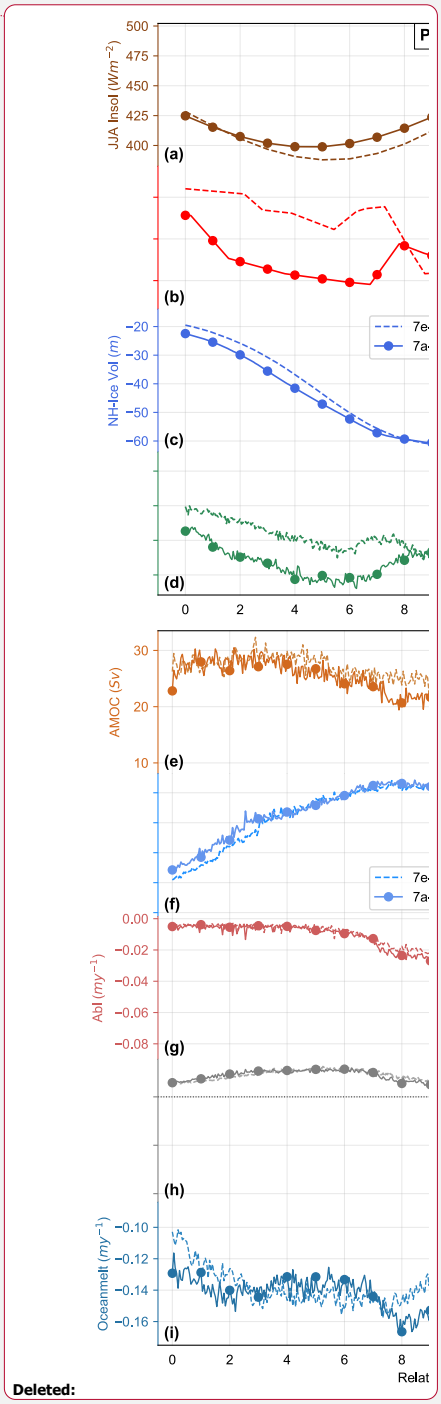
JJA Insol (Wm^{-2})
(a)
(b)
NH-Ice Vol (m)
(c)
(d)
AMOC (Sv)
(e)
(f)
Abl (my^{-1})
(g)
(h)
Oceanmelt (my^{-1})
(i)
Relat

Deleted:

Figure 6: Comparison between two glacial inception scenarios. Different variables over two 20k year periods (relative time) during pre-inception (left half) and post inception (right half) over the Northern Hemisphere are plotted. Variables from the earlier period (235-215ka) are plotted in dashed lines while that of the later period (190-170ka) are plotted in circled solid lines. (a) JJA mean insolation at 65°N (Wm^{-2}, *(Laskar et al., 2004)*). (b) CO_2 concentration (ppm, *(Lüthi et al., 2008)*). (c) Simulated Northern Hemisphere ice volume, in sea level equivalents (m). (d) Global average surface temperature anomaly (°C). (e) Temporal evolution of AMOC (Sv). (f) Net integrated accumulation rate over Northern Hemisphere ice (km^3y^{-1}). (g) Net integrated surface melt rate over Northern Hemisphere ice (km^3y^{-1}). (h) Net integrated surface mass balance over the Northern Hemisphere ice (km^3y^{-1}). (i) Net integrated subshelf melt rate over Northern Hemisphere (km^3y^{-1}).

Deleted: Average

Deleted: my

Deleted: Average

Deleted: my

Deleted: my

Deleted: Average

Deleted: my

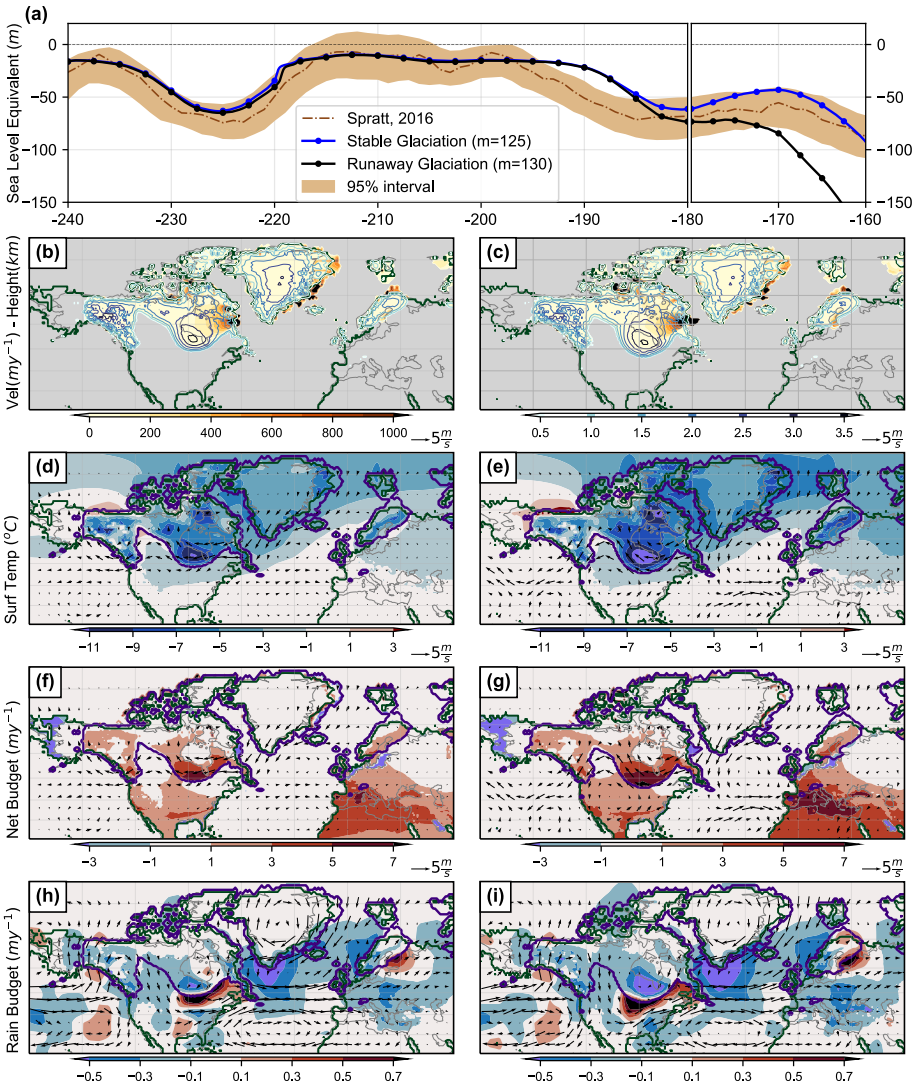

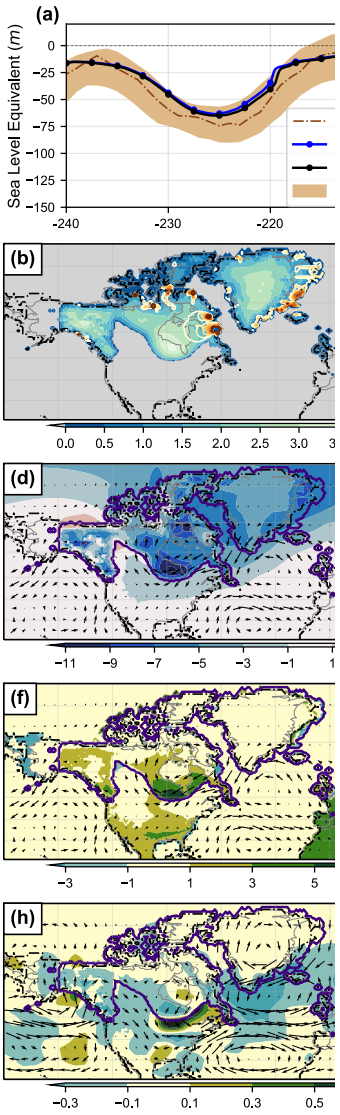

Figure 7: Bifurcation of the system at 180ka while transitioning into MIS 6 over Laurentide. (a) Sea level reconstruction (m) and 95% confidence interval of Spratt and Lisiecki (2016) (brown). Total ice volume (in terms of SLE, m) from two ensemble members of LOVECLIP, one that leads to a stable glacial inception (blue; α=2, m=125 Wm^{-2}) and another into a runaway glaciation (black; α=2, m=130 Wm^{-2}). Climate and ice sheet variables at 180ka from the stable glaciation on the left column (b, d, f and h) and runaway glaciation on the right (c, e, g and i). (b,c) Basal ice velocity (solid colors, my^{-1}) overlaid with ice thickness (colored contours, km) and the grounding line (solid green lines). (d,e) Surface temperature anomalies ($^{\circ}$C) overlaid with *anomalous* wind vectors at 800hPa (ms^{-1}). (f,g) Net mass balance anomalies (my^{-1}) overlaid with *anomalous* winds (ms^{-1}). (h,i) Rainfall anomalies (my^{-1}) overlaid with *absolute* winds (ms^{-1}). The purple contours in (d) to (i) mark the boundaries of the ice sheets from each run (stable for left and runaway for right). Anomalies here are with respect to the initial condition at 240ka. Anomalies over the Eurasian and Siberian ice sheets are small and not shown.

Deleted:
Deleted: ensembles
Deleted: Ice thickness (
Deleted: km
Deleted: basal
Deleted: velocity
Deleted: my^{-1})
Deleted: black dotted
Deleted: .
Deleted: Section Break (Next Page)